Sound Speed, Reflectivity, and Absorption Measurements in Arctic Ice in 1988

by
T. Wen
G.R. Garrison
R.E. Francois
R.P. Stein
W.J. Felton

Technical Report
APL-UW TR 9005
March 1991

Approved for public release.

Contract N00039-88-C-0054

Sound Speed, Reflectivity, and Absorption Measurements in Arctic Ice in 1988

by
T. Wen
G.R. Garrison
R.E. Francois
R.P. Stein
W.J. Felton

Technical Report
APL-UW TR 9005
March 1991

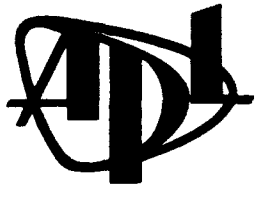

Applied Physics Laboratory University of Washington
1013 NE 40th Street Seattle, Washington 98105-6698

Approved for public release.

Contract N00039-88-C-0054

ACKNOWLEDGMENTS

This work was supported by the Office of Naval Technology (ONT) with technical management provided by the Naval Oceanographic and Atmospheric Research Laboratory (NOARL). The authors wish to thank Kevin Williams for his helpful suggestions.

ABSTRACT

Acoustic measurements at 20–300 kHz were made in the Arctic in Spring 1988 to study sound speed and absorption within the ice canopy and the reflectivity of the water–ice interface. An average sound speed of 3669 ±29 m/s was found for first-year ice, with evidence that the speed varied from 3800 m/s in solid ice to 2000 m/s in the so-called skeletal layer at the lower boundary. The absorption, α, for vertical transmissions was found to be three times as high as that given in the literature for horizontal transmissions; the recommended frequency and temperature dependence is $\alpha = 0.19f(-6/T)^{2/3}$ for temperatures between $T = -2$ and $T = -20$°C. The reflectivity of the lower surface of the ice decreased from 0.2 at 20 kHz to 0.04 at 200 kHz for sound impinging at normal incidence. A simple model that treats the echoes as the sum of reflections from two surfaces, one at the interface between the water and the skeletal layer and one at the transition from the porous skeletal layer to solid ice, matches the experimental results with reasonable accuracy.

TABLE OF CONTENTS

LIST OF FIGURES

LIST OF TABLES

I. EXECUTIVE SUMMARY

In Spring 1988 measurements were made of high-frequency (20–300 kHz) sound reflected at normal incidence from undisturbed first-year arctic ice—both from the 140-cm-thick ice canopy and from blocks of ice depressed below the surface—and of vertical transmissions through the ice to provide information on the acoustic properties of the ice. Such information is helpful in relating ice reflections to ice properties and thus in designing sonar systems for ice avoidance and ice thickness measurements.

A. Sound Speed in Ice

The average vertical sound speed in 140-cm-thick ice with the skeletal transition layer included was 3669 ± 29 m/s for ice with a temperature varying from −2°C at the bottom to −30°C at the top. The sound speed in solid ice was higher, near 3800 m/s. The sound speed in new ice up to 20 cm thick and in the lower 15 cm of thicker ice was lower than that for solid ice by about 20%. This lower speed is apparently a property of the skeletal transition layer, and there are indications that speeds lower than 2000 m/s may exist near the bottom surface of arctic sea ice.

B. Reflectivity of the Skeletal Layer

The reflectivity of the skeletal layer at the bottom of ice 140 cm thick varied roughly from 0.2 at 20 kHz to 0.04 at 200 kHz. The reflectivity was much higher in the first stages of freezing, gradually dropping to these values when the ice thickness reached about 25 cm.

If the reflecting medium has a lower acoustic impedance than the propagating medium, the reflected waveform will be inverted. The echoes recorded from the air–water interface were inverted, whereas those from the skeletal layer were not, indicating that the skeletal layer has an acoustic impedance greater than that of water. This would be expected, since solid ice has an impedance about twice that of seawater. However, when ice blocks were removed from the water and resubmerged, their reflections

were also inverted, indicating a low-impedance medium. A likely possibility is the presence of trapped air, which is easily envisioned for a drained skeletal layer lowered back into the water.

C. A Two-Interface Reflection from the Skeletal Layer

A shift was observed in the phase of the reflection from the skeletal layer at the bottom of a 58-cm ice block at all frequencies of measurement (20, 30, 40, 60, and 80 kHz). This shift appears to be caused by an overlapping reflection from the top of the skeletal layer. Visual observations of the skeletal layer indicated the structure was much firmer 1–2 cm into the ice. We demonstrate that a skeletal layer with a thickness of 1.4 cm, a density of 0.98, and a sound speed of 2462 m/s would produce a delayed reflection from the top with half the amplitude of the one from the bottom, and that this would result in the observed phase shift.

D. Absorption of Sound in Ice

Two methods were used to calculate sound absorption in sea ice from our vertical transmission experiments. The results were fitted to an absorption equation in the form adopted by McCammon and McDaniel[1] for sea ice,

$$\text{absorption} = k\, f\, (-6/T)^{2/3} \quad \text{dB/m}\,, \tag{1}$$

where T is the ice temperature in degrees Celsius and f is the frequency in kilohertz. They found that a value of 0.06 for the coefficient k gave a reasonable fit to the attenuation data available from other experimenters. For our vertical propagation measurements through the ice, we found that a much higher value, $k = 0.19$, gave a good fit for sea ice between −20 and −2°C.

In both methods we found that the absorption in the skeletal layer (the 1–3 cm thick porous ice layer at the water–ice interface) was anomalously high compared with the more dense ice above: 2 to 2.5 dB over the frequency range 37–96 kHz.

In the first method, sound absorption was calculated directly from one-way vertical transmissions through ice of varying thickness. The results showed an absorption of 2 dB in the combined skeletal layer and transition zone just above, and an absorption in the solid ice about three times that found by McCammon and McDaniel for horizontal transmissions.

In the second method, the absorption was calculated from reflections at normal incidence off the front and back faces of various configurations of arctic ice. For a submerged ice block, this method gave relatively high values of absorption: 12 dB/m at 30 kHz and 18 dB/m at 80 kHz. A possible reason for the high values is that the submerged block had warmed somewhat, causing higher absorption. For new, rapidly growing ice, this method gave an absorption in the skeletal layer of 2.5 dB at 37–92 kHz and an absorption coefficient in the ice about 10 times that given by the McCammon-McDaniel model for horizontal transmissions. For the 140-cm-thick ice canopy, the frequency dependence of the absorption was similar to that predicted by the McCammon-McDaniel model for horizontal transmissions, but the coefficient k was about three times as high, in agreement with the first method for the same ice thickness.

In all these reflection measurements, we assumed the back face of the ice, an air–ice interface, had a reflection coefficient of unity. If the coefficient was not unity, our results would be too high; nevertheless, they are applicable to measurements of ice thickness in which the reflection loss from the back face and the absorption in the ice are unavoidably combined. We also assumed that all sound not reflected back to the transducer entered the ice. Some scattering may have reduced the amount of sound entering the ice, causing our absorption values to be too high.

Our recommendation for calculating acoustic absorption in ice colder than –2°C, based mainly on the vertical measurements of transmission through the ice, is to use McCammon and McDaniel's frequency and temperature dependence, but with a higher constant, i.e.,

$$\text{absorption} = 0.19f(-6/T)^{2/3} \text{ dB/m}, \tag{2a}$$

for temperatures from −20 to −2°C. For the uniform temperature profile often observed in the ice, this becomes

$$\text{average absorption} = 1.9f\frac{(-T_2)^{1/3} - (-T_1)^{1/3}}{T_1 - T_2} \text{ dB/m}, \tag{2b}$$

where T_1 and T_2 are the temperature at the top and bottom of the ice, respectively.

II. INTRODUCTION

In Spring 1988, several experiments were conducted at an ice camp in the Arctic to measure some of the acoustic properties of flat, first-year ice, namely, the sound speed and absorption in the ice and the reflection coefficient of the under-ice surface at normal incidence. The effect of the skeletal layer and the adjacent transition zone on these properties was given special attention but was difficult to measure. The acoustic reflection from the ends of submerged blocks cored from the surface is described in Ref. 2. Here, we describe five separate investigations, summarized in Table 1.

Table 1. Summary of acoustic measurements in Spring 1988 discussed in this report.

Experiment	Transducer	Frequencies (kHz)	Ice Properties Calculated
Reflection from growing ice	Platter	37, 52, 92, 150, 200	Sound speed profile Reflection coefficient Sound absorption
Under-ice surface reflections for source depths of 10 and 28 m	ITC 1042 22×22 Platter	20, 30, 40, 60, 80 30, 40, 50, 80, 100, 120, 160, 200, 300 15, 37, 52, 92, 150, 220, 300	Average sound speed Reflection coefficient Sound absorption
Under-ice surface reflections for a source depth of 2 m	22×22	60, 80, 100, 120, 160, 200	Reflection coefficient Sound absorption
Phase change in ice-block reflections[a]	ITC 1042	20, 30, 40, 60, 80	Nature of reflecting medium Evidence of later arrivals
Transmissions through ice	ITC 1042 22×22	20, 30, 40, 60, 80 30, 40, 60, 80, 100, 120, 160, 200, 300	Sound speed profile Sound absorption

[a] The ice-block experiment is described in Ref. 2.

In the first experiment, reflections from the undersurface of ice formed in a large hole were monitored from the initial stages of freezing until the thickness reached 50 cm. Reflections from the front and back faces were analyzed to determine the reflection coefficient, sound speed, and absorption. This was intended as a study of the effect of the skeletal layer at different stages of growth.

In the second experiment, reflections at normal incidence were measured from the underside of the flat ice field used for the ice-block experiment,[2] using three different transducers. The reflections from the back face were recorded and used to calculate the reflection coefficient, sound speed, and absorption.

Reflections were also measured from the underside of a small area of ice similar to the flat ice field used for the previous experiment and located between it and the main camp. For these measurements, a transducer was supported on a rotating arm beneath the ice, and 72 slightly overlapping areas were ensonified in turn to provide statistics on the variations of the reflection coefficient. The reflections from the back face were used to determine absorption.

The ice-block reflections[2] were examined in detail for phase relationships that might disclose any additional reflecting surfaces. (The phase of the initial part of the reflection can indicate whether the reflecting medium has a higher or lower acoustic impedance than the water. Later phase changes may indicate the arrival of additional reflections from other surfaces in the skeletal layer or the transition zone.)

Finally, one-way transmissions were made from a transducer below the ice to a receiver in a hole on the surface. The hole was gradually deepened to give a path through less and less ice. A final reading was taken with the receiver in the water below the hole. These measurements were used to determine both sound speed and absorption.

The experimental site was about 100 m from the building housing the HP 85-controlled data-acquisition system. All operator/equipment interaction, other than gain setting changes, occurred at the computer. Pulses of desired frequency, length, and level were selected at the computer. The gains were read automatically by the computer, and the waveforms recorded on a Nicolet digital oscilloscope. Errors often made in the logging of important parameters were in effect eliminated with this system.

III. REFLECTIONS FROM GROWING ICE

A. Experimental Arrangement

To measure reflections from growing ice, a large hole was made in 1.4-m-thick ice in the flat ice field used to measure reflections from the ends of cylindrical ice blocks[2] cored out with APL's ice melter.[3] A transducer referred to as the "platter" transducer (described in Section IV.B) was suspended on lines from holes in the ice as shown in Figure 1. While pulses were transmitted, the lines were adjusted to bring the transducer directly under the hole, as ascertained by maximizing the returns from a calibration sphere suspended temporarily below the hole. Once in place, the transducer was fixed in position 11.3 m below the water surface. The transmitter and receiver electronics were located in a building 100 m away, where the received signals were monitored and recorded.

At various stages of freezing, cw pulses were transmitted at five frequencies (37, 52, 92, 150, and 220 kHz) and reflections recorded from the water surface or, after freezing started, from the ice.

Our first attempt, with a hole 86 cm in diameter, resulted in too much reflection from the edge of the hole. Before abandoning it, however, we measured sound speeds for the path to and from the upper surface of the ice through the surrounding ice cover. Later, a larger hole, about 2 m square, was made, and the reflections from the freezing surface were measured at intervals of 5–10 hours for 16 days.

B. Growth Rate

The first measurement was made before any ice had formed in order to calibrate the transducer and measure the distance between it and the water surface. The transducer and the upper surface of the ice were assumed to remain at these initial levels during the remainder of the experiment.

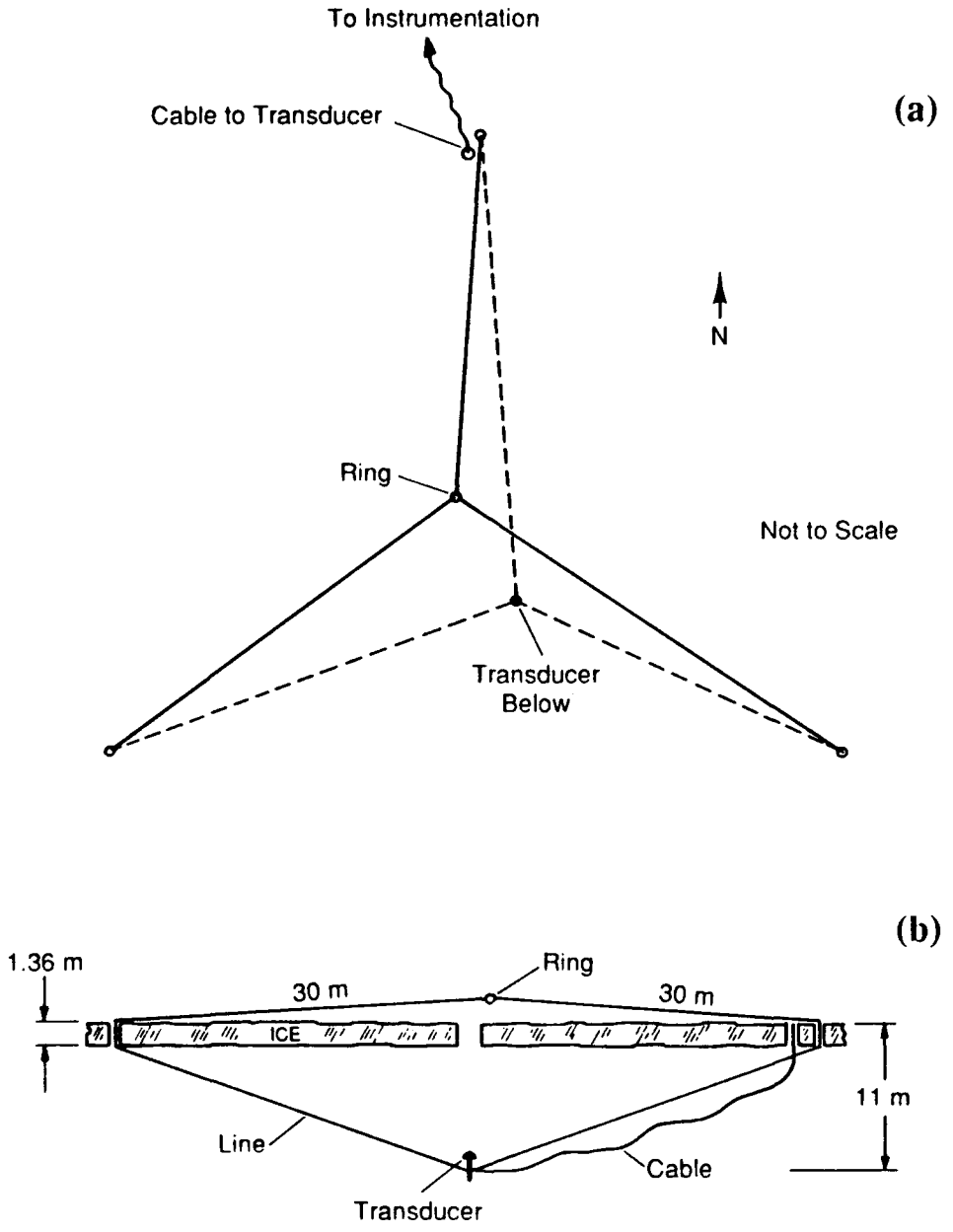

Figure 1. Suspension system used to support and move the transducer below the growing ice. Movement of the ring on top of the ice controls the movement of the transducer below. The ring is positioned on a grid of wooden pegs to ensure accurate movement. (a) Plan view. (b) Elevation view (two-dimensional simplification).

At various times thereafter, depending on other activities, measurements were made of the reflections from the undersurface of the ice in the hole. As the ice thickened, the reflections arrived earlier. The reflection time was converted into distance, i.e., ice thickness, using the known sound speed in the water (1436 m/s). The increase in thickness with time is shown in the upper plot of Figure 2 as a smoothed average. The lower plot, which was computed from the slope of the upper graph, shows the decrease in the freezing rate.

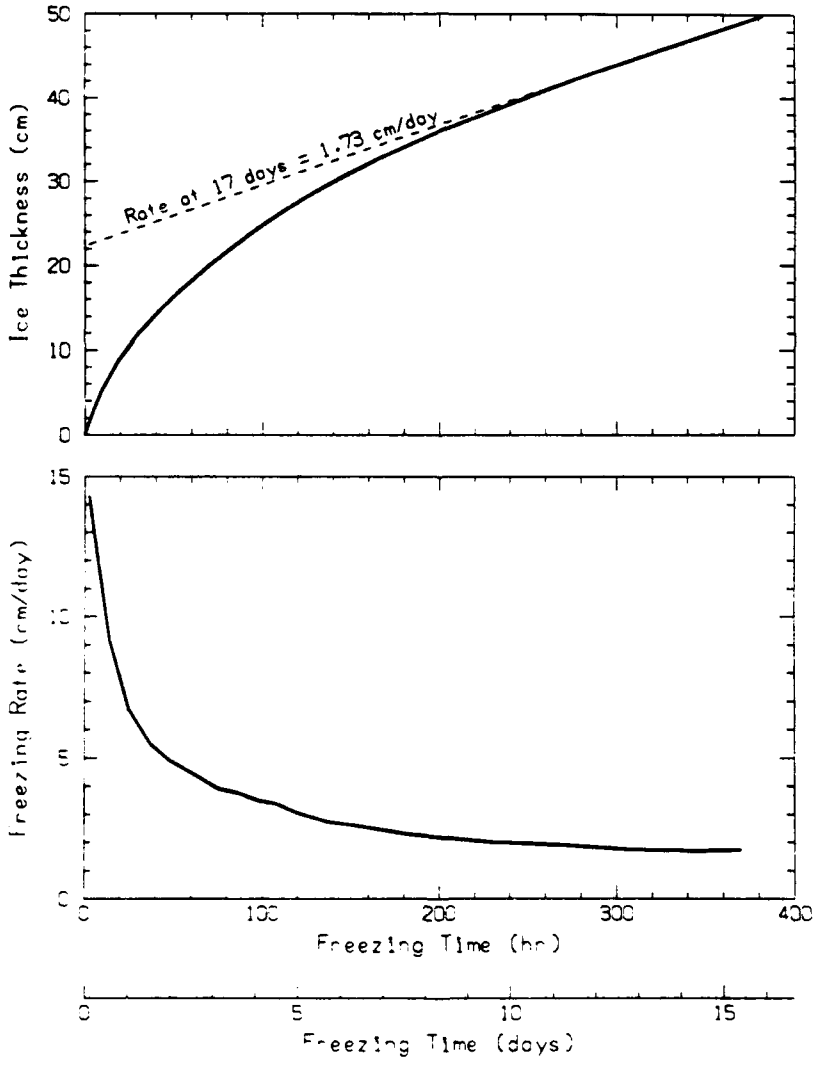

Figure 2. Increase in thickness of ice growing in a 2×2-m hole (top) and the corresponding freezing rate (bottom).

Table 2 compares our ice thickness measurements with those of Anderson[4] in 1956 and 1957 at Thule, Greenland, who related his thickness to degree-days of cooling (i.e., $\int \Delta T dt$, where ΔT is the freezing temperature of the water minus the air temperature and t is time). The air temperature during our measurements averaged −28°C for the first 6 days, −33 for the next 3 days, −29 for the next 4, and −25 the last 3 days. The agreement with Anderson's measurements is good even though our freezing took place in a 2×2 m hole surrounded by ice 1.4 m thick, a configuration which should have increased the freezing rate.

Table 2. Comparison of measured thickness with Anderson's measurements.[4]

Cumulative °C - Days	Measured Ice Thickness (cm)	
	APL 1988 in Beaufort Sea	Anderson 1956-7 at Thule, Greenland
0	0	0
20	8.2	9
40	13.5	14
100	22.3	24
200	32.5	37
400	46.4	50
457 (last)	50	52

C. Changes in Reflectivity of the Lower Surface

The reflections from the surface of the water before any ice had formed are plotted in Figure 3. The first, at 37 kHz, shows a fairly square pulse, taking only two cycles to reach full amplitude. The second, at 52 kHz, was near the resonant frequency of the transducer and has a slow build-up and a slow decay. A 0.35-ms pulse was used for both these frequencies.

A 0.2-ms pulse was used for the third and fourth frequencies. The 92-kHz echo showed a ringing at 52 kHz after the end of the pulse, which caused some confusion in sorting out the returns. For the fifth frequency, 220 kHz, a pulse only 0.035 ms long was used.

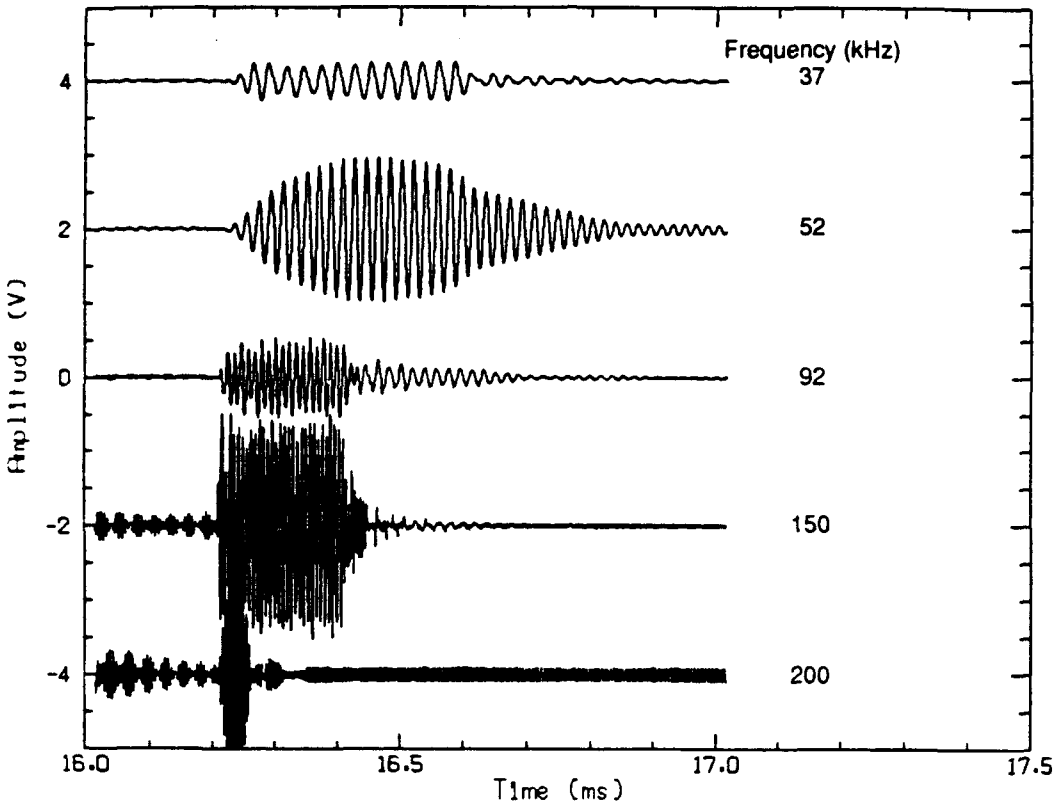

Figure 3. Waveforms of the reflections from the water surface in the 2×2-m hole at frequencies of 37–220 kHz. Waveforms are displaced vertically to avoid overlap.

A few of the echoes measured at various times during the following 16 days are shown in Figure 4. At first, the echoes from the lower and upper surfaces of the growing ice merged together. As the ice thickened, we were able to distinguish the reflections from the lower and upper faces. Table 3 shows the various items that were measured and calculated (some entries in this table will be explained later). The return from the lower surface, V_1, is tabulated just below the electrical voltage T_x applied to the transducer.

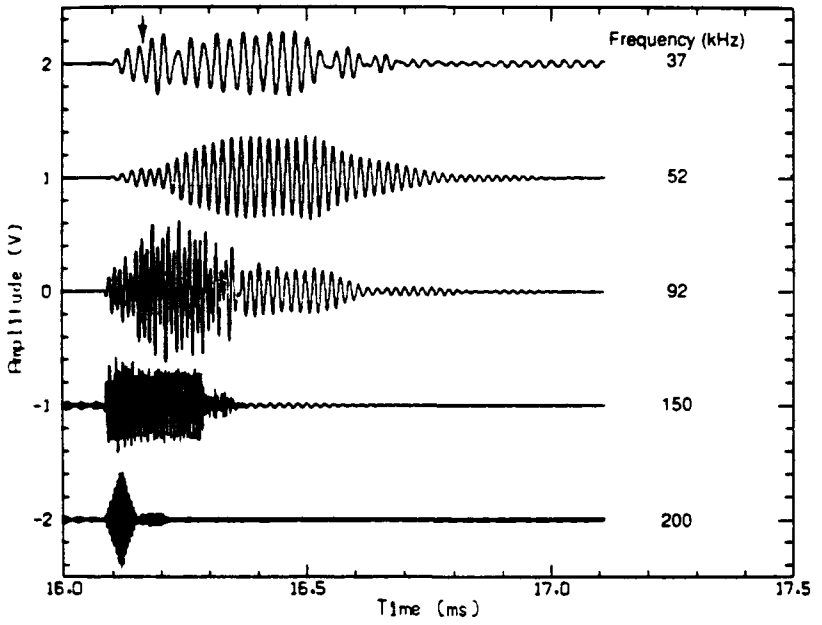

Figure 4a. Waveforms for the reflections from the newly frozen ice in the 2×2-m hole, after 18.8 hours of freezing. The arrow indicates the estimated start of the reflection from the upper face.

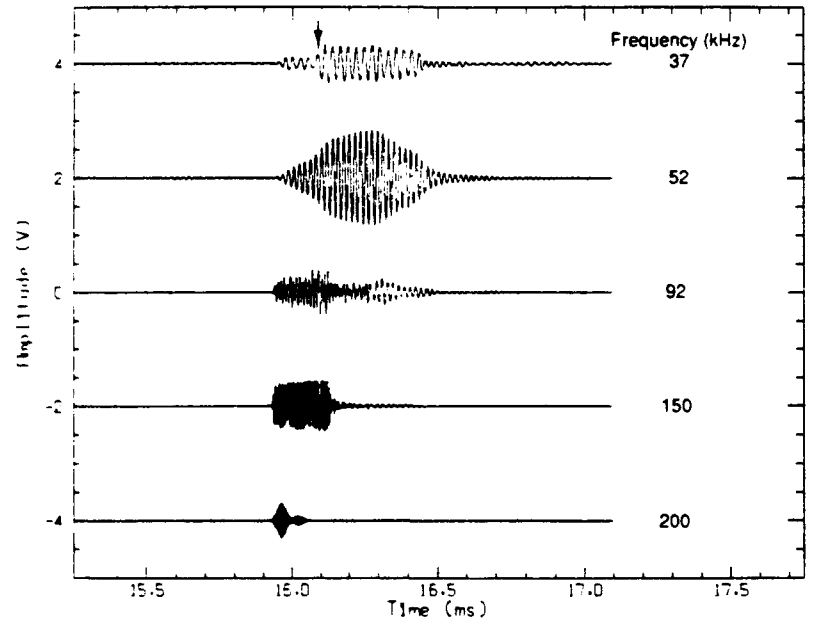

Figure 4b. Waveforms for the reflections from the newly frozen ice in the 2×2-m hole, after 70.5 hours of freezing. The arrow indicates the estimated start of the reflection from the upper face.

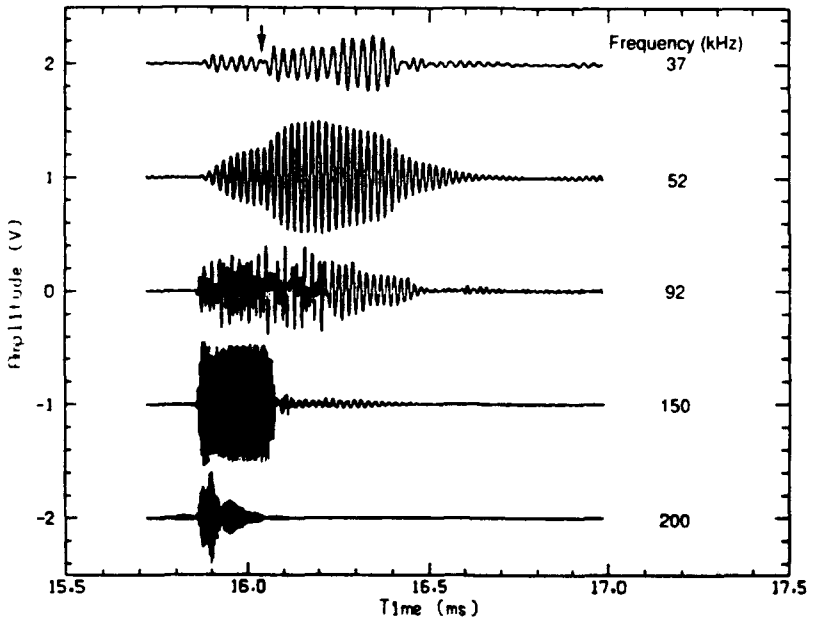

Figure 4c. Waveforms for the reflections from the newly frozen ice in the 2×2-m hole, after 102.5 hours of freezing. The arrow indicates the estimated start of the reflection from the upper face.

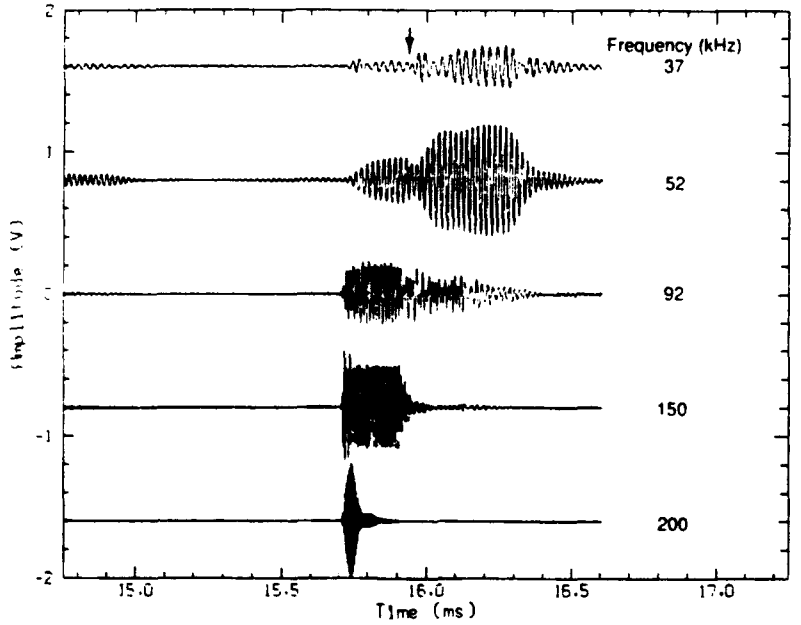

Figure 4d. Waveforms for the reflections from the newly frozen ice in the 2×2-m hole, after 200 hours of freezing. The arrow indicates the estimated start of the reflection from the upper face.

Table 3. Acoustic measurements during freezing in the hole.

Hours of Freezing		0.0	5.0	9.0	18.8	31.2	43.0	52.0
Smoothed T_1 (ms)		16.209	16.167	16.139	16.087	16.039	16.001	15.976
T_0-T_1 (ms)			0.042	0.070	0.122	0.170	0.208	0.233
Range (m)		11.64	11.61	11.59	11.55	11.52	11.49	11.47
Thickness (cm)			2.98	5.01	8.75	12.21	14.91	16.76
T_2-T_1; 37 kHz (ms)				0.030	0.065	0.110	0.120	0.122
52 kHz (ms)				0.020	0.082	0.110	0.130	
92 kHz (ms)				0.060	0.065	0.085	0.100	0.100
Smoothed T_2-T_1 (ms)			0.0300	0.0470	0.0740	0.0950	0.1101	0.1204
Sound speed in ice (m/s)			1986.	2133.	2364.	2570.	2709.	2784.
Refraction correction			1.0036	1.0064	1.0125	1.0190	1.0245	1.0283
37 kHz;	T_x (V_{pp})	10.12	26.60	26.20	25.50	33.00	32.90	32.40
	V_1 (V_{pp})	0.520		0.280	0.320	0.360	0.330	0.305
	V_2 (V_{pp})		0.650	0.640	0.535	0.425	0.675	0.135
	V_3 (V_{pp})			0.410	0.400	0.650	0.635	0.380
Amplitude check				Yes	Yes	Yes	Yes	Yes
2-way absorption (dB)				10.1	9.9	8.0	8.2	12.6
Absorption coef. (dB/m)				100.5	56.6	32.8	27.6	37.5
52 kHz;	T_x (V_{pp})	4.98	7.56	18.60	4.36	4.60	11.90	12.40
	V_1 (V_{pp})	2.000			0.400	0.700	1.103	1.290
	V_2 (V_{pp})		1.450	3.000				
	V_3 (V_{pp})							
Amplitude check								
2-way absorption (dB)								
Absorption coef. (dB/m)								
92 kHz;	T_x (V_{pp})	11.20	77.00	63.60	28.60	63.20	128.70	62.20
	V_1 (V_{pp})	1.050			0.410	1.030	1.020	0.500
	V_2 (V_{pp})		1.400	2.450	0.940	1.550		
	V_3 (V_{pp})				0.590	0.450		
Amplitude check					Yes	No		
2-way absorption (dB)					12.6	21.7		
Absorption coef. (dB/m)					71.8	88.9		
150 kHz;	T_x (V_{pp})	33.00	104.80	96.80	38.40	82.20	154.40	84.80
	V_1 (V_{pp})	2.800	1.600	1.650	0.700	1.300	1.300	0.500
220 kHz;	T_x (V_{pp})	4.50	24.20	9.90	4.68	7.11	12.90	8.60
	V_1 (V_{pp})	2.800	1.300	2.190	0.850	1.150	0.900	0.800
R_e;	37 kHz	0.984		0.204	0.239	0.207	0.190	0.178
	52 kHz	0.989			0.230	0.380	0.225	0.252
	92 kHz	1.039			0.158	0.179	0.087	0.088
	150 kHz	1.019		0.204	0.217	0.188	0.100	0.070
	220 kHz	0.924		0.327	0.268	0.238	0.102	0.136

T_0 = time of return from water surface
T_1 = time of return from lower ice surface
T_2 = time of return from upper ice surface
T_x = voltage applied to transmitter
V_1 = voltage of return from lower ice surface
V_2 = voltage of combined returns from lower and upper surfaces
V_3 = voltage of return from upper ice surface
Amplitude check: Is V_2 between V_1-V_3 and V_1+V_3?

Table 3. (cont)

Hours of Freezing		70.5	80.5	94.5	102.5	112.5	128.0	145.0
Smoothed T_1 (ms)		15.928	15.905	15.875	15.859	15.839	15.812	15.785
T_0-T_1 (ms)		0.281	0.304	0.334	0.350	0.370	0.397	0.424
Range (m)		11.44	11.42	11.40	11.39	11.37	11.35	11.33
Thickness (cm)		20.18	21.81	23.99	25.15	26.56	28.52	30.46
T_2-T_1; 37 kHz (ms)		0.135	0.147	0.145	0.175	0.165	0.185	0.195
52 kHz (ms)		0.150	0.155	0.165	0.180	0.167	0.180	0.207
92 kHz (ms)		0.130	0.140	0.160	0.165	0.170	0.185	0.195
Smoothed T_2-T_1 (ms)		0.1389	0.1476	0.1592	0.1653	0.1729	0.1835	0.1942
Sound speed in ice (m/s)		2905.	2956.	3014.	3043.	3072.	3108.	3137.
Refraction correction		1.0357	1.0393	1.0442	1.0468	1.0500	1.0544	1.0587
37 kHz;	T_x (V_{pp})	32.80	64.40	32.20	33.20	32.40	33.60	32.80
	V_1 (V_{pp})	0.250	0.340	0.220	0.140	0.120	0.055	0.040
	V_2 (V_{pp})	0.625	0.600	0.380	0.350	0.370	0.500	0.540
	V_3 (V_{pp})	0.540	1.030	0.560	0.460	0.610	0.675	0.652
Amplitude check		Yes	No	Yes	Yes	No	No	No
2-way absorption (dB)		9.7	10.0	9.2	11.3	8.6	8.0	8.1
Absorption coef. (dB/m)		24.0	23.0	19.2	22.4	16.2	14.1	13.3
52 kHz;	T_x (V_{pp})	12.00	8.51	12.10	12.00	12.10	12.30	12.00
	V_1 (V_{pp})	0.990	0.390	0.650	0.540	0.670	0.370	0.170
	V_2 (V_{pp})							
	V_3 (V_{pp})							0.850
Amplitude check								
2-way absorption (dB)								14.9
Absorption coef. (dB/m)								24.4
92 kHz;	T_x (V_{pp})	62.60	62.40	61.50	124.40	125.60	126.80	126.80
	V_1 (V_{pp})	0.480	0.720	0.330	0.340	0.270	0.215	0.500
	V_2 (V_{pp})							
	V_3 (V_{pp})			0.380	0.510	0.470	0.300	
Amplitude check								
2-way absorption (dB)				23.1	26.6	27.4	31.4	
Absorption coef. (dB/m)				48.1	53.0	51.6	55.0	
150 kHz;	T_x (V_{pp})	84.20	155.60	157.20	158.00	155.60	158.40	156.80
	V_1 (V_{pp})	0.900	0.840	0.400	1.040	0.500	1.000	0.360
220 kHz;	T_x (V_{pp})	15.80	15.40	31.40	33.00	17.50	17.20	32.20
	V_1 (V_{pp})	0.700	0.600	0.650	0.600	0.760	0.630	0.620
R_a;	37 kHz	0.143	0.099	0.128	0.079	0.069	0.031	0.023
	52 kHz	0.200	0.111	0.130	0.108	0.133	0.072	0.034
	92 kHz	0.083	0.125	0.058	0.030	0.023	0.018	0.042
	150 kHz	0.126	0.064	0.030	0.077	0.038	0.074	0.027
	220 kHz	0.065	0.057	0.030	0.026	0.063	0.053	0.028

Table 3. (cont)

Hours of Freezing	163.5	200.0	261.0	281.0	333.0	358.0	382.0
Smoothed T_1 (ms)	15.757	15.708	15.638	15.615	15.563	15.538	15.514
T_0-T_1 (ms)	0.452	0.500	0.571	0.594	0.646	0.670	0.694
Range (m)	11.31	11.28	11.23	11.21	11.17	11.16	11.14
Thickness (cm)	32.45	35.94	41.03	42.61	46.38	48.14	49.87
T_2-T_1; 37 kHz (ms)	0.182	0.220	0.265	0.260	0.330	0.270	0.373
52 kHz (ms)	0.202	0.227	0.260	0.260	0.310		0.400
92 kHz (ms)	0.211	0.229	0.248	0.254	0.274		0.298
Smoothed T_2-T_1 (ms)	0.2052	0.2244	0.2523	0.2607	0.2802	0.2890	0.2975
Sound speed in ice (m/s)	3163.	3203.	3252.	3269.	3311.	3332.	3352.
Refraction correction	1.0632	1.0711	1.0828	1.0865	1.0957	1.1001	1.1045
37 kHz; T_x (V_{pp})	32.00	16.10	33.40	32.60	32.60	162.50	31.80
V_1 (V_{pp})	0.120	0.080	0.080	0.060	0.065	0.280	0.110
V_2 (V_{pp})	0.455		0.206	0.220	0.112	0.330	
V_3 (V_{pp})			0.310	0.250	0.080	0.140	0.065
Amplitude check			No	Yes	Yes	Yes	
2-way absorption (dB)			14.6	16.3	26.1	35.2	27.6
Absorption coef. (dB/m)			17.8	19.1	28.1	36.5	27.7
52 kHz; T_x (V_{pp})	12.10	7.70	24.00	23.20	23.30	23.80	23.80
V_1 (V_{pp})	0.380	0.320	0.505	0.380	0.225		0.570
V_2 (V_{pp})		0.730	1.380				
V_3 (V_{pp})	1.200	0.780	1.130	0.830			
Amplitude check		Yes	Yes				
2-way absorption (dB)	11.9	11.7	18.3	20.7			
Absorption coef. (dB/m)	18.4	16.2	22.3	24.3			
92 kHz; T_x (V_{pp})	126.40	65.90	124.80	63.20	120.80	119.20	124.00
V_1 (V_{pp})	0.570	0.430	0.400	0.220	0.100		0.270
V_2 (V_{pp})							
V_3 (V_{pp})							
Amplitude check							
2-way absorption (dB)							
Absorption coef. (dB/m)							
150 kHz; T_x (V_{pp})	156.80	93.10	159.20	79.20	159.60	162.40	158.40
V_1 (V_{pp})	0.750	0.600	0.300	0.380	0.170	0.100	0.400
220 kHz; T_x (V_{pp})	32.20	12.20	34.00	32.80	30.20	34.00	18.30
V_1 (V_{pp})	1.050	0.800	1.060	0.600	0.180	0.020	
R_a; 37 kHz	0.070	0.092	0.044	0.034	0.037	0.032	0.063
52 kHz	0.075	0.099	0.050	0.039	0.023		0.056
92 kHz	0.048	0.070	0.034	0.037	0.009		0.023
150 kHz	0.056	0.075	0.022	0.055	0.012	0.007	0.029
220 kHz	0.047	0.094	0.045	0.026	0.008	0.001	

Knowing the calibration properties of the transducer and the voltage applied, we calculated the amplitude reflection coefficient for the under-ice surface in the hole. The change in the reflection coefficient as the ice froze is shown in Figure 5. At all frequencies, the reflection coefficient plunged from unity (assumed for the water surface) to less than 0.5 in the first 10 hours and then decreased to a nearly constant value in about 100 hours, when the ice thickness was 25 cm.

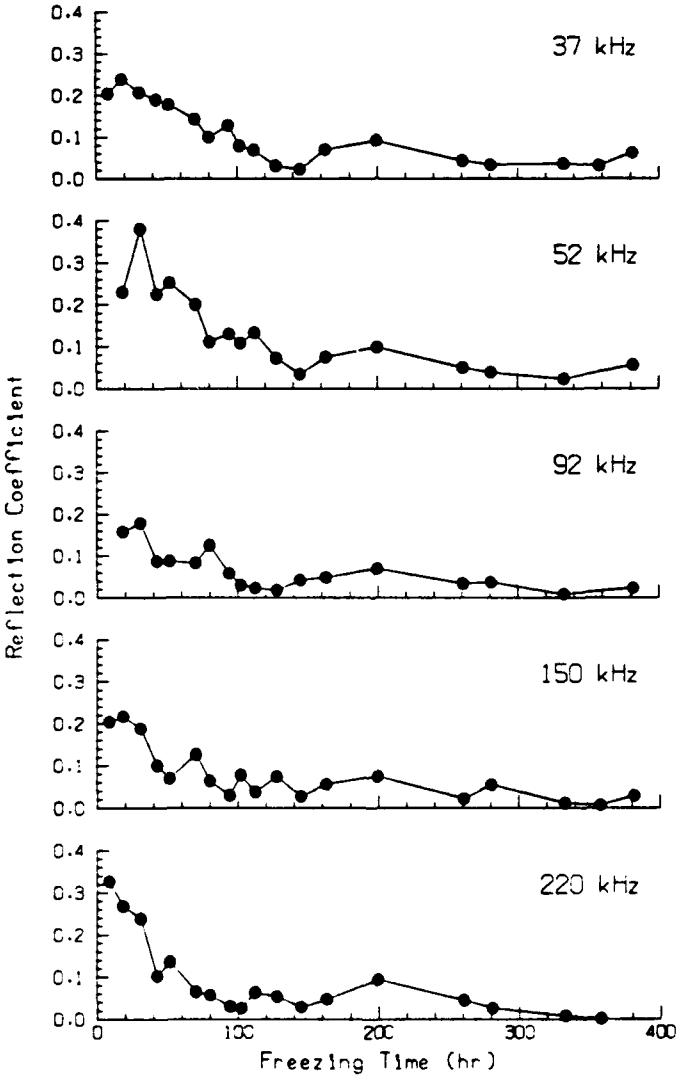

Figure 5. Dropoff of amplitude reflection coefficient as the ice in the hole thickened.

D. Reflections from Upper Surface of Growing Ice

Before we try to identify the reflection from the upper surface of the growing ice, we will review the various sound paths and reflections present in the return. Figure 6 shows an echo at 37 kHz after 94.5 hours of freezing. The phase with respect to an arbitrary reference signal at the same frequency is plotted below as an aid in separating the reflections present in the echo. The first reflection (a) occurred from the bottom of the ice surrounding the hole. Overlapping this was a small return of sound that had entered this surface, traveled through the ice, and reflected off the upper surface of the ice cover. These two reflections were unwanted, and occurred because the transducer pattern was too wide. They usually ended before the arrival of the reflection of main interest (b) from the bottom of the newly frozen surface; however, after 200 hours had elapsed, the reflection from the freezing surface arrived sufficiently early that there was some overlap. The reflection from the upper surface of the growing ice (c) generally overlapped that from the lower surface (b). Phase changes usually occur when a contribution starts or ends; thus the lower plot in Figure 6 was useful in determining the arrival time of pulse (c).

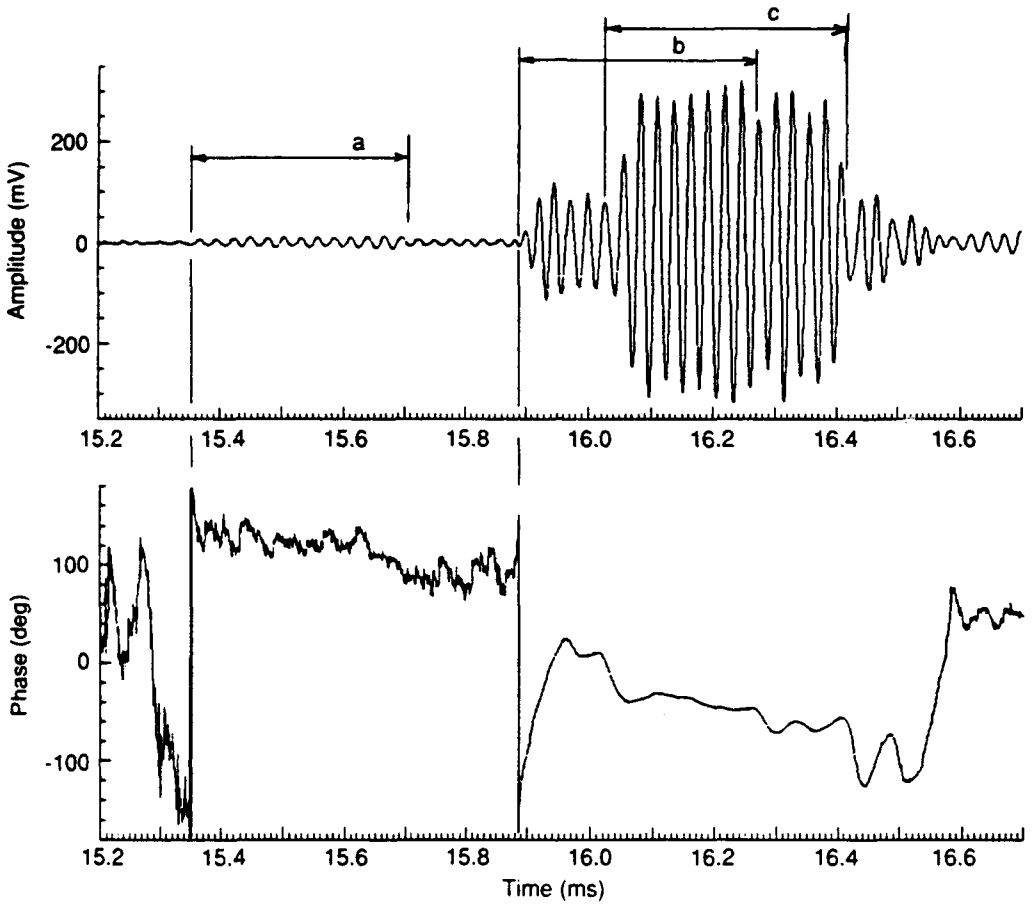

Figure 6. An example of the return showing the various reflections (top) and the use of corresponding phase changes to detect each arrival (bottom). These data are for a frequency of 37 kHz and a freezing time of 94.5 hours.

E. Change in Sound Speed with Thickness

The growing-ice experiment gave an opportunity to measure the sound speed in ice of varying thickness, always with the skeletal layer present. The time of arrival T_1 of the echoes from the surface where freezing was taking place (reflection (b) in Figure 6) is plotted in Figure 7. The plotted results show a fairly smooth rate of freezing. By comparing these times with T_0, the time of the return from the initial water surface, and using the known sound speed in the water, we can calculate the thickness of the ice as it grew. This assumes that the freezing plug in the hole did not rise or bulge as its buoyancy increased; the surface appeared to remain flat and well bonded to the sides of the hole. This thickness is used in both the sound speed and absorption calculations.

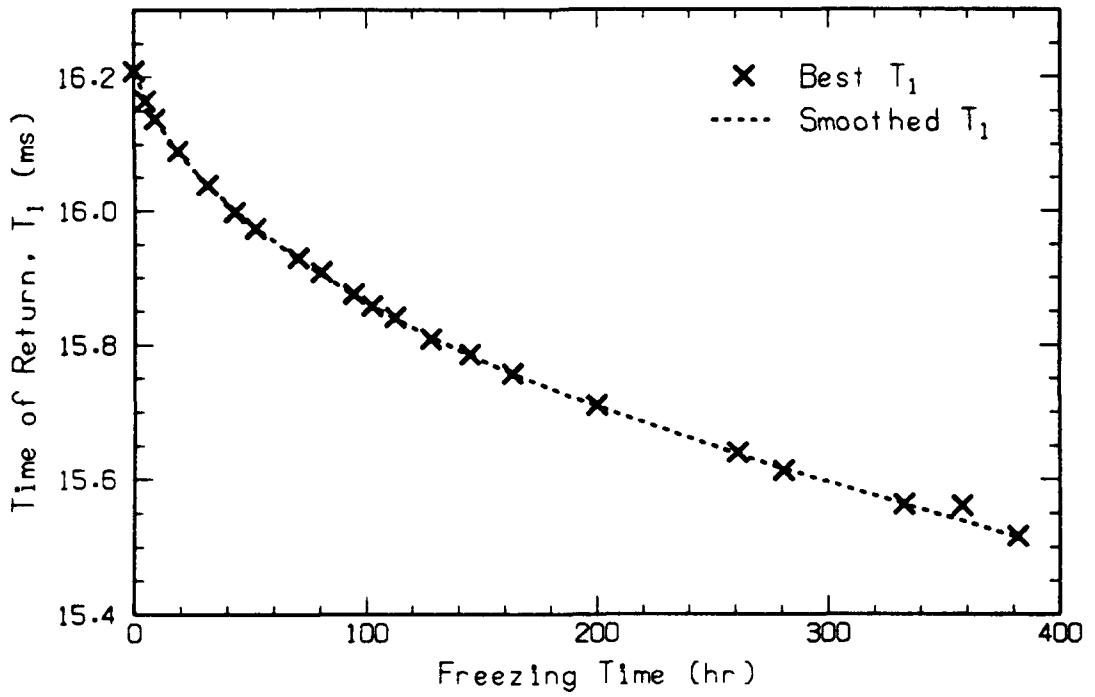

Figure 7. The travel time of the return from the bottom of growing ice.

The reflection from the upper surface (reflection (c) in Figure 6) was identified, and the time between the reflections was measured. This time difference, labeled $T_2 - T_1$, is tabulated in Table 3 and plotted in Figure 8 versus freezing time and ice thickness. A smooth line has been drawn as an estimate of $T_2 - T_1$ as the ice froze and the thickness increased. The smoothed two-way travel times shown in Figure 8 and the thickness calculated from the smoothed T_1 values in Figure 7 were used to calculate the average sound speed in the ice versus time and thickness (Figure 9).

From one measurement to the next, the sound speed at any depth increases because the ice is becoming less porous. If we assume that from one measurement to the next the sound speed in the lower few centimeters remains the same, we can calculate the sound speed in the incremental layer at the top of the ice that has the same thickness as the amount added at the bottom. In other words, the next average will involve an "additional" ice layer at the top, and the change in the average can be used to calculate the sound speed in that layer. The sound speeds calculated are plotted in Figure 10 along with the average sound speed. Note that the incremental sound speed increases rapidly until a thickness of 14 cm is obtained, indicating a skeletal layer transition zone of that thickness.

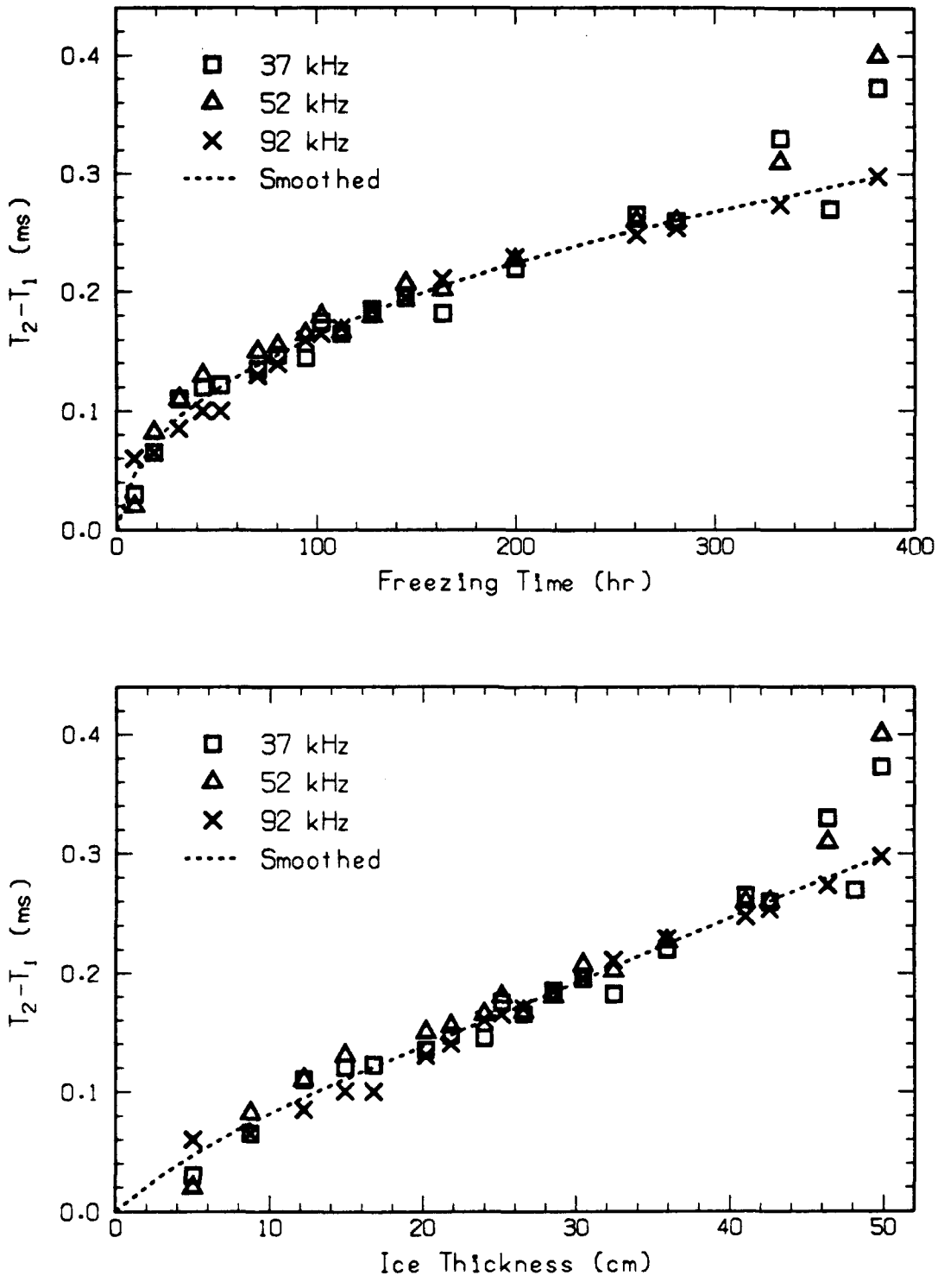

Figure 8. Time interval between returns from front and back faces of growing ice versus freezing time (top) and ice thickness (bottom).

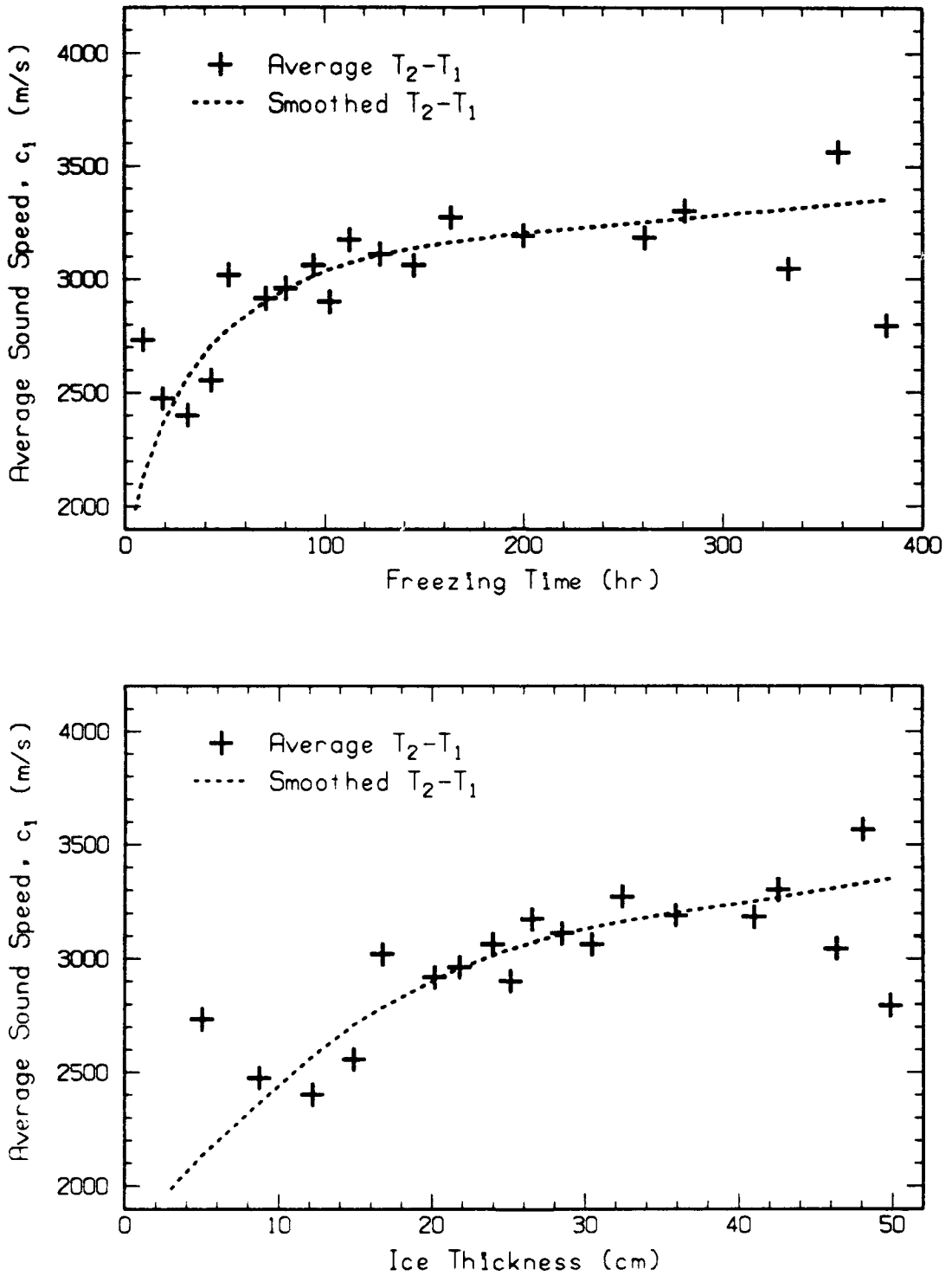

Figure 9. Average sound speed in the newly frozen ice as determined from reflections from the front and back faces, plotted versus freezing time (top) and ice thickness (bottom).

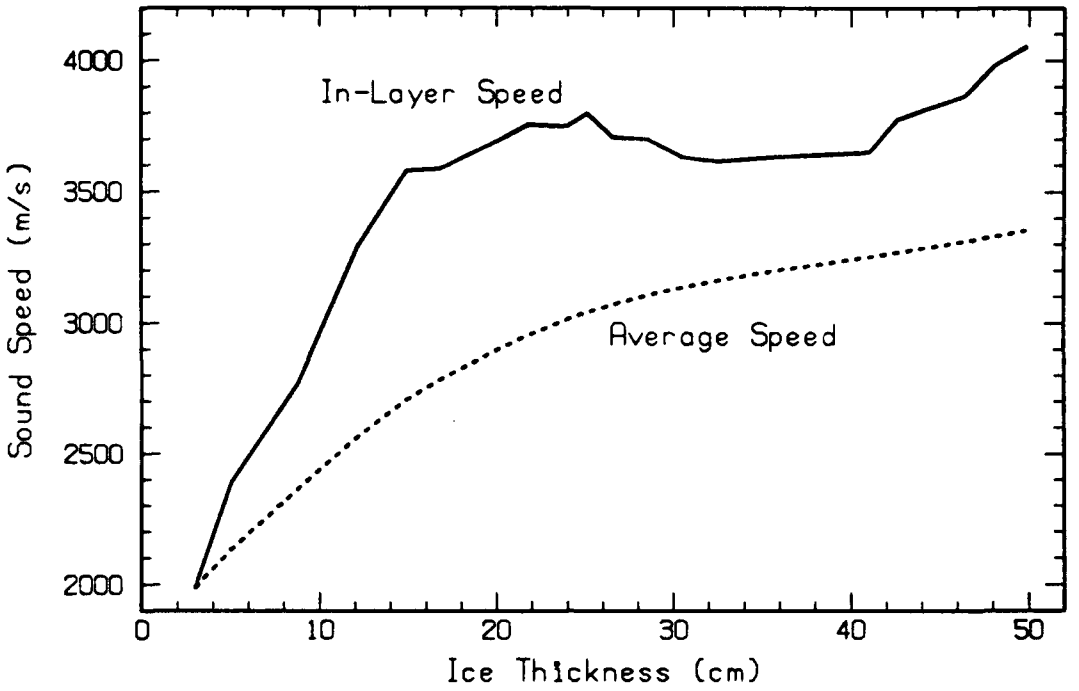

Figure 10. Sound speed in an increment at the top of the ice (solid curve) calculated from the change in the average (dotted curve) as freezing progressed. The first points are not very accurate, but a low speed in the skeletal layer is indicated.

F. Sound Speed for a Path through the Surrounding Ice

During the growing-ice experiment, we also observed a reflection from the bottom of the ice cover and a second reflection which appeared to be from the top surface of the ice cover. Knowing the thickness of the ice cover, we compared the times of the two returns in an attempt to calculate the sound speed in the ice.

The times of the echoes from the top and bottom of the ice cover are tabulated in Table 4 and plotted in Figure 11. If we assume that the transducer did not move vertically, the decrease in travel time for the echo from the bottom indicates an increase of about 0.27 cm per day in the ice surrounding the bottom of the hole, one-half the growth observed during various investigations of the undisturbed ice in the area. The travel times of the echoes from the upper face show a gradual decrease in the first 200 hours.

Table 4. The times of the returns from the upper and lower surfaces of the ice cover (37 and 52 kHz data), and the calculated sound speed.

Freezing Time (hr)	Disc	Track	Time (ms)		
			T1, lower	T2, upper	T2-T1
43	13	6,7	14.53	15.40	0.87
52		11,12	14.54	15.37	0.83
81	14	1,2	14.54	15.32	0.78
95		6,7	14.54	15.34	0.78
103		11,12	14.53	15.35	0.82
113		16,17	14.52	15.28	0.76
128	15	1,2	14.52	15.28	0.76
164		11,12	14.52	15.21	0.69
200		16,17	14.51	15.28	0.77
261	16	1,2	14.50	15.24	0.74
333		11,12	14.52	15.28	0.76
358		16,17	14.51	15.29	0.78
382	17	1,2	14.45	15.27	0.82
				average difference	0.78
				std. dev.	± 0.05
				std. dev. of mean	± 0.013

For average thickness of 142 cm,

$$\text{Sound speed} = \frac{1.42\ (2)}{0.78\times10^{-3}} = 3640 \pm 60 \text{ m/s}$$

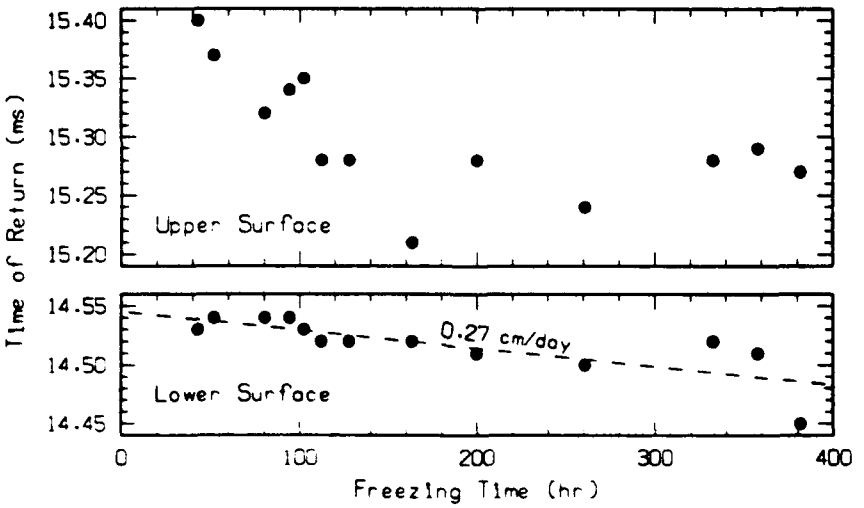

Figure 11. Return times for reflections from the upper and lower surfaces of the ice canopy (37 and 52 kHz data). The difference is the two-way travel time through the ice cover.

To correspond to the extra ice added on the bottom, this decrease should be 0.063 ms, but instead is three times that. We think that the arrival times for the pulses traveling through the ice are not as accurately measured as those of the pulses reflected from the bottom, and that the variation in the returns from the upper face is probably merely timing error.

The thickness of the ice canopy was measured at various times and places in the vicinity of the ice-growth experiment. The thickness was approximately 140 cm at the beginning of the experiment and increased 0.25 cm per day to 144 cm at the end. Based on the average thickness of 142 cm and the average time difference of 0.78 m/s given in Table 4, we calculate an average sound speed of 3640 ± 60 m/s for the 142-cm-thick ice.

Returns from the ice canopy were also recorded during an earlier attempt to monitor ice growth in a smaller-diameter hole. This attempt was aborted after the ice had grown to a thickness of 38 cm, because of reflections from the lower edge of the hole. However, the timing of the returns from the upper and lower surfaces of the ice cover was fairly accurate. These times (Table 5) increased slightly for both the upper and lower surfaces; however, the differences were fairly constant, indicating that the increase was due to a slight downward movement of the transducer. The ice thickness was taken as 139 cm, compared with the 140 cm measured later at the beginning of the measurements at the larger hole. This gives a mean sound speed of 3757 m/s with a standard deviation of 15 m/s for the 14 readings.

G. Change in Absorption with Thickness of Growing Ice

The amplitudes of the returns from the upper and lower faces of the growing ice in the hole were used to calculate the absorption. Near the beginning of the experiment, these amplitudes were difficult to read because of the overlapping of the two returns. The readings are shown in Table 3 for the three lower frequencies (37, 52, and 92 kHz). At the two higher frequencies (150 and 220 kHz), the return from the upper face was too small to read.

Table 5. The times of the returns from the upper and lower surfaces of the ice cover during the preliminary experiment using an 86-cm-diameter hole; platter transducer, 37 kHz only.

Disc	Track	Time (ms)		
		T1, lower	T2, upper	T2-T1
6	7	14.44	15.17	0.73
	13	14.44	15.17	0.73
7	1	14.44	15.17	0.73
	7	14.44	15.17	0.73
	13	14.44	15.17	0.73
8	1	14.45	15.19	0.74
	7	14.45	15.19	0.74
	13	14.46	15.21	0.75
9	1	14.46	15.19	0.73
	8	14.46	15.21	0.75
	15	14.46	15.21	0.75
10	2	14.47	15.22	0.75
	9	14.51	15.25	0.74
11	1	14.51	15.26	0.75
			average difference	0.74
			std. dev.	± 0.01
			std. dev. of mean	± 0.003

For thickness 139 cm,

$$\text{Sound speed} = \frac{1.39\ (2)}{0.74\times10^{-3}} = 3757 \pm 15 \text{ m/s}$$

The returns were corrected for refraction effects as described in Section IV.G. The value of the correction changes with thickness and is tabulated in Table 3.

Because we suspect that the skeletal layer provides most of the absorption, we first calculated the total absorption rather than the absorption per meter. The relationship[2,5] used to calculate the total two-way absorption loss in the ice from the reflections from the lower and upper surfaces is

$$\text{loss} = 20\log\left[\frac{1-R_a^2}{R_a} - R_b\frac{V_1/V_2}{1+tN/R}\right], \qquad (3)$$

where R_a is the amplitude reflection coefficient at the lower surface, R_b is the amplitude reflection coefficient at the upper surface, t is the thickness of the ice, and V_1 and V_2 are the returns received from the lower and upper faces, respectively. The factor $1 + tN/R$ is the refraction correction (see Section IV.G). The average absorption coefficient could then be obtained by dividing by $2t$.

The results are tabulated in Table 6 and plotted in Figure 12. The three points at the far right for 37 kHz are considered unreliable because of the interference from other paths through the ice.

Table 6. One-way absorption loss in growing ice, calculated from measurements using platter transducer.

Freezing Time (h)	t Thickness (cm)	qt			One-Way Absorption Loss, L (dB)		
		37 kHz[a]	52 kHz[b]	92 kHz[c]	37 kHz	52 kHz	92 kHz
0	0	-	-	-	-	-	-
5	3.0	-	-	-	-	-	-
9	5.0	1.21	-	3.01	5.0	-	7.3
19	8.8	2.13	-	5.30	4.9	-	6.3
31	12.2	2.96	-	7.35	4.0	-	10.8
43	14.9	3.61	-	-	4.1	-	-
52	16.8	4.07	-	-	6.3	-	-
71	20.2	4.90	-	-	4.8	-	-
81	21.8	5.28	-	-	5.0	-	-
95	24.0	5.82	-	14.46	4.6	-	11.5
103	25.2	6.11	-	15.19	5.6	-	13.3
113	26.6	6.45	-	16.03	4.3	-	13.7
128	28.5	6.91	-	17.17	4.0	-	15.7
145	30.5	7.39	10.39	-	4.0	7.4	-
164	32.5	-	11.07	-	-	5.9	-
200	35.9	-	12.23	-	-	5.8	-
261	41.0	9.94	13.96	-	7.3	9.1	-
281	42.6	10.33	14.51	-	8.1	10.3	-
333	46.4	11.25	-	-	13.0	-	-
358	48.1	11.66	-	-	17.6	-	-
382	49.9	12.10	-	-	13.8	-	-

[a] $q = 24.24$; [b] $q = 34.06$; [c] $q = 60.26$

The variation in absorption loss with ice thickness indicates there is a constant amount of scattering and absorption caused by the skeletal layer plus an amount that is proportional to thickness. In Section III.H we discuss modifying an absorption model to accommodate these measurements of average absorption in the ice.

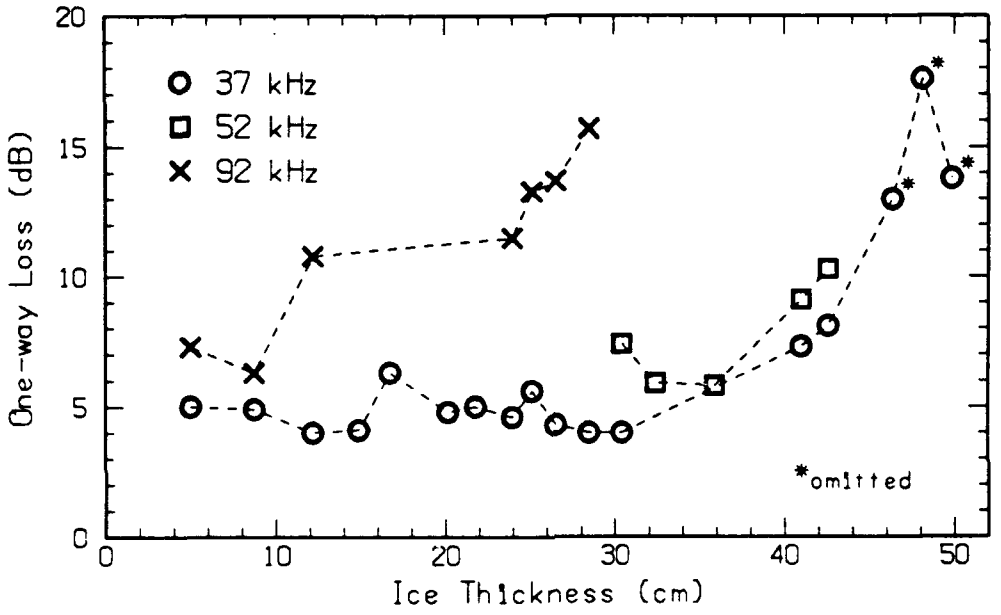

Figure 12. One-way absorption loss in the newly frozen ice, assuming that the amplitude reflection coefficient at the upper surface is unity ($R_b = -1$). The three 37-kHz points at the far right are unreliable and were omitted when calculating absorption.

H. Absorption Coefficient Versus Temperature of Growing Ice

1. Average Absorption

Before we can calculate the average absorption through a given thickness of ice, we must examine the expected variation with temperature to determine how the measured average can be used to determine constants in a temperature-dependent absorption equation.

McCammon and McDaniel[1] have expressed the absorption coefficient in ice as a function of frequency f (kHz) and temperature T (°C) for temperatures between −20 and −2°C:

$$\alpha = kf(-6/T)^{2/3} \quad \text{dB/m} \tag{4}$$

with coefficient $k = 0.06$.

During periods with a stable ambient temperature, the ice has been found to have a constant gradient between the air temperature and the water temperature. For this linear temperature profile, the one-way absorption loss in ice of thickness t is

$$\text{loss} = \int_0^t \alpha \, dy \, . \tag{5}$$

For temperatures varying from T_1 to T_2,

$$\text{loss} = (3)kft6^{2/3} \frac{(T_2^{1/3} - T_1^{1/3})}{T_2 - T_1} \quad \text{dB} \, . \tag{6}$$

Let us assume that the skeletal layer has a loss p (in decibels) due to scattering and absorption. The total apparent one-way absorption loss for an ice canopy of thickness t with temperature varying linearly from T_1 to T_2 can then be expressed

$$\text{total loss} = p + kqt \, , \tag{7}$$

where

$$q = 3f6^{2/3} \frac{(-T_2)^{1/3} - (-T_1)^{1/3}}{T_1 - T_2} \, . \tag{8a}$$

2. *Absorption Measurement*

The total absorption calculated for the growing-ice data was tabulated in Table 3 and plotted in Figure 12. During the experiment, the thickness of the ice in the hole increased to 50 cm. The air temperature at the time was −30°C, and the water temperature was about −2°C. If we ignore a possible change in the temperature gradient across the skeletal layer and take these as the top and bottom temperatures of the ice, we obtain

$$q = 0.655f\,. \tag{8b}$$

From Eq. (7) we see that a plot of the loss versus qt should give a straight line with slope k. The data are plotted in Figure 13 together with a least-squares regression line. This line indicates an absorption of 2.5 dB (one-way) in the skeletal transition zone ($qt = 0$) and has a value of $k = 0.57$ (with a standard deviation of 0.08). This value is nearly 10 times the value of 0.06 found by McCammon and McDaniel for horizontal transmissions.

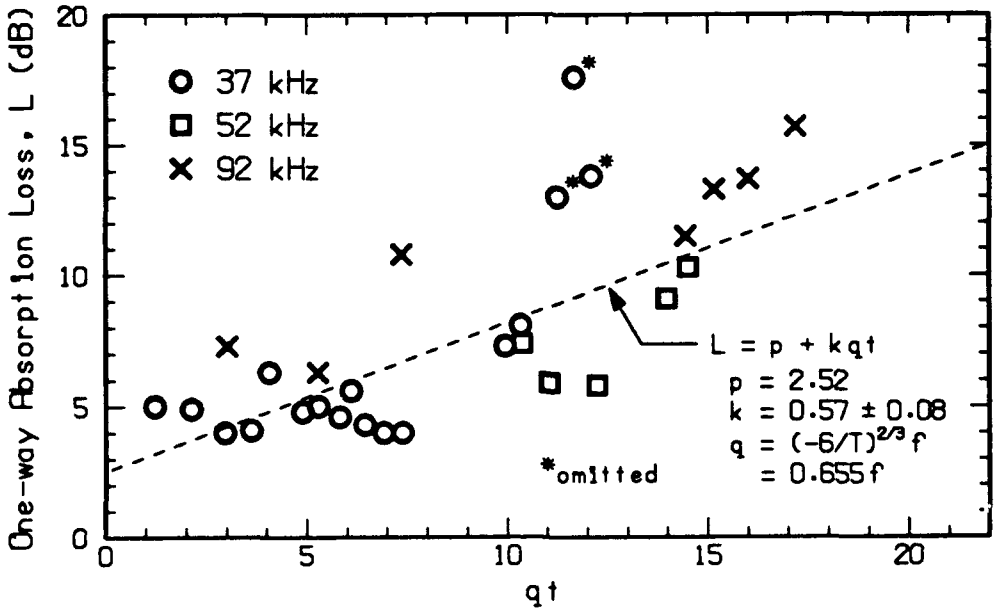

Figure 13. Absorption loss calculated from upper- and lower-surface reflections in growing ice. The three points marked with an asterisk were omitted when calculating absorption.

In calculating Eq. (3), we assumed that all sound not specularly reflected entered the ice. The amplitude reflection coefficient (Figure 5) drops to about 0.05 after 140 hours of freezing, when, according to Figure 2, the thickness was 30 cm. Note from Table 6 that, at least for the first two frequencies, there is a sudden increase in absorption at a thickness of 41 cm (261 hours). This may be due to an increase in scattering at this thickness, which shows up in the calculation of Eq. (7) as an increase in absorption.

IV. REFLECTIONS FROM UNDER-ICE SURFACE

Reflections from the undersurface of the ice canopy were measured at several locations, using three different transducers. Most of the experiments utilized the same configuration used for the ice-block experiment,[2] but some were made with the transducer mounted on a rotating arm suspended beneath the ice. The transducers consisted of an ITC 1042 (a 2.5-cm-diameter sphere with a nearly omnidirectional pattern), the "platter" transducer used for the growing-ice experiments (described in Section III), and the "22×22," a multielement array constructed at APL. In addition to providing data on the reflectivity of the under-ice surface, the returns were used to calculate sound speed and absorption.

A. Experimental Arrangement

1. Measurements with the ITC 1042 Transducer

For these measurements, the transducer was suspended on three polypropylene lines 28 m below the under-ice surface and pointed upward as in the ice-block experiment (see Figure 1). The ice was 1.36 m thick, and the lower surface appeared uniform over the whole area.

The locations of the measurements are shown in Figure 14, which gives the position of the ring on the frame as x's and the corresponding position of the transducer as dots. A typical reflection area is shown at the lower right, based on the return amplitude leveling off at about 1/3 the pulse length. Any return outside the circle would arrive later than this. A considerable overlapping of areas is indicated. The directive patterns of the platter and 22×22 transducers used at the higher frequencies would reduce the area to less than that shown.

Short (0.5 ms) cw pulses were transmitted, and the echoes from the surface were received on the same transducer. A series of five frequencies (20, 30, 40, 60 and 80 kHz) was transmitted at a spacing of 0.1 s.

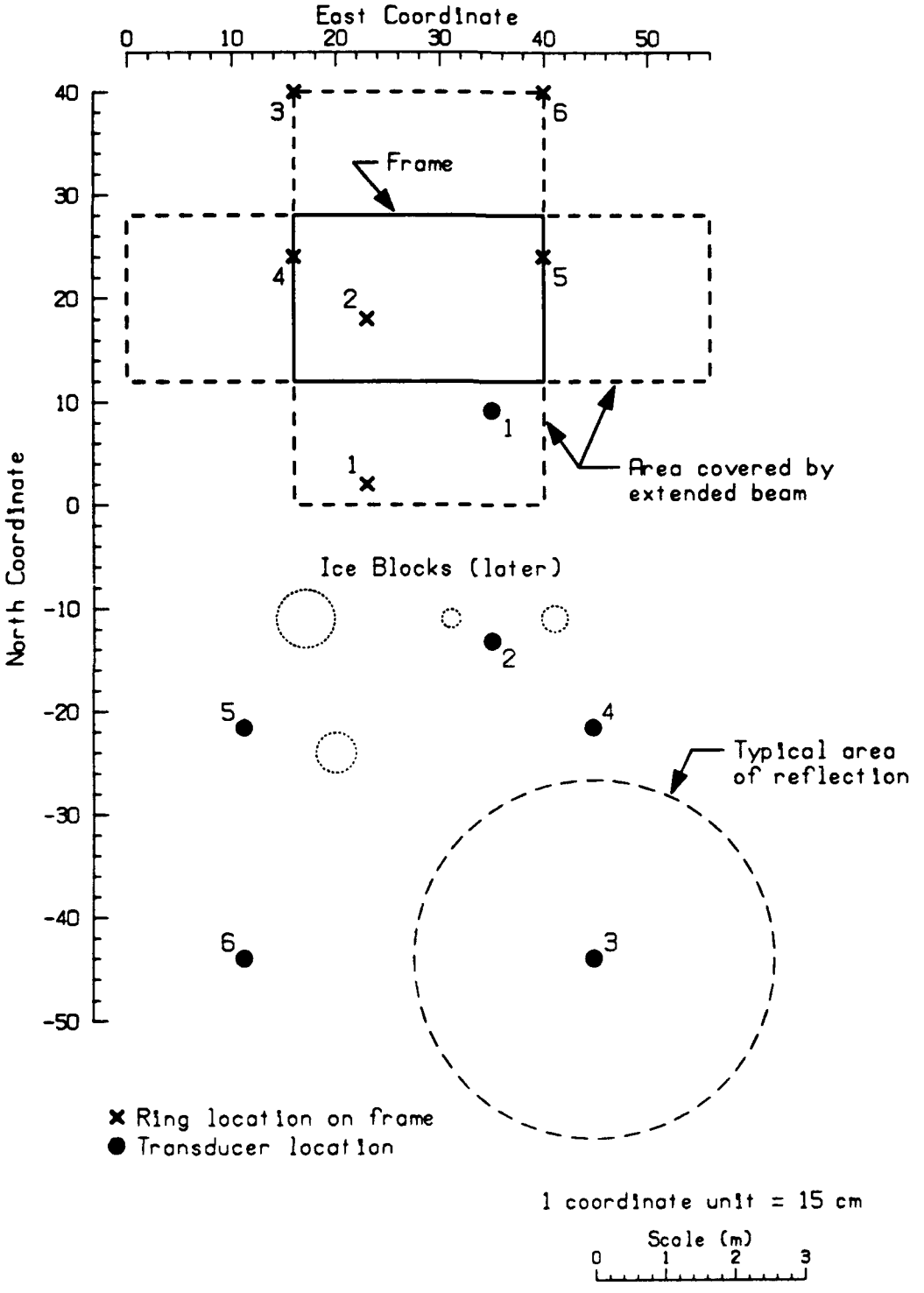

Figure 14. Locations of ITC 1042 transducer used for the surface-reflection measurements.

2. Measurements with Other Transducers

The platter transducer was suspended in the same manner as the sphere. The 22×22 was suspended in the same manner at first, but later some additional measurements were made with the transducer mounted on a rotating arm as shown in Figure 15. Both the platter and the 22×22 transducers were calibrated using reflections from a Freon-filled stainless-steel sphere and from an air–water interface. The latter was more accurate, but the sphere calibration was closer in time to the reflection measurement.

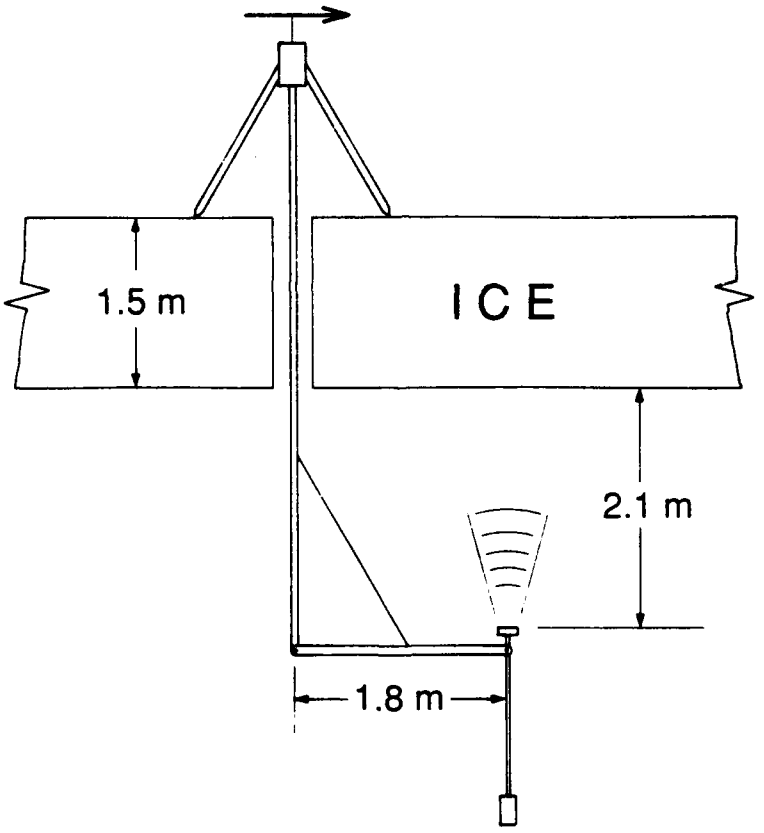

Figure 15. Apparatus for measuring short-range surface reflections with the 22×22 transducer. The arm was rotated in 10° increments to obtain 36 samples of the surface.

3. *Calibration Sphere*

A 20-cm diameter, stainless-steel sphere filled with Freon TF was used as an aid in calibrating the measurements. The sphere was suspended 1–2 m below the ice and near the center of the transducer beam. The return from the sphere came before the return from the ice and was easy to recognize and measure.

The best calibration was obtained during the ice-block experiment[2] using the ITC 1042, when both the sphere and an air–water interface were in the field of view at the same time. The calibration values for the ITC 1042, the target strengths obtained for the sphere during the ice-block experiment, and those obtained during the surface-reflection measurements with the ITC 1042 are shown in the first four columns of Table 7.

Table 7. Target strengths of calibration sphere calculated from several measurements.

Freq. (kHz)	CAL[a] (dB)	SPHERE TARGET STRENGTH (dB)				
		Ice-Block Experiment	Surface[b] Reflection Measurements	At Barge Using Mk 46	At Barge Using 22×22	Selected For Arctic Use
20	–75	–9.0	–9.4	–9.2		–9.2
25				–13.6		
30	–70	–7.1	–9.6	–12.1		–8.0
35				–10.8		
40	–65	–6.0	–8.1	–9.3		–7.5
45				–11.8		
50				–9.0	–9.3	
55				–10.4	–9.5	
60	–50	–8.4	–10.3		–9.4	–8.8
65					–10.0	
70					–9.9	
75					–10.4	
80	–50	–8.1	–11.6		–11.0	–9.8
100					–10.2	–10.2
120					–12.2	–11.0
160					–17.3	–16.0
200					–18.5	–17.5
250					–20.4	
300					–20.9	–20.0

[a] Transmitting response plus receiving sensitivity of ITC 1042 transducer.
[b] See Table 14 in Section IV.D.1.

The target strength of the sphere was also measured at the APL acoustic calibration barge after the field trip. These measurements were made in fresh water at 15°C. Marks and Mikeska[6] have shown that the target strength of a 6-in. fluid-filled sphere at 50–130 kHz is maximum when the index of refraction of the fluid in the sphere relative to that of the surrounding water is 1.77; the strength drops off 2 dB when it increases to 1.8, and drops another 3 dB when it increases to 2.0. At arctic temperatures, the Freon would have an index of refraction of 1.8, whereas at the calibration barge the index would be 2.0. This difference would make the target strength of the sphere 3 dB higher in the Arctic. The measurements at the barge were made with a transducer using Torpedo Mk 46 elements at 20–55 kHz and with the 22×22 transducer at 50–300 kHz. The range was about 2 m. The results are shown in the fifth and sixth columns of Table 7.

All values in the table are plotted for comparison in Figure 16. As expected, the low-frequency calibration measurements at the barge are lower than those in the Arctic.

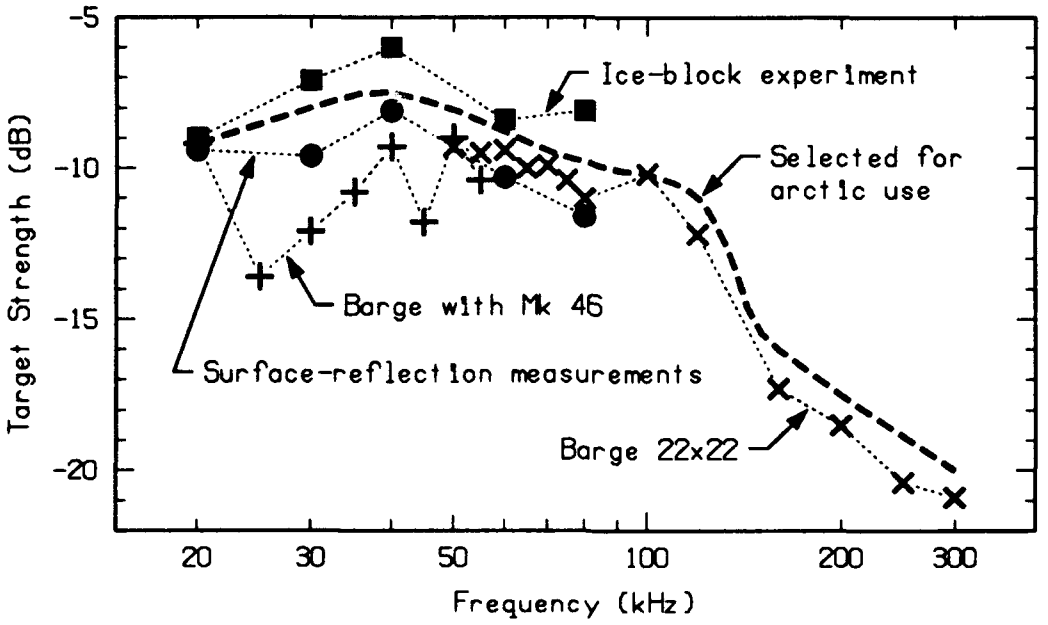

Figure 16. Measured target strength of 20-cm Freon-filled sphere. The measurements at the acoustic barge were at 15°C. At this temperature, the sound is not focused well onto the back face; therefore, the barge data are not accurate for arctic conditions.

(There were no high-frequency arctic calibration measurements.) The best estimate selected for the target strength of the sphere in the Arctic is given in the last column of Table 7. Above 100 kHz, where there are no field calibration measurements, we have estimated a value 1 dB higher than the barge calibration, based on comparisons at 50–80 kHz.

Our results are in good agreement with those of Marks and Mikeska,[6] who measured the reflections from several spheres 15–45 cm in diameter in the laboratory at 70°F. They used a mixture of Freon and carbon tetrachloride to obtain the desired index of refraction, whereas we obtained the same result by operating at a lower temperature.

B. Transducers

1. ITC 1042

The ITC 1042 was a 2.5-cm-diameter sphere with a nearly omnidirectional pattern. It was calibrated during the experiment by measuring the reflections from a level air–water interface. The air–water interface was obtained by installing a flat metal pan with a diameter about the same as that of the ice block, open end down, just below the ice and filling it with air. The target strength at normal incidence for such a circular flat area is given by Urick[7] as

$$TS = 20 \log (\text{area/wavelength}) .$$

The transducer calibration value CAL, which is the sum of the transmitting response and the receiving sensitivity, was chosen as the value that would give this target strength. Results are given in the second column of Table 7 for five frequencies.

During the surface-reflection measurements, a 20-cm-diameter, stainless-steel sphere filled with Freon was suspended in the center of the area so that all returns

included an echo from this sphere. The measured sphere echoes and the transmitted voltages are shown in Section D for each of the six surface-reflection measurements taken in the ice-block area. The average target strengths of the sphere for the six measurements were calculated using the CAL values in Table 7. At 20 kHz, they agreed with the sphere target strengths determined during the ice-block experiment; at the other frequencies, they were about 2 dB lower. This agreement gave confidence that the transducer calibration for the surface-reflection measurements was correct.

2. *Platter Transducer*

The platter transducer was a narrow-beam, multi-element array arranged within a 28-cm-diameter disk. The beam patterns, as measured in October 1988 at the APL acoustic calibration barge, are shown in Figure 17.

The platter was calibrated in the field and again later at the acoustic barge in Seattle. The first field calibration was from the return from the water surface in the 2×2 m hole used for the growing-ice experiment. The measurements and their results are shown in Table 8.

Table 8. Platter calibration using reflections from a free surface in the 2×2 m hole at a range of 11.7 m.

Frequency (kHz)	Nicolet Frame No.	Time (ms)	Tx (V_{pp})	Rec (V_{pp})	CAL[a] (dB)
37	1	16.20	10.08	0.528	-38.1
52	2	16.22	4.82	1.960	-20.2
92	3	16.21	11.60	1.048	-33.1
150	4	16.21	34.80	2.897	-33.6
220	5	16.21	4.50	3.040	-15.1

[a] Transmitting response plus receiving sensitivity of platter transducer.

$$CAL = 20 \log \frac{Rec}{Tx} + 20 \log 2R + 2\alpha R - G$$

where α = absorption coefficient in water
R = range
G = receiver gain = 40 dB

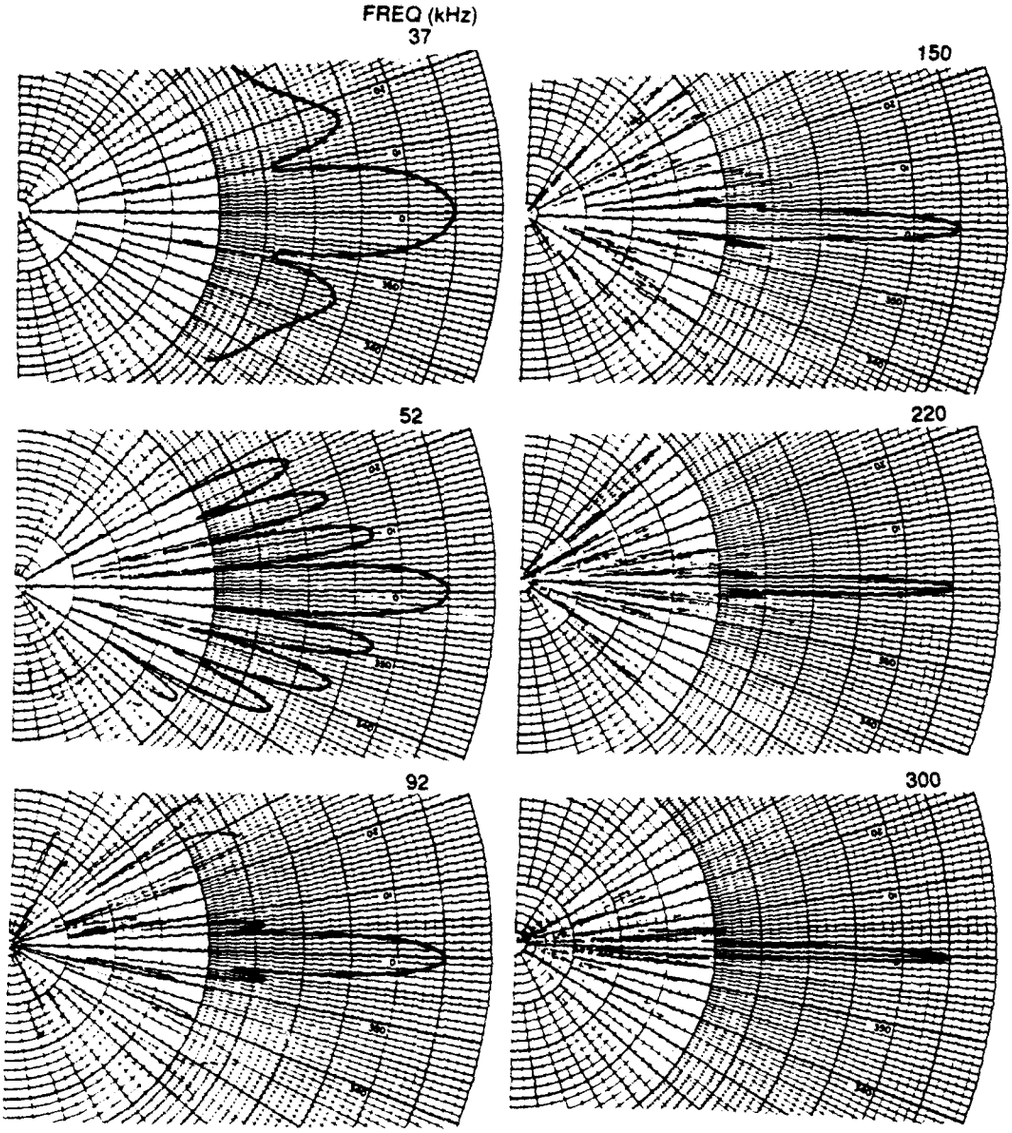

Figure 17. Beam patterns of platter transducer at several frequencies (same for transmit and receive).

The second field calibration was obtained from returns from a 20-cm-diameter sphere at a range of about 10 m. The target strength of the sphere selected for arctic use is shown in Figure 16. The calibration data and results are shown in Table 9.

Table 9. Platter transducer calibration using the sphere at a range of 9.78 m.

Frequency (kHz)	Nicolet Frame No.	Tx (V_{pp})	Rec (V_{pp})	TS[a] of Sphere (dB)	CAL[b] (dB)
15	8	97.6	0.524	-9.3	-36.4
37	9	160.8	1.776	-7.7	-31.6
52	10	23.4	1.704	-8.3	-14.6
92	11	122.4	1.176	-10.0	-30.2
150	12	157.6	1.176	-14.0	-28.0
220	13	179.1	1.760	-18.1	-21.9
300	14	185.6	1.528	-20.0	-21.0

[a] Target strength of sphere from Table 7

[b] $CAL = 20 \log \frac{Rec}{Tx} + 40 \log R + 2\alpha R - TS - G$

The acoustic barge calibrations, performed in November 1988, are compared with the field calibrations in Table 10 and Figure 18. At frequencies up to 150 kHz, the barge and sphere calibrations agree well. We believe that the measurements in the 2×2 m hole were influenced by returns from the sides of the hole. The sphere values were used for calibration instead of the barge values mainly because the sphere returns were from the same ping as the surface-reflection measurements.

Table 10. Summary of platter transducer calibrations.

Frequency (kHz)	CAL (dB)		
	At Barge	Using Free Surface in a 2×2 m Hole	Using[a] Sphere
15			-36.4
37	-30.4	-38.1	-31.6
52	-15.0	-20.2	-14.6
92	-29.8	-33.1	-30.2
150	-27.0	-33.6	-28.0
220	2.8	-15.1	-21.9
300	-33.9		-21.0

[a] These CAL values were selected for arctic use.

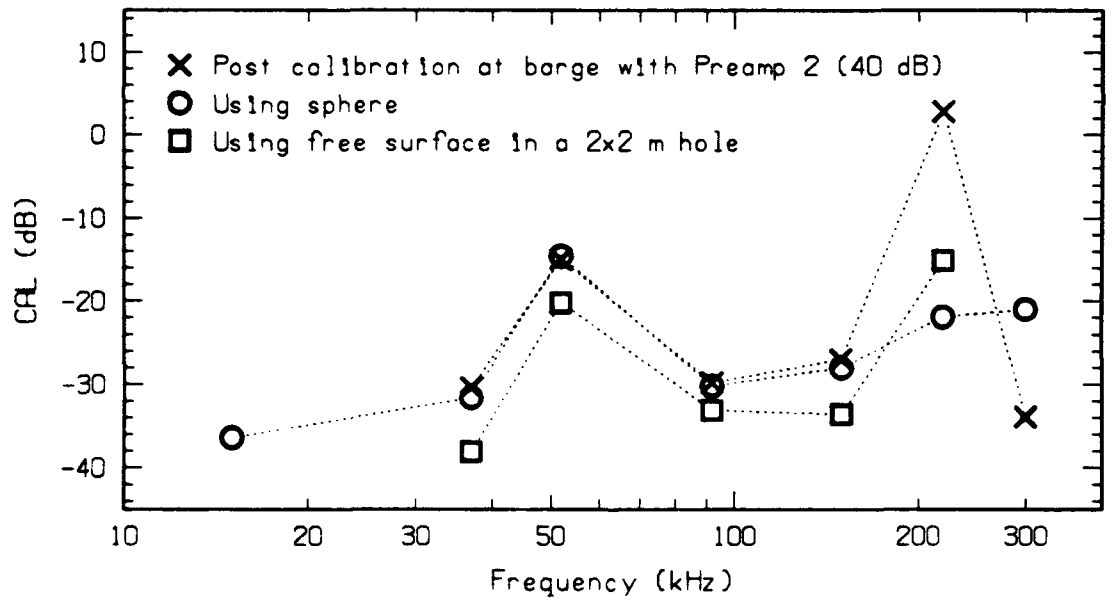

Figure 18. Platter transducer calibrations. The sphere calibration was selected for use in the data analysis.

3. *22×22 Transducer*

This transducer consisted of an array of 22×22 elements built at APL from an 8.26-cm-square ceramic plate. When potted in polyurethane and mounted for use, it had a beamwidth (between −3 dB points, one-way) of 8° at 100 kHz. The one-way beam patterns at 100, 145, 200, and 300 kHz are shown in Figure 19.

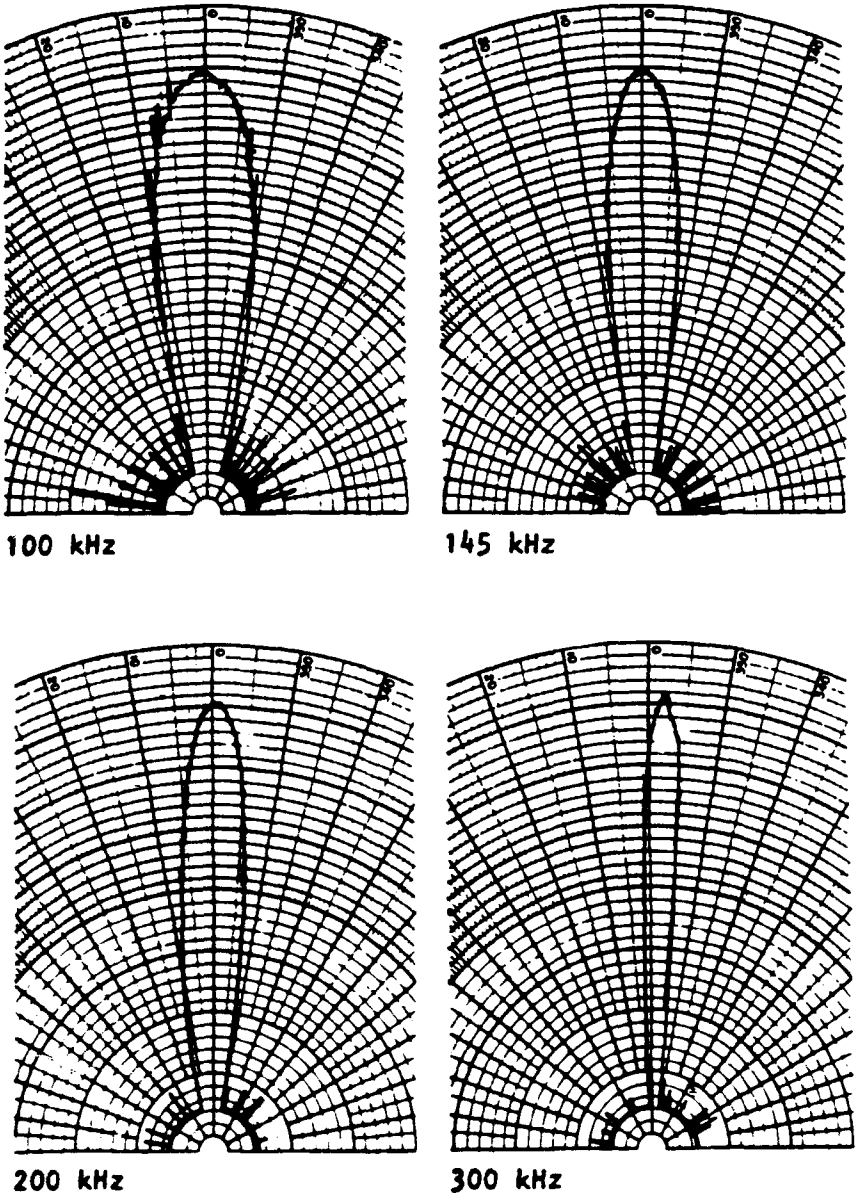

Figure 19. Beam patterns of the 22×22 transducer.

Two calibrations were performed for this transducer in the field. One was done specifically for the short-range measurements from the rotating arm. For this calibration, the apparatus was set up in a large open hole so that reflections could be measured from the free air–water interface. Three trials, each with the transducer at slightly different distances below the water, were run. The results are shown in Table 11.

Table 11. Calibration of 22×22 transducer using reflections from a water–air interface in a 1×13-m hole. The transmit/receive box and cables are included.

Freqency (kHz)	Range (m)	T_x[a] (V_{pp})	Rec. (V_p)	20log2R (dB)	2αR (dB)	Gain (dB)	CAL[b]
Run 7							
60	2.19	66.6	0.205	12.8	0.1	20	–51.3
80	2.19	55.6	0.389	12.8	0.1	20	–44.2
100	2.19	26.6	0.381	12.8	0.1	20	–37.9
120	2.19	10.6	0.277	12.8	0.1	20	–32.7
160	2.19	4.6	0.454	12.8	0.1	20	–21.2
200	2.19	1.1	0.436	12.8	0.2	20	–9.0
Run 8							
60	2.10	66.6	0.218	12.5	0.1	20	–51.1
80	2.10	55.6	0.404	12.5	0.1	20	–44.2
100	2.10	26.6	0.400	12.5	0.1	20	–37.0
120	2.10	10.6	0.291	12.5	0.1	20	–32.6
160	2.10	4.6	0.470	12.5	0.1	20	–21.2
200	2.10	1.1	0.459	12.5	0.2	20	–8.9
Run 9							
60	2.28	66.6	0.202	13.2	0.1	20	–51.0
80	2.28	55.6	0.376	13.2	0.1	20	–44.1
100	2.28	26.6	0.367	13.2	0.1	20	–37.9
120	2.28	10.6	0.267	13.2	0.1	20	–30.7
160	2.28	4.6	0.439	13.2	0.1	20	–21.1
200	2.28	1.1	0.417	13.2	0.2	20	–9.0

[a]Corrected by –1.4 V for TR box
[b]CAL = 20 log (Rec/T_x) + 20 log2R + 2αR – Gain

Average of Three Runs	
Freq.	CAL
60	–51.1
80	–44.2
100	–37.9
120	–30.7
160	–21.1
200	–9.0

The calibration was also checked by measuring reflections from the stainless-steel sphere installed for the ice-block experiment. The transducer was located below the sphere, and returns from the sphere were measured at several frequencies. The transmitted and received voltages and the assumed target strength of the sphere are shown in Table 12. The calculated calibration values (CAL) of the transducer appear in the last column. This method is limited by the accuracy of the assumption used for the target strength of the sphere. Some uncertainty in the sphere calibration is evident in the summary plot in Figure 16.

Table 12. Calibration of 22×22 transducer using reflections from the sphere.

Frequency	Frame	T_x (V_p)	Rec. (mV_p)	$2\alpha R$ (dB)	Sphere[a] TS (dB)	CAL[b] (dB)
30	1	183	54	0.3	–8.0	–67.3
40	2	91	42.5	0.5	–7.5	–63.7
60	3	152	131.5	0.8	–8.8	–57.0
80	4	184	336	0.9	–9.8	–49.4
100	5	46.9	105	1.0	–10.2	–47.2
120	6	31.2	126	1.1	–11.0	–40.8
160	7	27.7	230	1.5	–16.0	–29.1
200	8	28.6	513	2.0	–17.5	–20.4
300	9	28.4	88	3.1	–20.0	–32.1

[a]See Table 7.
[b]$CAL = 20\log(Rec/T_x) + 40\log R + 2\alpha R - Gain$ – Sphere TS, where $R = 23.8$ m, Gain = 60 dB.

The 22×22 transducer was calibrated at the acoustic barge in November 1988 after the field trip. The results are compared with the two field calibrations in Table 13 and Figure 20. The sphere calibration is used for analyzing the surface reflection-measurements in the ice-block area because the cable and preamplifier configuration were the same in both cases.

Table 13. Comparison of calibration values for 22×22 transducer and values selected for use.

Frequency (kHz)	CAL (dB)			
	Water–Air Interface[a] (Table 11)	Barge Nov. 1988	Sphere (Table 12)	Selected for Use in Ice-Block Area
30	--	–62.0	–67.3	–67.8
40	--	--	–63.7	–64.4
60	–51.1	–50.3	–57.0	–57.7
80	–44.2	--	–49.4	–51.1
100	–37.9	–38.5	–47.2	–45.0
120	–30.7	--	–40.8	–39.0
150	--	–21.5	--	–30.5
160	–21.1	--	–29.1	–28.0
200	–9.0	–5.2	–20.4	–20.3
300	--	–15.8	–32.1	–30.5

[a]Used for measurements with the rotating arm.

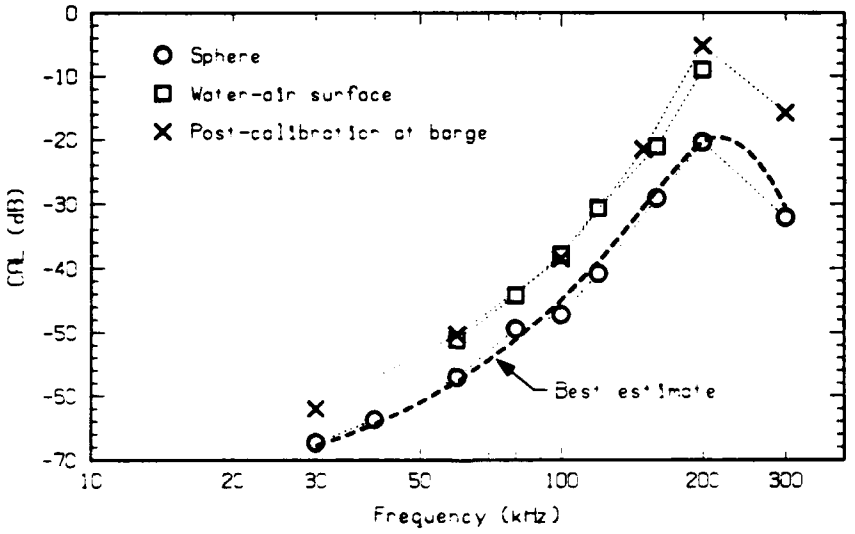

Figure 20. Comparison of calibrations of 22×22 transducer. The sphere calibration was used for the surface-reflection measurements in the ice-block area because the transducer had the same accessories used for those measurements. The water–air interface and barge calibrations were used in analysis of the surface-reflection measurements with the 22×22 transducer mounted on a rotating arm, since these three measurements all used the same accessories.

C. Amplitude Reflection Coefficient

The returns at normal incidence from the undersurface of the ice cover include contributions from both coherent reflections and incoherent scatter. With the understanding that an "effective" amplitude reflection coefficient will include both, we now consider ways to determine this coefficient from the field measurements.

1. Comparison with an Air–Water Interface

The straightforward way is to repeat the measurements, using exactly the same geometry, with a flat water–air interface replacing the undersurface of the ice. The amplitude reflection coefficient is then the ratio between the amplitude of the return from the ice and that from the water–air interface.

2. Mirror Image Calculation

An alternative is to calibrate the transducer accurately and then compare the return with that expected from a mirror surface, i.e., the signal from an image source with a range twice that of the ice. This method may include a small error because of beam-pattern effects. If the surface is slightly rough, some of the sound energy within the beam will be lost because of incoherent scattering from the surface, with no compensating energy being gained by scattering from the surface lying outside the beam. For the measurements reported here, this effect would be small because measurements of the under-ice surface[2] indicated undulations with maximum slopes of 1°, which is exceeded by the transducer pattern except for the extreme case of the platter at 300 kHz. Another indication that scattering had a small effect is the fast rise of the return pulse, as shown in Figure 21.

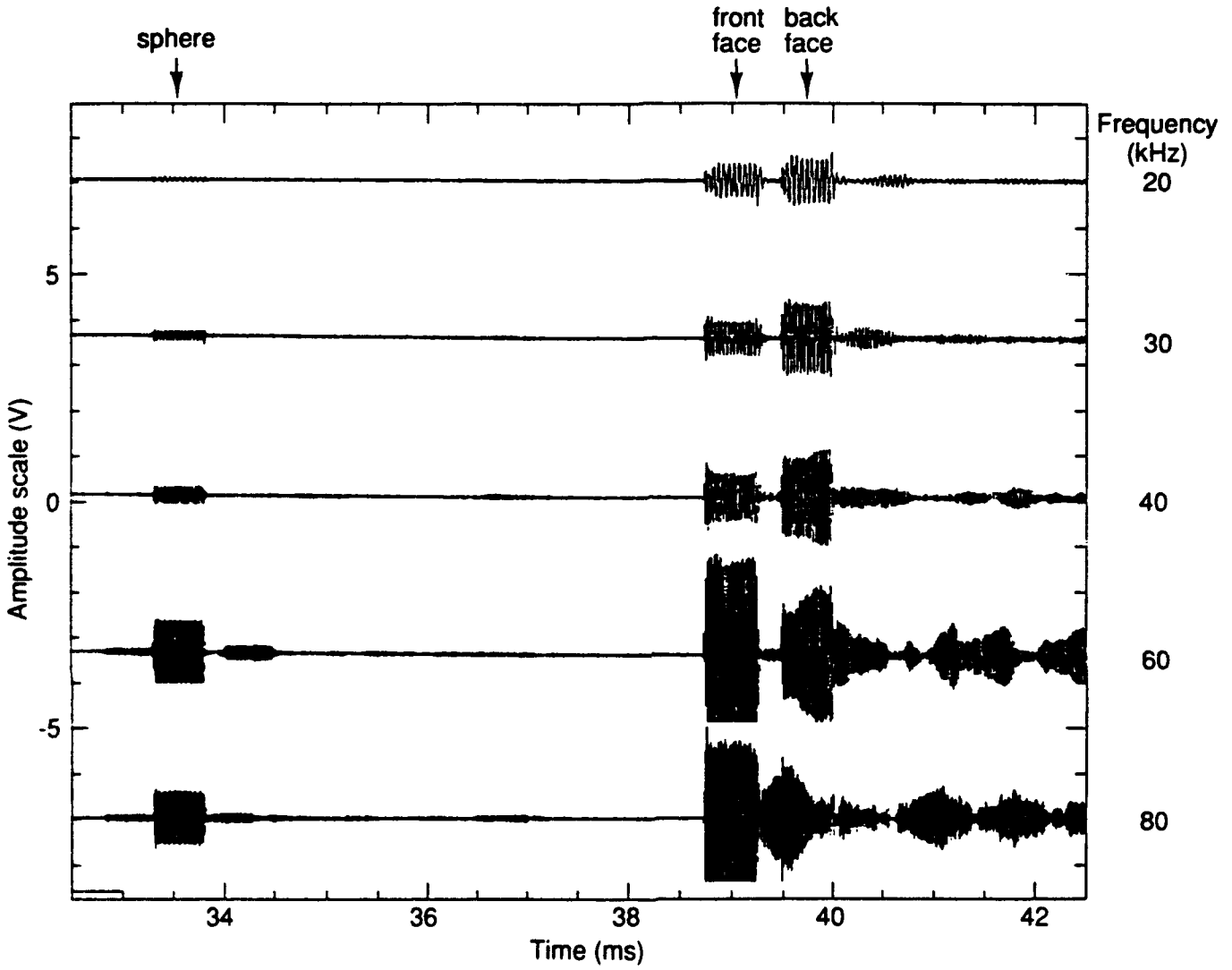

Figure 21. Example of the returns from the calibration sphere and the ice cover at normal incidence.

3. *Calculation of Amplitude Reflection Coefficient*

The nominal steady-state return is for a specular reflection from an infinite, rigid (or fully compliant) surface. For measurements from any other surface, the reflectivity is represented by an amplitude reflection coefficient that is accordingly less than unity. Therefore, if we measure the amplitude of a reflection from the surface, we can calculate the reflection coefficient from the following equation by considering a source at distance $2R$:

$$20\log V_1 = 20\log Vx + \mathrm{CAL} - 20\log 2R - 2\alpha R + 20\log R_a + G\,, \qquad (9)$$

where V_1 is the amplitude of the surface reflection, CAL is the sum of the transmitting response and receiving sensitivity of the transducer, V_x is the amplitude of the voltage applied to the transmitter, R is the range, α is the absorption in seawater, R_a is the amplitude reflection coefficient for the front face, and G is the receiver gain. Transposing, we obtain

$$20\log R_a = 20\log(V_1/V_x) - \mathrm{CAL} + 20\log 2R + 2\alpha R - G\,. \qquad (10)$$

D. Measured Returns

The returns from the ice usually consisted of two cw pulses, one from the lower face and one from the upper. Some examples of the returns measured with the ITC 1042 are shown in Figure 21. The pulse at the left is the return from the sphere. The returns from the upper and lower faces of the ice were usually well separated, but there were extra reflections at the higher frequencies that caused confusion. For these returns, the reflection gain ($20\log R_a$) at the lower surface is given by Eq. (10).

1. *Returns Measured with the ITC 1042 Transducer*

The amplitudes of the ITC 1042 returns from the calibration sphere and those from the two faces of the ice at the six locations shown in Figure 14 are tabulated in Table A1 in Appendix A. The average amplitude-reflection coefficients for the six locations are

shown in Table 14 along with the average target strengths of the calibration sphere for the same pings. These were discussed earlier and plotted in Figure 16.

Table 14. Summary of under-ice amplitude-reflection coefficients for six locations measured using the ITC 1042 transducer. The target strength of the calibration sphere measured for the same pings is given below.

Frame Coordinates	Amplitude Reflection Coefficient				
	20 kHz	30 kHz	40 kHz	60 kHz	80 kHz
N2, E23	0.33	0.15	0.10	0.08	0.05
N18, E23	0.20	0.13	0.14	0.11	0.08
N40, E16	0.20	0.12	0.16	0.14	0.10
N24, E16	0.15	0.11	0.12	0.11	0.10
N24, E40	0.33	0.20	0.18	0.13	0.12
N40, E40	0.25	0.17	0.17	0.17	0.11
Mean	0.24	0.15	0.14	0.12	0.09
Std. Dev.	0.07	0.03	0.03	0.03	0.03
Std. Dev. of Mean	0.03	0.01	0.01	0.01	0.01
	Average Target Strength of Calibration Sphere				
TS (dB)	-9.4	-9.6	-8.1	-10.3	-11.6
Std. Dev. (dB)	4.6	4.0	3.2	3.7	3.5
Std. Dev. of Mean (dB)	1.9	1.6	1.3	1.5	1.4

2. *Returns Measured with the Platter Transducer*

The transmit voltages and received amplitudes for the five locations measured with the platter transducer are shown in Table A2 in Appendix A. The results are summarized in Table 15.

3. *Returns Measured with 22×22 Transducer*

The transmit voltages and received amplitudes for the 10 locations measured with the 22×22 transducer are shown in Table A3 in Appendix A. The results are summarized in Table 16.

Table 15. Summary of under-ice amplitude reflection coefficients measured at five locations using the platter transducer.

Location	Amplitude Reflection Coefficient, R_a						
	Frequency (kHz)						
	15	37	52	92	150	220	300
1a	0.30	0.13	0.08	0.09	0.04	0.02	0.03
1b	0.30	0.16	0.12	0.21	0.06	0.09	0.06
2a	--	0.14	0.08	0.13	0.05	0.04	0.03
2b	0.34	0.15	0.10	0.21	0.05	0.08	0.04
3a	0.33	0.16	0.10	0.18	0.08	0.08	0.06
Mean	0.32	0.15	0.10	0.16	0.06	0.06	0.04
Std. Dev.	0.02	0.01	0.02	0.05	0.02	0.03	0.02
Std. Dev. of Mean	0.01	0.01	0.01	0.02	0.01	0.01	0.01

Table 16. Summary of under-ice amplitude reflection coefficients measured at ten locations using the 22×22 transducer.

Location	Amplitude Reflection Coefficient, R_a								
	Frequency (kHz)								
	30	40	60	80	100	120	160	200	300
N13,E32	0.10	0.07	0.08	0.08	0.11	0.06	0.009	0.013	0.016
N22,E30	0.09	0.07	0.06	0.09	0.08	0.06	0.005	0.011	0.018
N12,E22	0.11	0.08	0.06	0.08	0.08	0.05	0.012	0.006	0.013
N13,E14	0.09	0.08	0.07	0.09	0.12	0.06	0.009	0.006	0.013
N28,E16	0.09	0.06	0.08	0.07	0.09	0.06	0.013	0.006	0.017
N40,E16	0.11	0.08	0.09	0.05	0.10	0.06	0.011	0.008	0.020
N28,E28	0.09	0.08	0.07	0.07	0.09	0.06	0.008	0.012	0.018
N40,E28	0.11	0.07	0.08	0.11	0.11	0.06	0.011	0.005	0.016
N40,E40	0.10	0.09	0.10	0.09	0.13	0.11	0.013	0.009	0.018
N28,E40	0.11	0.10	0.11	0.07	0.13	0.11	0.019	0.013	0.015
Mean	0.100	0.077	0.080	0.081	0.104	0.068	0.011	0.009	0.017
Std. Dev.	0.009	0.011	0.016	0.015	0.019	0.022	0.004	0.003	0.002
Std. Dev. of Mean	0.003	0.003	0.005	0.005	0.006	0.007	0.001	0.001	0.001

4. Returns Measured with the 22×22 on the Rotating Arm

At each of two holes, the 22×22 transducer was mounted on a 1.8-m-long arm and rotated to 36 locations spaced at 10° in azimuth. At 100 kHz the spot size (to the −3 dB points, two-way) was 0.26-m in diameter. The holes were spaced 0.32 m apart; therefore, the reflections were independent above 100 kHz but slightly overlapping at 60 and 80 kHz.

The transducer was calibrated by placing it 2 m below the surface in a 1×13 m hole that had been cut for other experiments. All cables and electronic equipment were the same as for the ice-reflection measurements. In analyzing the data, the ice reflection was simply compared with the reflection from the free surface to obtain the amplitude reflection coefficient.

The results are summarized in Table 17. These data contain 72 nearly independent samples of the return from the under-ice surface. The transducer calibration values were about 3 dB higher than those obtained from the sphere reflection, as shown in Figure 20. Histograms of the reflection coefficients are plotted in Figure 22; these histograms were used to test the effect of roughness.[8]

Table 17. Summary of under-ice amplitude reflection coefficients measured at 72 locations when using the 22×22 transducer on the rotating arm.

	Amplitude Reflection Coefficient, R_a					
Frequency (kHz)	60	80	100	120	160	200
CAL	-51	-44	-37	-33	-21	-9
36 at Hole 1	0.126	0.090	0.035	0.053	0.046	0.040
36 at Hole 2	0.115	0.071	0.041	0.056	0.041	0.040
Mean	0.120	0.081	0.038	0.055	0.044	0.040
Std. Dev.	0.020	0.020	0.014	0.016	0.017	0.017
Std. Dev. of Mean	0.002	0.002	0.002	0.002	0.002	0.002

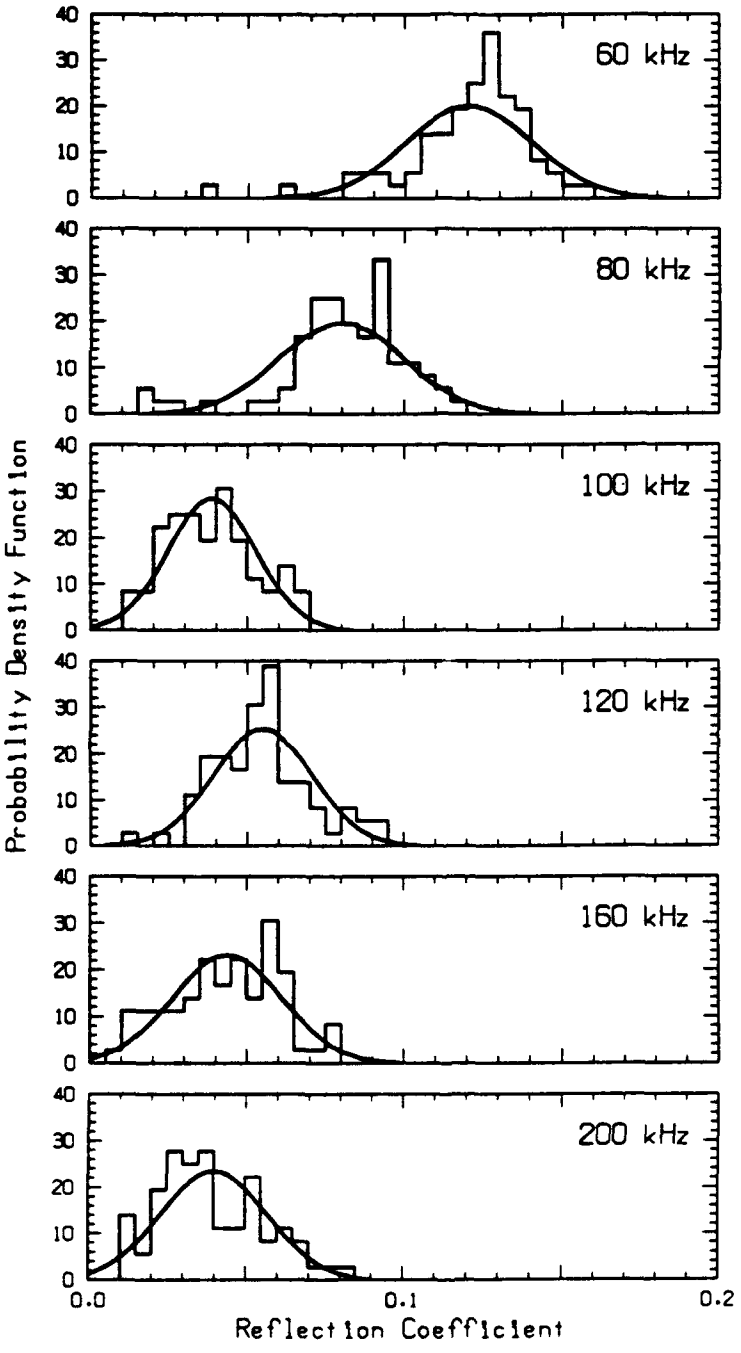

Figure 22. Histograms of reflection coefficients for returns at normal incidence obtained at 72 locations and at several frequencies. The smooth curves are a best fit with a Rice probability function.

E. Reflection Coefficients Compared

The amplitude reflection coefficients tabulated in Tables 14–17 for the lower face are summarized in Table 18 and plotted in Figure 23. The reflection coefficient decreases as the frequency increases.

There is good agreement considering the different methods and geometries used to measure the reflection. The results for the deep 22×22 transducer are low; a review of the measurements and calculations shows no explanation.

Table 18. Summary of amplitude reflection coefficients measured in Spring 1988.

Freq. (kHz)	TRANSDUCER								Ice Block	
	ITC 1042		Platter		22×22		22×22 on arm			
	R_a	σ	R_a	σ	R_a	σ	R_a	σ	R_a	σ
15			0.32	0.01						
20	0.24	0.03							0.20	0.02
30	0.15	0.01			0.100	0.003			0.17	0.02
37			0.15	0.01						
40	0.14	0.01			0.077	0.003			0.19	0.02
52			0.10	0.01						
60	0.12	0.01			0.080	0.005	0.120	0.002	0.13	0.02
80	0.09	0.01			0.081	0.005	0.081	0.002	0.12	0.01
92			0.16	0.02						
100					0.104	0.006	0.038	0.002		
120					0.068	0.007	0.055	0.002		
150			0.06	0.01						
160					0.011	0.001	0.044	0.002		
200					0.009	0.001	0.040	0.002		
220			0.06	0.01						
300			0.04	0.01	0.017	0.001				
Source	*Table 14*		*Table 15*		*Table 16*		*Table 17*		*Fig. 41 in Ref. 2*	

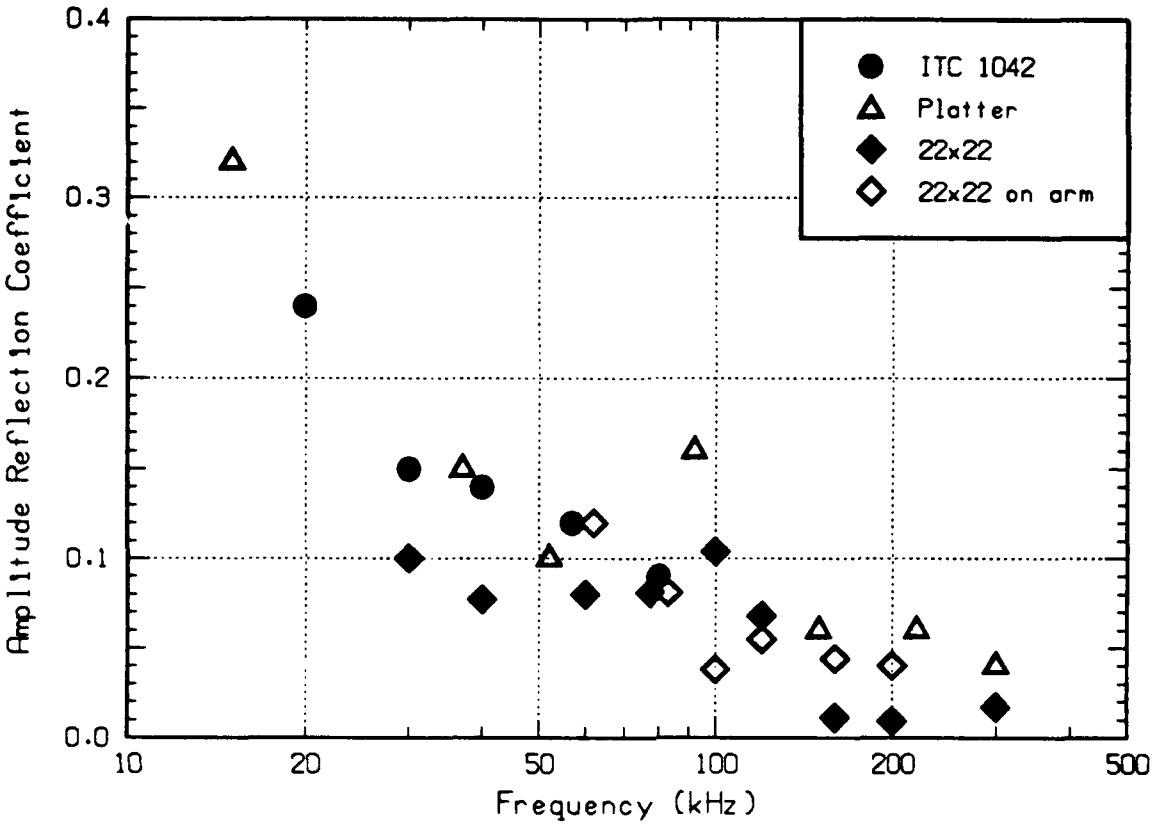

Figure 23. Comparison of all amplitude reflection coefficients calculated for returns at normal incidence from the under-ice surface in Spring 1988.

F. Sound Speed Calculations

The time between the arrival of the reflections from the front and back faces can be used to calculate the average sound speed in the ice. For the six locations ensonified by the ITC 1042 transducer, the average time difference was 0.750 ± 0.005 ms. For two locations ensonified by the platter transducer that gave distinct arrival times, it was 0.726 ± 0.007 ms for all frequencies (37–300 kHz). For seven locations measured with the 22×22 transducer it was 0.750 ± 0.006 ms at all frequencies (30–60 kHz). The ice thickness was measured several times with a boat hook, and averaged 136 ± 1 cm. Thus, the average measured sound speed in the vertical direction for this ice is

$$c = 3642 \pm 70 \text{ m/s} . \tag{11}$$

G. Refraction Correction

As sound enters the ice, it is refracted. At normal incidence, the spreading increases as if the sound had originated from a shorter range. As a result, sound entering the ice will have a greater spreading loss than sound reflected from the lower face. After the sound is reflected from the upper face, it will be somewhat focused as it passes through the lower face back into the water. The net decrease in amplitude suffered by reflections from the upper face as a result of these two effects is derived in Appendix B, and is given by the factor $1/F$.

$$F = (1 + Nt/R) , \tag{12}$$

where N is the ratio of sound speed in ice to that in water, t is the thickness of the ice, and R is the distance from transducer to the bottom of the ice.

The return from the upper face will be lower than that from the bottom face because of the refraction both ways, and its amplitude must be multiplied by F to compensate for the loss.

H. Absorption Calculated from Two Reflections

1. Measurements with the ITC 1042 Transducer

Table 19 shows the absorption values calculated for the reflection measurements with the ITC 1042 at the six locations in the area of the ice-block experiment. The amplitude reflection coefficient for the lower surface (R_a) was computed in Section D and shown in Table 14. The amplitude reflection coefficient for the upper surface, R_b, cannot be determined from these measurements—it must be assumed. In calculating the absorption, we assume there is no loss in amplitude upon reflection at the upper surface (i.e., $R_b = -1$), as if the upper surface were a sharp transition between hard ice and air. With a partially packed snow surface, R_b might be as low in magnitude as R_a at the skeletal surface below, but surely no lower.

Table 19. Absorption calculations for ice reflections measured with the ITC 1042 transducer. The ice was 1.36 m thick.

Location	Ratio of Upper-Face Reflection to Lower-Face Reflection (V_2/V_1)				
	20 kHz	30 kHz	40 kHz	60 kHz	80 kHz
1	1.53	1.67	1.80	0.93	0.70
2	1.47	1.69	0.60	0.69	0.63
3	0.93	1.44	0.69	0.31	0.32
4	1.45	1.20	0.75	0.23	0.31
5	1.26	2.09	1.57	0.56	0.63
6	1.24	1.16	0.96	0.48	0.50
Mean	1.31	1.54	1.06	0.53	0.52
Std. Dev.	0.22	0.35	0.50	0.26	0.17
Std. Dev. of Mean	0.08	0.14	0.20	0.11	0.07
R_a from Table 14	0.24	0.15	0.14	0.12	0.09
One-Way Absorption Loss (dB) for $R_b = -1$	4.3	5.8	7.5	11.5	12.6

2. *Measurements with the Platter Transducer*

Similar calculations were made for the measurements at five locations with the platter transducer using data from Table A2 and the R_a values from Table 15. The results are tabulated in Table 20.

Table 20. Absorption calculations for ice reflections measured with the platter transducer.

Location	Ratio of Upper-Face Reflection to Lower-Face Reflection (V_2/V_1)						
	15 kHz	37 kHz	52 kHz	92 kHz	150 kHz	220 kHz	300 kHz
1a	1.58	0.68	0.28	0.24	0.38	0.42	0.29
1b	--	0.69	0.51	0.22	0.41	0.13	0.21
2a	--	0.67	0.47	0.21	0.36	0.22	0.33
2b	1.19	1.32	0.49	0.16	0.42	0.12	0.29
3a	1.46	0.77	0.62	0.25	0.35	0.15	0.32
Avg.	1.41	0.83	0.47	0.22	0.38	0.21	0.29
σ	0.20	0.28	0.12	0.03	0.03	0.12	0.05
σ mean	0.09	0.13	0.06	0.02	0.01	0.06	0.02
R_a from Table 15	0.32	0.15	0.10	0.16	0.06	0.06	0.04
One-Way Absorption Loss (dB) for $R_b = -1$	2.5	8.7	12.6	13.9	15.9	18.5	18.8

3. *Measurements with the 22×22 Transducer*

The results for the measurements at the 10 locations with the 22×22 transducer, made using data from Tables A3 and 16, are tabulated in Table 21.

Table 21. Absorption calculations for ice reflections measured with the 22×22 transducer.

Location	Ratio of Upper-Face Reflection to Lower-Face Reflection (V_2/V_1)						
	30 kHz	40 kHz	60 kHz	80 kHz	100 kHz	120 kHz	160 kHz
N13,E32	0.69	0.78	0.36	--	--	--	--
N22,E30	1.35	1.02	0.26	0.18	--	--	--
N12,E22	1.19	1.62	0.49	0.26	--	--	--
N13,E14	1.54	1.00	0.44	0.22	--	--	0.78
N28,E16	1.72	1.38	0.74	--	--	--	--
N40,E16	1.15	1.07	0.38	0.34	--	--	--
N28,E28	1.47	1.19	0.49	--	--	--	--
N40,E28	1.13	1.04	0.45	0.109	--	--	--
N40,E40	1.33	1.16	0.49	0.20	--	--	--
N28,E40	1.60	1.24	0.37	--	--	--	--
Mean.	1.32	1.15	0.45	0.22	--	--	0.78
σ	0.30	0.23	0.13	0.08	--	--	--
σ mean	0.09	0.07	0.04	0.03	--	--	--
R_a from Table 16	0.10	0.08	0.08	0.08	--	--	0.01
One-Way Absorption Loss (dB) for $R_b = -1$	8.2	9.8	13.9	17.0	--	--	20.1

4. *Measurements with the 22×22 Transducer on the Rotating Arm*

The absorption calculated for the returns as the arm was rotated to 36 different locations at two holes is listed in Tables 22a and 22b. The absorption was calculated from the

Table 22a. Absorption calculated for data obtained with the 22×22 transducer on the rotating arm; frequency, 60 kHz.

	Hole 1				Hole 2			
Azimuth (deg)	R_a	V_1 (mV)	V_2 (mV)	Absorption[a] (dB)	R_a	V_1 (mV)	V_2 (mV)	Absorption[a] (dB)
0	0.12	209	23	14.4	0.15	252	26	13.5
10	0.12	212	18	15.4	0.14	224	16	15.7
20	0.13	219	15	16.2	0.13	214	21	14.5
30	0.12	217	26	13.9	0.12	193	38	11.9
40	0.10	182	39	12.1	0.14	235	27	13.4
50	0.08	146	15	16.4	0.14	227	20	14.8
60	0.04	63	39	12.2	0.14	227	35	12.3
70	0.06	111	45	11.5	0.13	208	38	11.9
80	0.09	158	39	12.1	0.11	181	14	16.4
90	0.09	140	16	15.7	0.14	231	26	13.6
100	0.08	139	24	14.0	0.14	227	17	15.5
110	0.11	186	14	16.5	0.13	220	12	16.9
120	0.12	206	20	14.9	0.13	218	42	11.5
130	0.12	217	16	16.0	0.13	212	21	14.6
140	0.13	224	20	15.0	0.13	212	23	14.0
150	0.12	213	23	14.4	0.13	211	19	15.0
160	0.14	250	6	20.2	0.16	258	34	12.3
170	0.11	197	7	19.5	0.13	210	18	15.2
180	0.12	204	20	15.0	0.13	221	25	13.7
190	0.13	228	17	15.6	0.11	188	20	14.8
200	0.12	202	7	19.5	0.11	176	28	13.2
210	0.12	207	21	14.9	0.09	148	23	14.0
220	0.12	218	19	15.2	0.14	224	16	15.6
230	0.12	217	23	14.4	0.13	205	25	13.7
240	0.11	198	24	14.2	0.11	181	16	15.7
250	0.13	225	27	13.7	0.12	198	15	16.0
260	0.14	254	26	14.0	0.11	171	12	16.9
270	0.11	197	20	15.0	0.13	207	13	16.6
280	0.09	155	18	15.5	0.11	189	26	13.6
290	0.12	203	33	12.8	0.10	159	26	13.4
300	0.12	202	33	12.7	0.12	202	28	13.2
310	0.13	231	38	12.2	0.13	214	14	16.3
320	0.15	255	40	11.9	0.13	218	36	12.2
330	0.14	238	34	12.7	0.13	206	22	14.3
340	0.15	254	39	12.0	0.13	209	12	16.9
350	0.13	226	23	14.4	0.10	169	37	12.2
Mean	0.11			14.6	0.13			14.3
Std. Dev.	0.02			2.1	0.01			1.6
Std. Dev. of Mean	0.004			0.4	0.002			0.3

[a]One-way loss for an assumed $R_b = -1$.

ratios between the reflections from the upper and lower faces, assuming no loss upon reflection at the upper surface ($R_b = -1$). Table 22a is for 60 kHz and Table 22b for 80 kHz. At higher frequencies, the reflections from the back face were unreadable.

Table 22b. Absorption calculated for data obtained with the 22×22 transducer on the rotating arm; frequency, 80 kHz.

	Hole 1				Hole 2			
Azimuth (deg)	R_a	V_1 (mV)	V_2 (mV)	Absorption[a] (dB)	R_a	V_1 (mV)	V_2 (mV)	Absorption[a] (dB)
0	0.07	404	17	21.0	0.08	464	9	23.7
10	0.08	461	15	21.6	0.09	539	11	22.9
20	0.07	450	14	22.0	0.09	521	7	24.8
30	0.09	542	27	19.1	0.08	484	28	19.0
40	0.07	450	13	22.3	0.10	613	28	18.8
50	0.03	173	29	18.9	0.08	458	11	22.8
60	0.02	127	44	17.1	0.11	674	52	16.1
70	0.02	118	47	16.8	0.10	589	9	23.7
80	0.02	101	23	19.9	0.10	606	19	20.5
90	0.08	512	13	22.3	0.07	390	18	20.7
100	0.11	654	19	20.6	0.08	480	16	21.3
110	0.10	602	7	25.0	0.09	547	15	21.5
120	0.10	591	10	23.4	0.09	559	34	18.0
130	0.09	578	16	21.5	0.09	526	29	18.6
140	0.07	455	11	23.0	0.07	407	29	18.5
150	0.06	385	7	25.0	0.09	536	8	24.3
160	0.07	393	10	23.4	0.11	678	27	19.0
170	0.06	375	9	24.0	0.09	531	13	22.2
180	0.04	229	8	24.3	0.10	571	15	21.5
190	0.08	520	16	21.5	0.10	581	19	20.4
200	0.07	454	7	25.1	0.11	623	18	20.7
210	0.06	344	7	24.9	0.10	562	13	22.2
220	0.08	509	15	21.8	0.08	482	9	23.8
230	0.07	421	17	21.2	0.08	446	26	19.2
240	0.08	479	13	22.5	0.09	510	14	21.8
250	0.07	418	12	22.8	0.07	424	10	23.3
260	0.08	474	9	23.9	0.09	551	10	23.2
270	0.09	550	16	21.4	0.05	298	7	24.7
280	0.07	455	20	20.5	0.09	523	15	21.5
290	0.09	532	10	23.5	0.09	540	13	22.1
300	0.09	524	24	19.7	0.08	459	9	23.8
310	0.07	457	31	18.7	0.08	470	5	26.4
320	0.07	449	28	19.0	0.08	452	15	21.6
330	0.09	533	39	17.6	0.08	494	12	22.5
340	0.07	435	38	17.8	0.12	683	21	20.1
350	0.09	537	12	22.6	0.11	634	10	23.4
Mean	0.07			21.5	0.09			21.6
Std. Dev.	0.02			2.4	0.01			2.3
Std. Dev. of Mean	0.004			0.4	0.002			0.4

[a]One-way loss for an assumed $R_b = -1$.

5. *Summary of Absorption in the Ice Cover*

We now use the equations developed in Section III.H to take into account the variation of absorption with temperature and to allow for extra absorption in the skeletal layer. As in Eq. (7),

$$L = p + kqt \tag{13}$$

for the total one-way absorption loss. The values calculated for L and qt are summarized in Table 23 and plotted in Figure 24. The absorption values for $q > 95$ are low compared with the trend at the lower frequencies. Omitting these data, we computed least-squares values for p and q. The resulting line is plotted in Figure 24 and indicates $p = 0.8$ dB and $k = 0.22$.

Table 23. Summary of absorption measurements in the ice cover (using unity for the reflectivity of the upper face).

Transducer	Frequency	One-Way Absorp. Loss (dB)	q	qt
ITC 1042	20	4.3	13.1	17.8
Table 19	30	5.8	19.7	26.8
t = 1.36 m	40	7.5	26.2	35.6
	60	11.5	39.3	53.4
	80	12.6	52.4	71.3
Platter	15	2.5	9.8	13.3
(Table 20)	37	8.7	24.2	32.9
t = 1.36 m	52	12.6	34.1	46.4
	92	13.9	60.3	82.0
	150	15.9	98.3[a]	134[a]
	220	18.5	144[a]	196[a]
	330	18.8	216[a]	294[a]
22×22	30	8.2	19.7	26.8
(Table 21)	40	9.8	26.2	35.6
t = 1.36 m	60	13.9	39.3	53.4
	80	17.0	52.4	71.3
	160	20.1	105[a]	143[a]
22×22 on	60 (hole 1)	14.6	39.3	59.0
Arm	60 (hole 2)	14.3	39.3	59.0
(Table 22)	80 (hole 1)	21.5	52.4	78.6
t = 1.50 m	80 (hole 2)	21.6	52.4	78.6

[a]Data for $q > 95$ omitted in calculation of best-fit line.

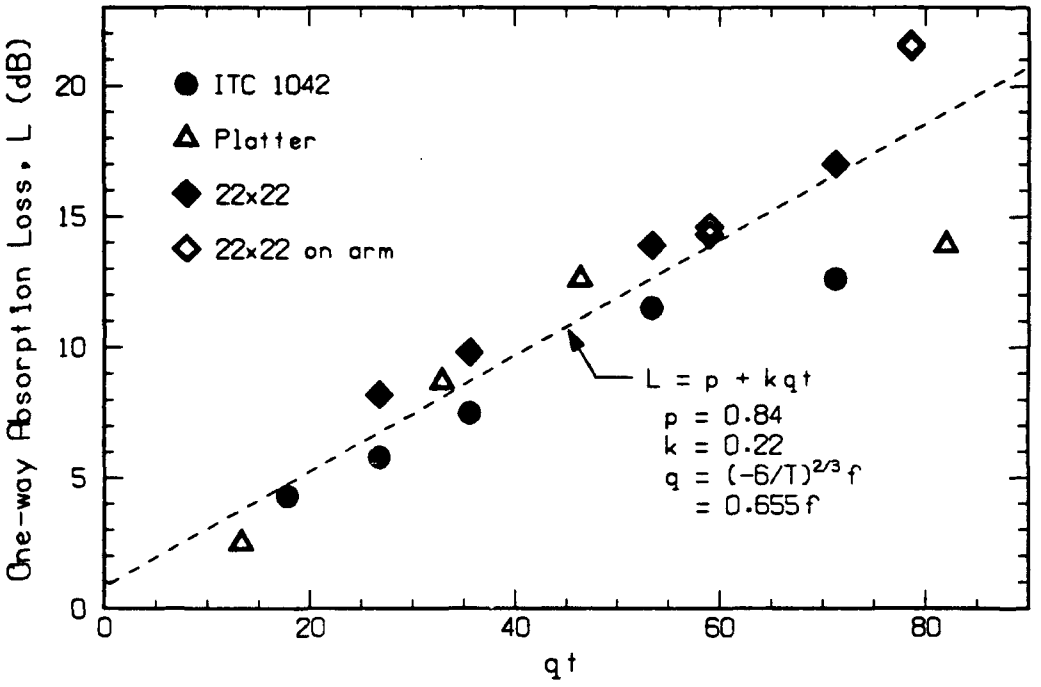

Figure 24. Acoustic absorption determined from reflections off the upper surface of ice cover of thickness t in Spring 1988. The absorption is expressed as an initial loss in the skeletal layer plus an absorption per meter in the form of the McCammon-McDaniel model.[1]

V. PHASE RELATIONSHIPS IN REFLECTIONS FROM SKELETAL LAYER

The phase of the first cycles of the signal reflected at normal incidence from the skeletal layer at the bottom of the ice during the ice-block experiment was examined to determine the acoustic nature of the reflecting medium. A plane wave traveling from one medium to another will be transmitted completely only if the acoustic impedances of the two media are exactly equal. If the impedances are unequal, a reflection will occur at the interface. If the impedance of medium 2 is greater than that of medium 1, the reflection will be in phase with the incident wave. If the impedance of medium 2 is less than that of medium 1, the reflection will be 180° out of phase. In the foregoing, we assume that the reactive component of the impedance is zero.

We were able to compare the reflections from the skeletal layer with reflections from two media with known phase shifts—a water–air interface (~180° phase shift) and a Freon-filled sphere (approx. zero phase shift)—to determine whether the impedance of the skeletal layer was lower or higher than that of the water. Also, we were able to detect additional reflecting layers within the ice by looking for slightly later arrivals which would shift the phase and elongate the pulse. The use of these properties to determine the nature of the skeletal layer is discussed in this section.

A. Review of Ice Reflection Measurements

Before we discuss the echoes measured, we will review the ice-block experiment.[2] Reflections were measured from ice blocks of four diameters: 27, 38, 58, and 84 cm. Reflections from four inverted, air-filled metal pans of about the same diameters (28, 40, 60, and 86 cm) were used to calibrate the transducer.

In addition, various modifications were made to 58-cm blocks. (1) After the standard reflection measurements, the 58-cm block was pulled just out of the water and allowed to drain for half an hour. During that time, the lower portion of the block was surrounded with fiberglass insulation in an attempt to keep it from cooling. The block

was then lowered back into the water, and the reflection measurement repeated. (2) The block was removed from the water, and the top portion was sawed off. The block was then lowered beneath the ice and turned over to release any air trapped in the skeletal layer. After the block was turned back to its original orientation, the reflection was again measured. (3) For comparison, another 58-cm block that had been exposed to −25 to −30°C air for 3 days was cut off at both ends, providing a 62-cm long cylinder of cold, brittle ice. This block was lowered into the water, and its reflection was measured. The variations in target strength for these modifications are shown in Figure 25.

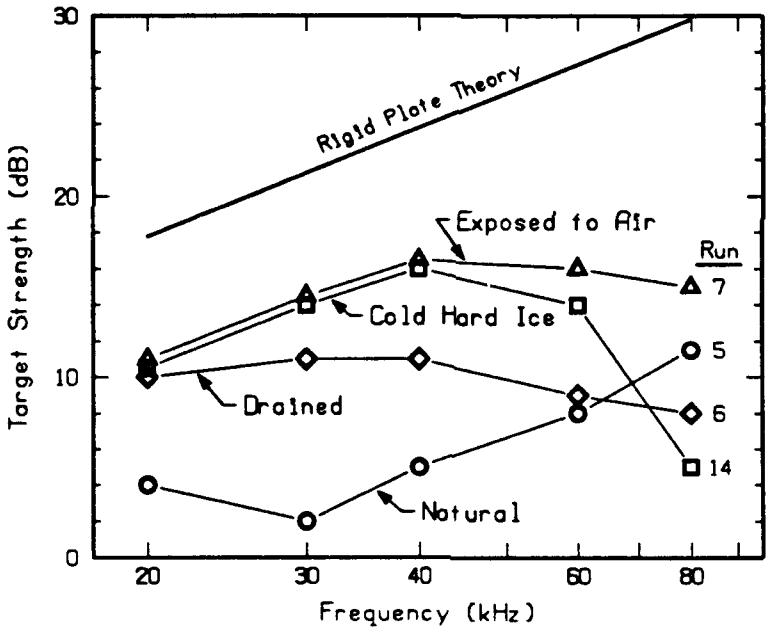

Figure 25. Target strength measurements at normal incidence for 58-cm blocks with several modifications. The target strengths have been normalized to the area of the 84-cm block.

The 84-cm block was remeasured after it had been in the water for 28 hours, showing a large reduction in reflectivity. The variations in target strength with time for both the 58- and 84-cm blocks are shown in Figure 26.

In addition to the ice-block measurements, measurements were made of one-way vertical transmissions through the ice and to depths within the ice (Section VI). Measurements were also made of reflection from the under-ice surface at various locations in the area (Section IV).

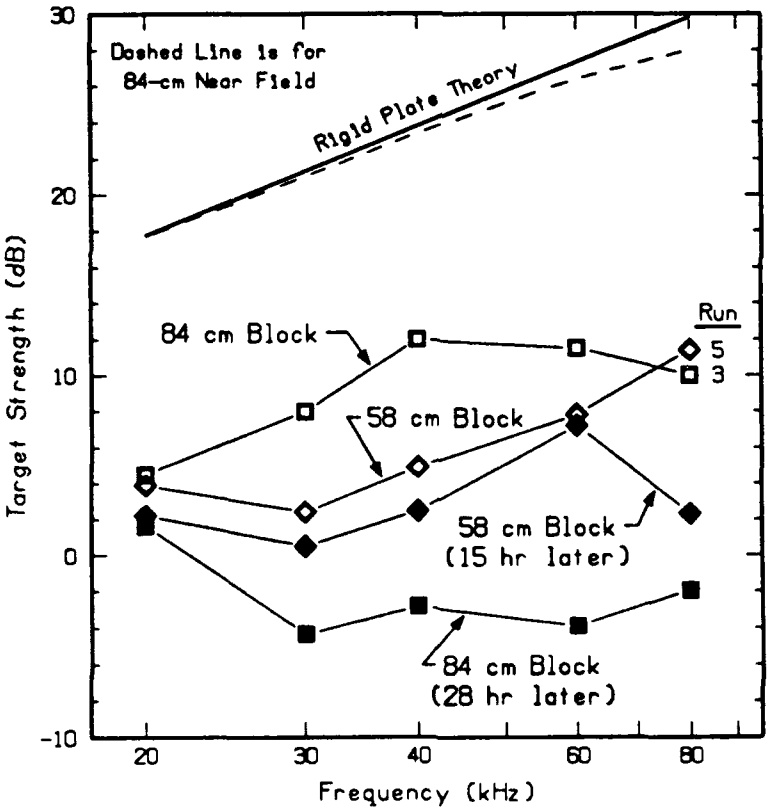

Figure 26. Changes in the returns at normal incidence from the 58- and 84-cm blocks after several hours of submergence. The target strengths have been normalized to the area of the 84-cm block.

B. The Transmitted Pulse

The shape of the pulse can be seen in the reflections from the air-filled pans. Figure 27 shows the return from the ITC 1042 transducer at 20 kHz. (In this and the following figures in this section, pulses longer than 0.2 ms have been split and a central portion removed so that the ends of the pulse can be compared at the same scale.) At the lower frequencies, the pulse begins near the resonant frequency of the transducer (80–100 kHz) and then, after two or three cycles, settles to the driving frequency. At the end of the pulse, the transducer again oscillates a few cycles at its resonant frequency. At the higher frequencies, which are near the transducer resonance, the transition is hardly noticeable. In the composite at the bottom of the figure, times are matched for best fit, and amplitudes are adjusted to match in the steady-state region. The return from the 86-cm block saturated the oscilloscope; thus the peaks are lower than those for the other blocks. The echoes from the 60-cm air-filled pan at all frequencies are shown in Figure 28. Figure 29 is a composite of echoes from all four air-filled pans, amplitude adjusted for best match; the echoes show excellent agreement at all frequencies. The constancy of the waveform for the four pan sizes indicates that this signal represents the in-water signal, with possibly some variation in amplitude as the frequency of the cycles changes.

The asymmetry of the waveform allows us to determine the phase of reflections even if we are unable to determine exactly the starting time of the signal as it rises above the noise. The asymmetry is also helpful in determining the time and amplitude of additional reflections.

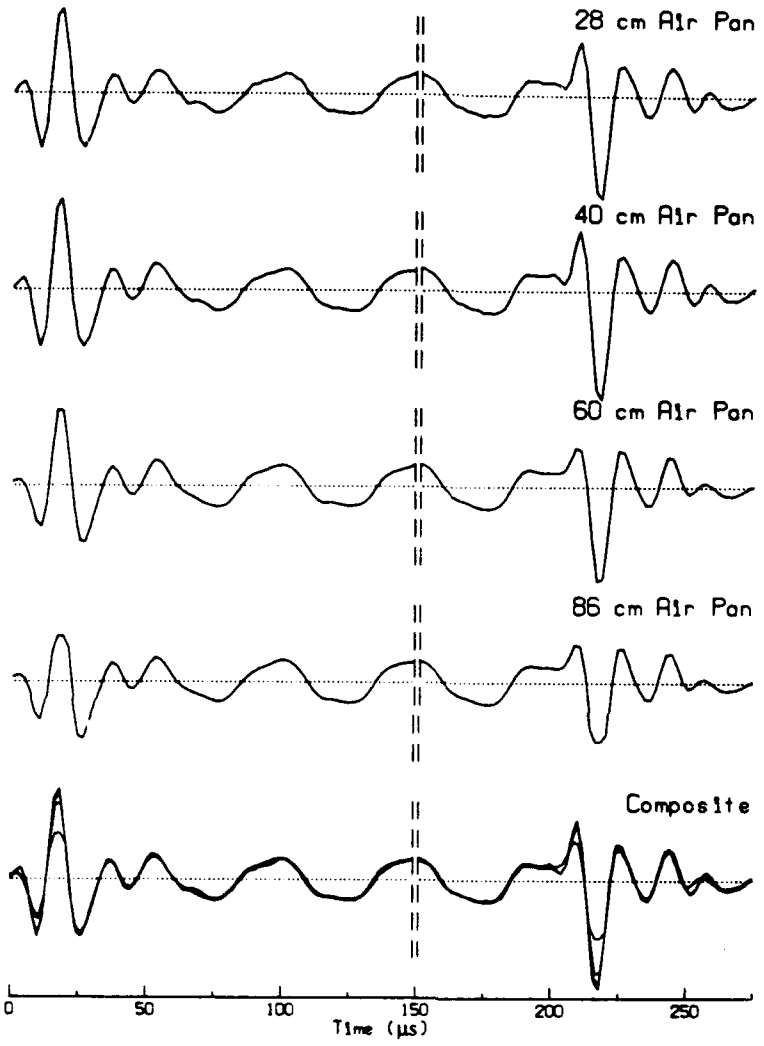

Figure 27. The 20-kHz echoes from air-filled pans of four diameters when using an ITC 1042 transducer. The composite at the bottom shows the consistency in the shape. A portion in the center of the pulse has been removed so that both ends can be presented at a large scale.

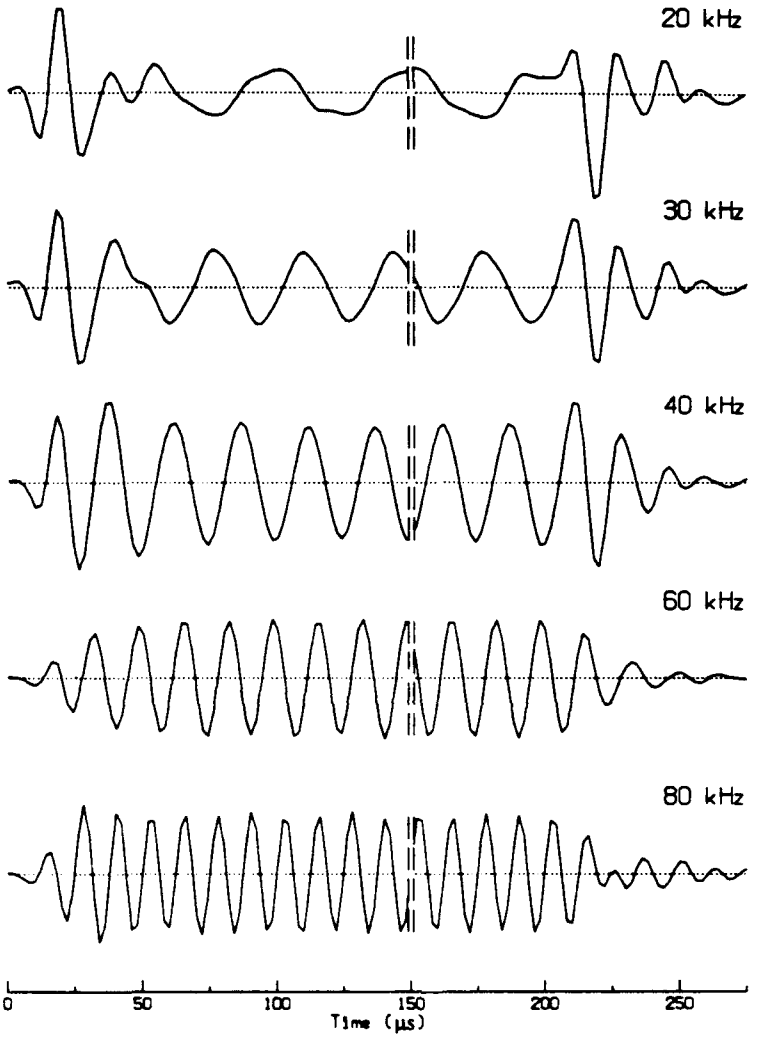

Figure 28. The echoes from the 60-cm air-filled pan at all frequencies.

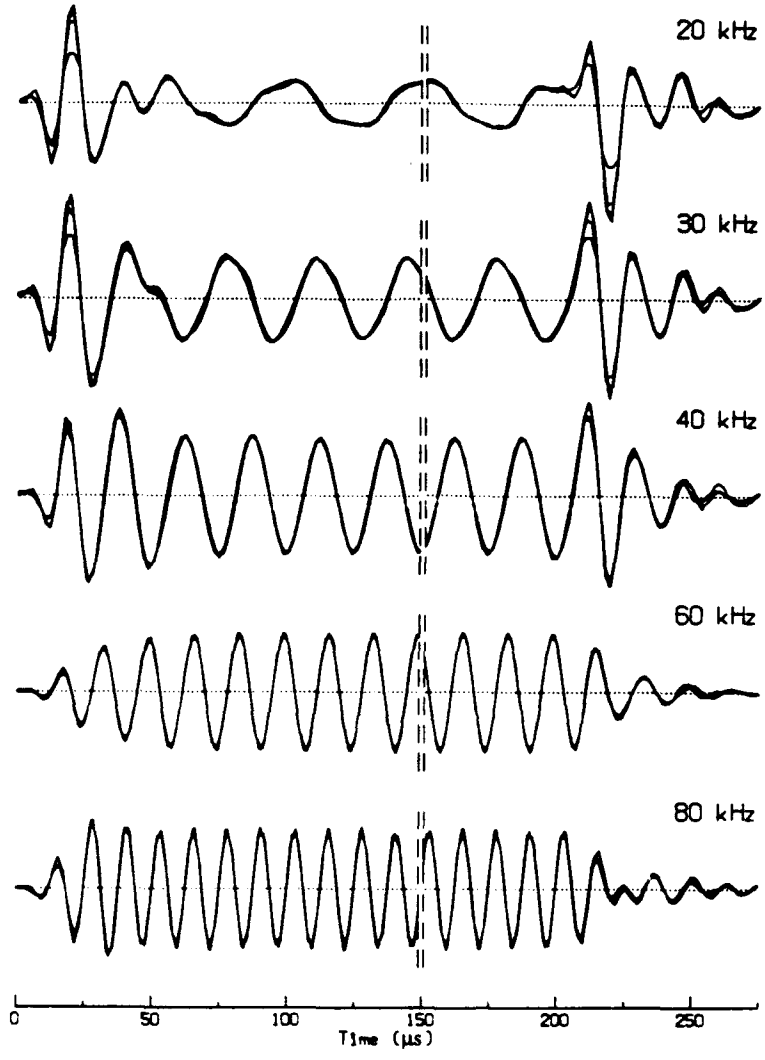

Figure 29. Composites of echoes from four sizes of air-filled pans, aligned for best fit at each frequency.

C. Phase of the Reflections

A calibration sphere was placed so that its echo was present in every ping during the ice-block experiment. To compare the phase of the returns from the air-filled calibrations pans and that of the ice-block reflections, we examined the accompanying sphere echoes for all pings. The sphere echoes accompanying the air-pan returns at 20 kHz are shown in Figure 30. Those accompanying the ice-block echoes at 20 kHz are shown in Figure 31. The transmitted pulse is the same shape, with no polarity inversion, for both measurements.

Some sample waveforms of the various ice-block echoes at the five frequencies are shown in Figures 32–36. To test whether the reflections are essentially in phase with a water–air echo (air-type) or 180° out of phase (ice-type), we compared them with both the echoes recorded from the air-filled pans and inverted versions of those echoes. For each block, we then plotted the comparison with the better correlation.

As expected, the unmodified 58-cm block (Figure 32) gave ice-type reflections. Surprisingly, however, all the modified 58-cm blocks gave air-type echoes at all frequencies, including the cold ice block with the sawed-off surface (Figure 35). For the blocks with a skeletal layer that had been removed from the water and then resubmerged (Figures 33 and 34), we suspect that sufficient air was trapped to cause the phase reversal. For the cold ice block with the sawed-off surface (Figure 35) it is difficult to envision any trapped air. However, the high target strength of this block shown in Figure 25 requires that the reflection be from a plane surface with a large impedance mismatch, and air trapped in the rough saw cut seems the only answer.

The echoes from the smaller ice blocks (27 and 28 cm) had a low signal-to-noise ratio and were not examined in detail. In contrast to the 58-cm block, the echo from the 84-cm block (Figure 36) was more air-type than ice-type, which is also difficult to explain. A complex impedance model, incorporating our ice absorption results (see Section VII.C) may provide more insight into these issues.

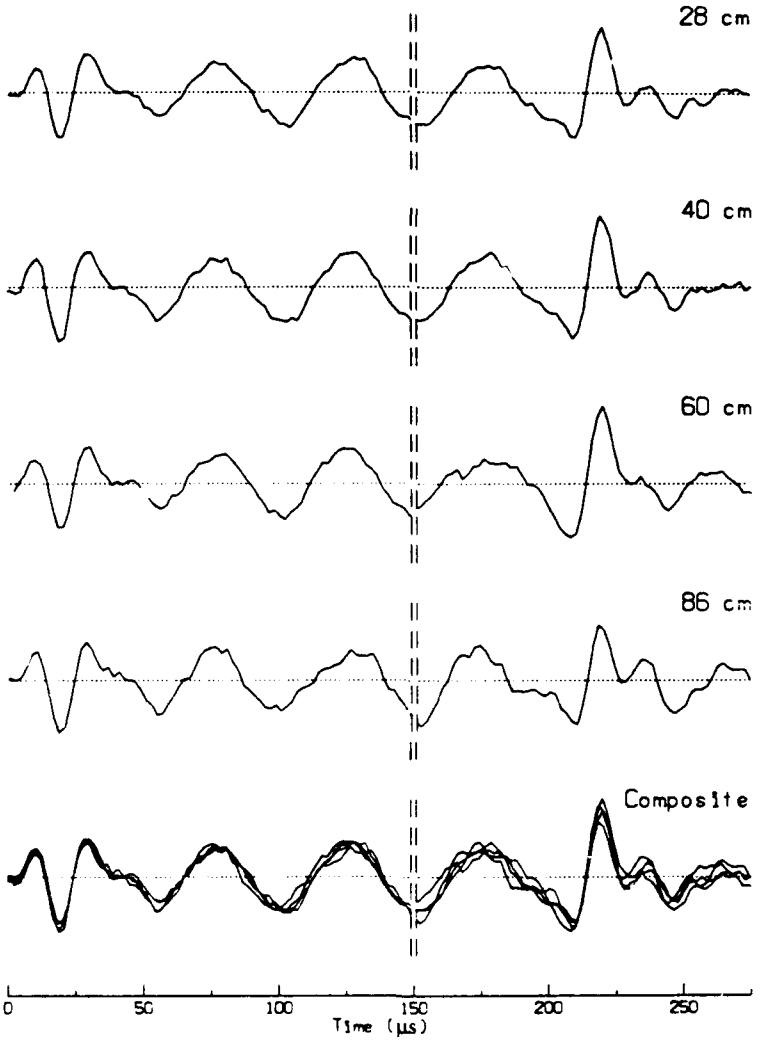

Figure 30. Sphere echoes at 20 kHz that accompanied the echoes from the air-filled pans.

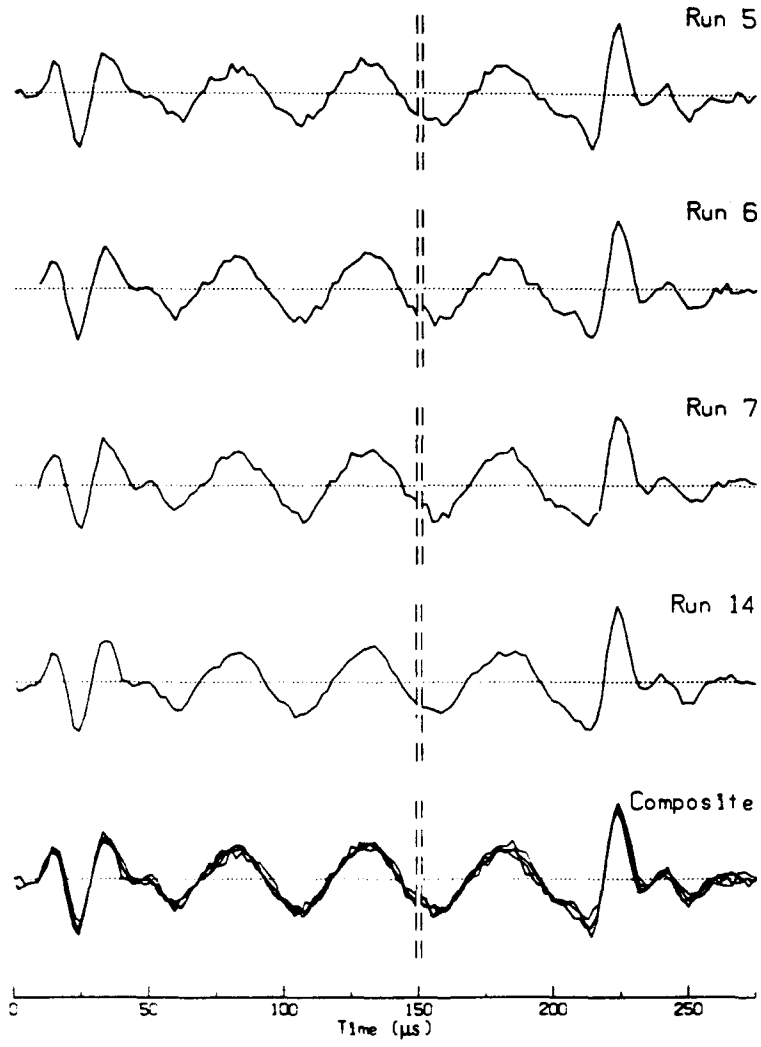

Figure 31. Sphere echoes at 20 kHz that accompanied the echoes from various 58-cm ice blocks.

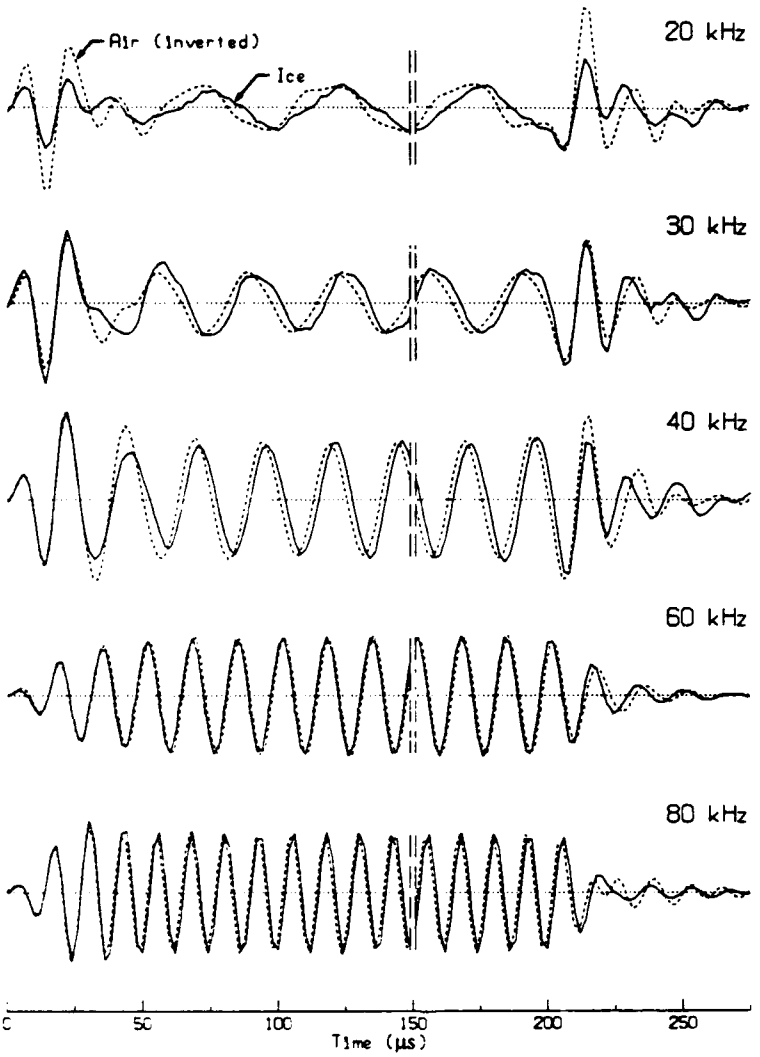

Figure 32. Echoes from the unmodified 58-cm ice block (solid lines) compared with inverted echoes from an air-filled pan (dotted lines). Conclusion: The 58-cm ice block is an ice-type reflector.

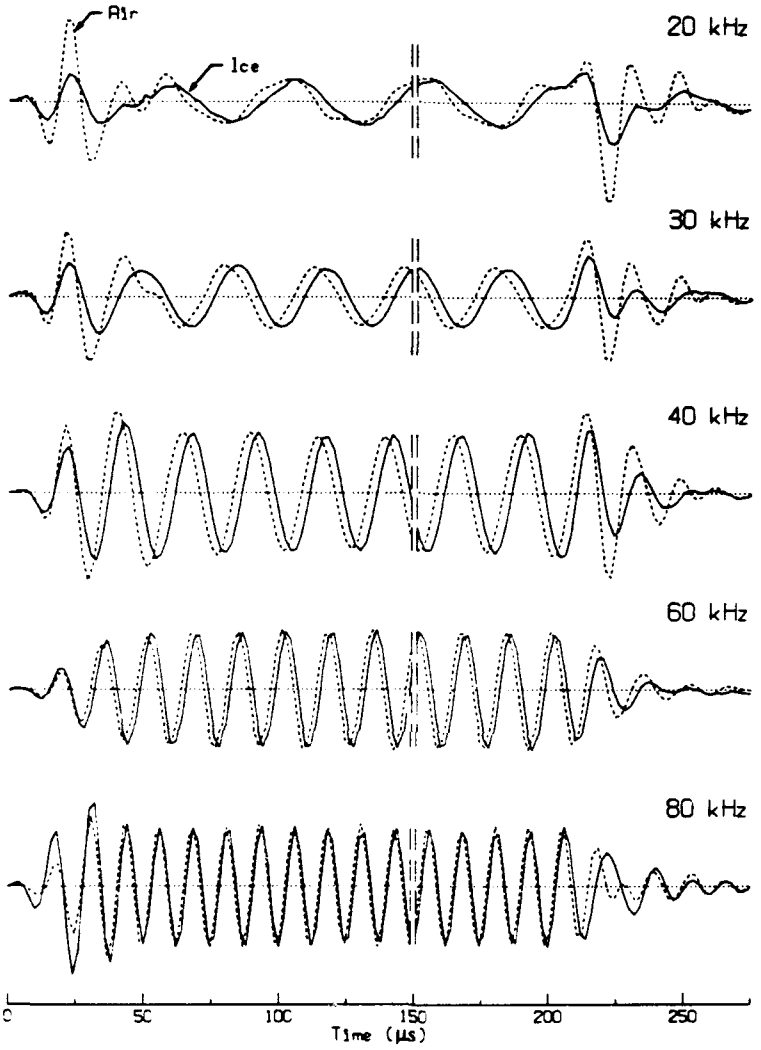

Figure 33. Echoes from the drained 58 cm ice block (solid lines) compared with echoes from the air-filled pan. Conclusion: The drained ice is an air-type reflector.

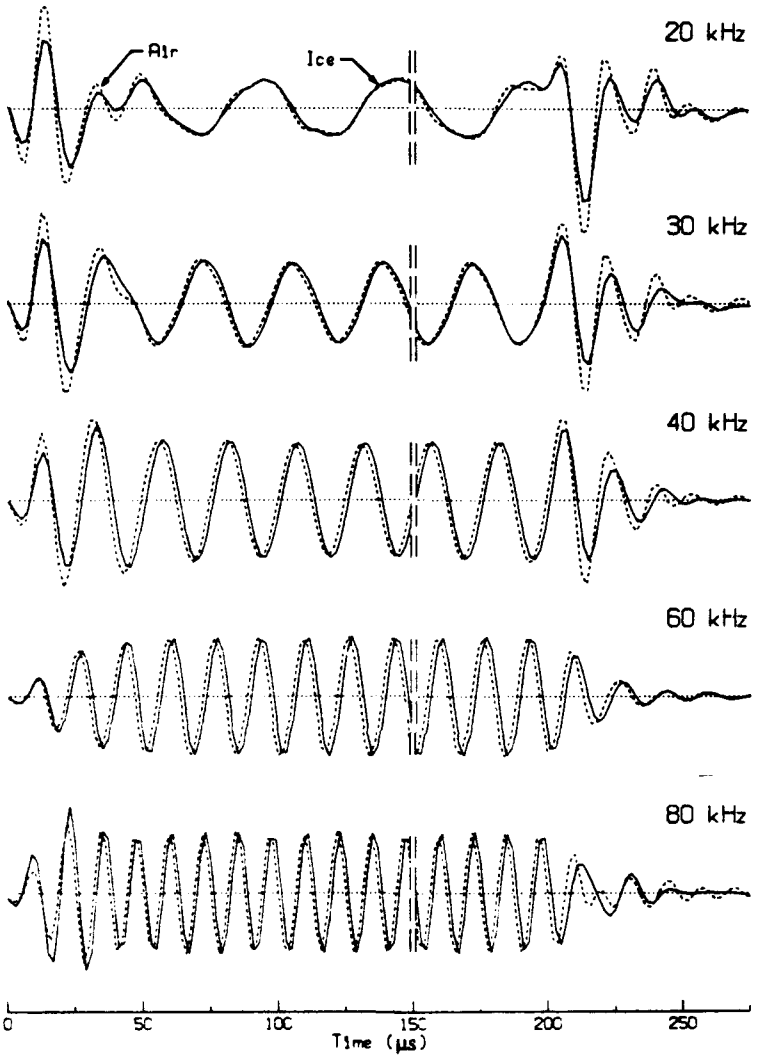

Figure 34. Echoes from the 58-cm ice block that was removed from the water and the top sawed off (solid lines) compared with echoes from the air-filled pan. Conclusion: This ice is an air-type reflector.

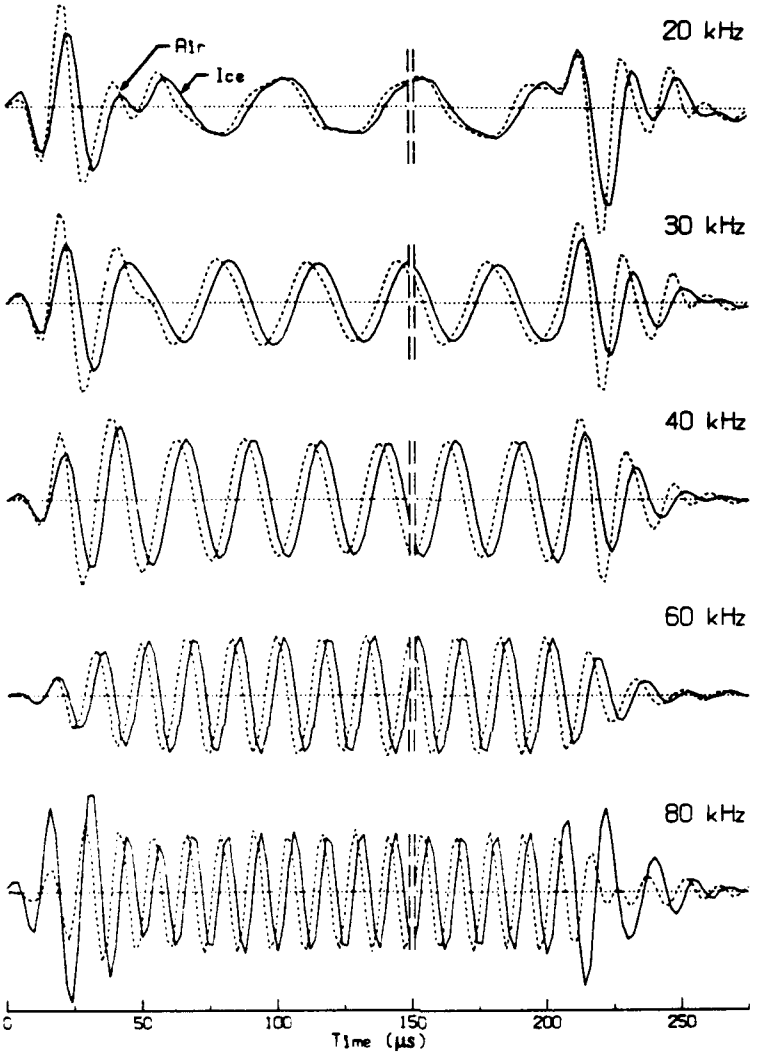

Figure 35. Echoes from the 58-cm cold, hard ice block (solid lines) compared with echoes from an air-filled pan. Conclusion: This hard ice is an air-type reflector.

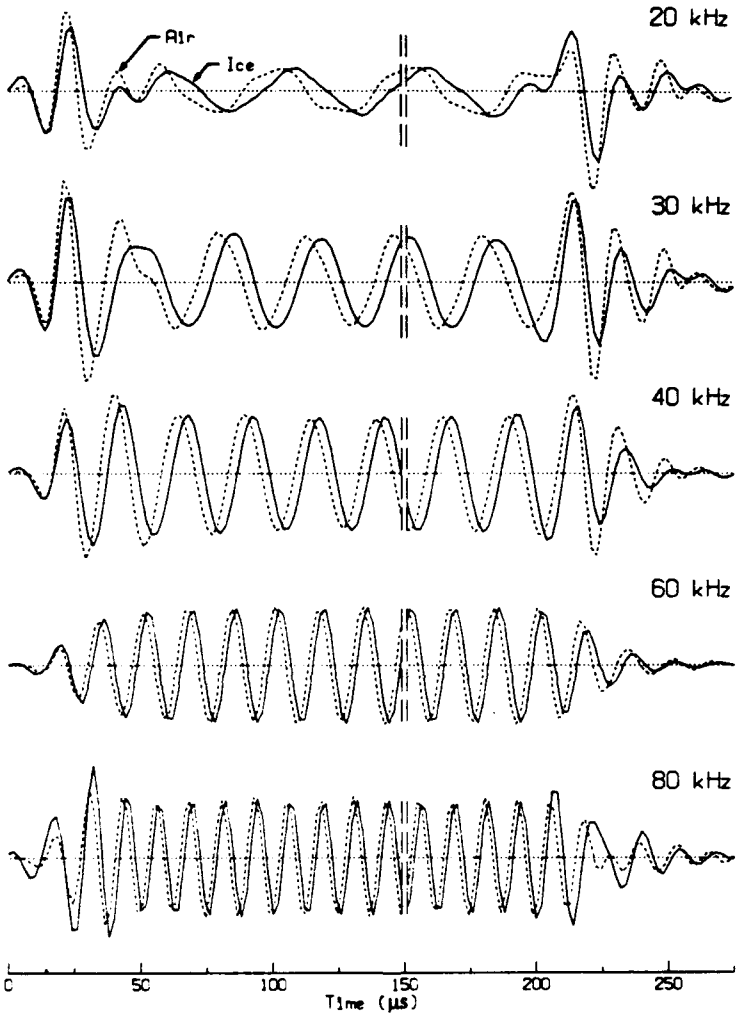

Figure 36. Echoes from the 84-cm ice block (solid lines) compared with echoes from an air-filled pan. Conclusion: The 84-cm ice-block reflection is more air-type than ice-type.

The reflections from the 84-cm ice block were remeasured after it had been underwater for 28 hours (Figure 37). The target strength decreased 3 dB at 20 kHz and progressively more as the frequency increased, reaching a decrease of 12 dB at the higher frequencies (Figure 26). (In the echoes shown in Figure 37, the amplitudes have been adjusted to about the same size for plotting.) At the lower frequencies, the higher-frequency first cycle has decreased considerably more than the following cycles, consistent with the observation that higher frequencies are reduced more. A change in the

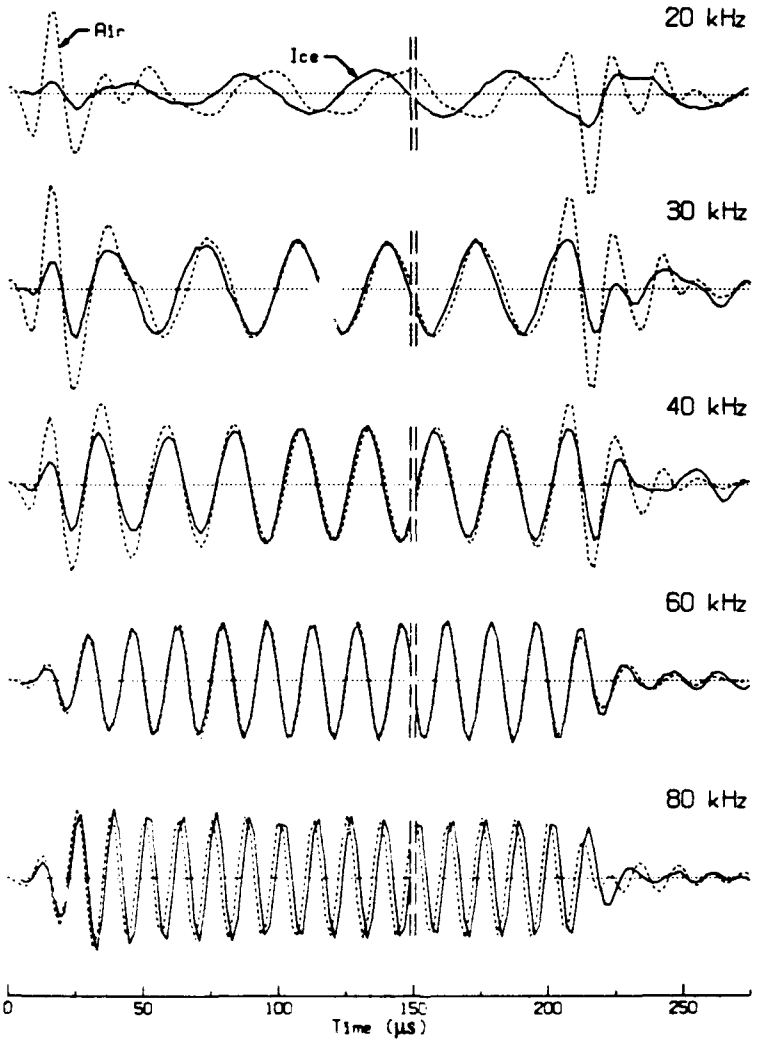

Figure 37. Echoes from the 84-cm ice block after a one-day submergence compared with echoes from an air-filled pan. Conclusion: This ice block is an air-type reflector.

surface as the block warmed in the water is not surprising, considering the delicate balance between brine drainage and pore closure; however, we cannot explain just how this causes the reflectivity to change.

The reflection from the underside of the ice canopy, using the ITC 1042 with its very broad pattern, is compared with the echo from the sphere and the inverted echo from the air-filled pan in Figure 38. For the first cycle, the ice-canopy and sphere echoes are similar. Also, the agreement with the inverted air echo is good except for the first

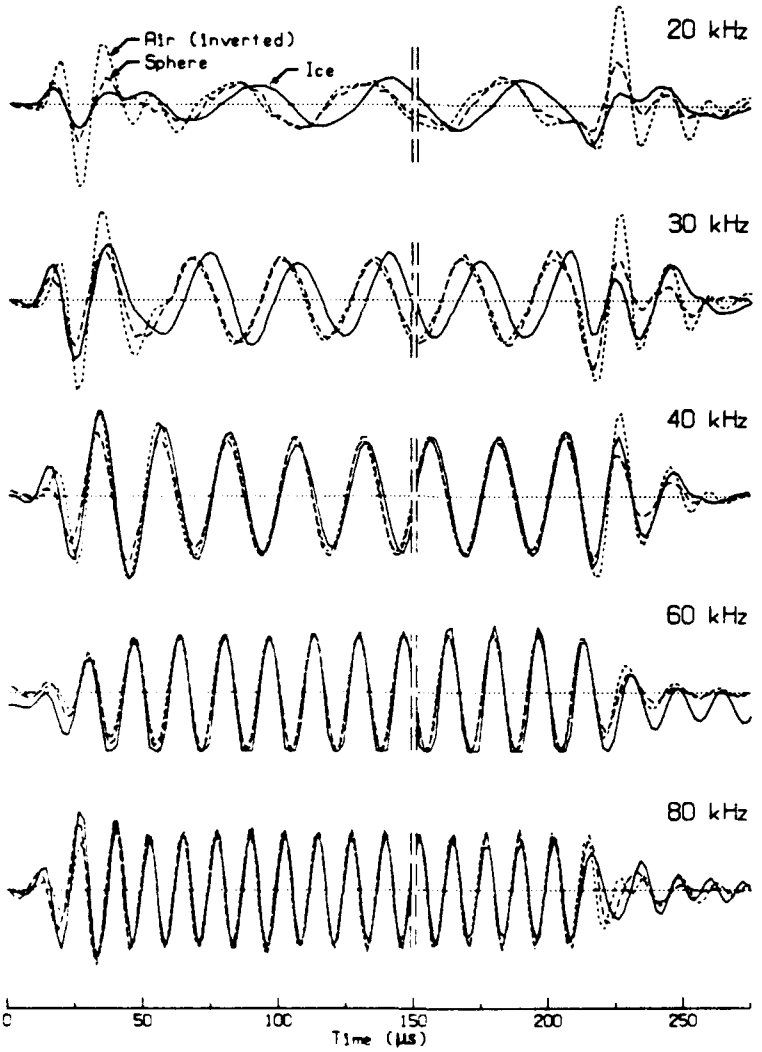

Figure 38. Reflection from the underside of the ice canopy (solid lines) compared with echoes from the Freon-filled sphere (dashed lines) and the inverted return from the air-filled pan (dotted lines). Conclusion: The canopy reflection is more ice-type than air-type.

cycle, which is at a higher frequency and thus theoretically would have a higher return. Beyond the first cycle or two, the canopy returns lag the other returns by about 75°. The lag may result because the canopy return involves larger incident angles, which have later arrival times.

D. Additional Reflecting Layers

The phases of the skeletal-layer reflections shown in Figures 32 and 33 appear to shift with respect to those of the air return after the first cycle or two. We suspected this was caused by an additional reflecting layer. To test this hypothesis, a computer simulation was made by taking the appropriate air-pan reflection and adding to it a replica with delay g (in microseconds) and amplitude ratio f. The simulation results for various values of f and g were then compared with the 58-cm ice-block reflection, and the best fit selected.

The waveforms for the 58-cm ice block and the 60-cm air pan are shown in Figure 39. First the ice echo (solid line) is compared with the air echo (dashed line) and then with the simulated echo, which is an air echo plus a delayed replica at lower amplitude. In all these comparisons, the relative amplitude has been arbitrarily adjusted to give the best match for the whole pulse. At the higher frequencies, the presence of a delayed echo is not so evident because the anomalous first cycle is not present and the delay is approximately the period of one cycle. In general, the simulated echoes are close fits to the ice echoes, verifying that the two-layer model is adequate.

To quantify the analysis, we computed the cross-correlation coefficient

$$r = \frac{\frac{1}{N}\sum xy - \bar{x}\,\bar{y}}{\sigma_x \sigma_y} . \qquad (14)$$

The sensitivity of the comparison to f and g was determined by computing the correlation coefficient for many values of f and g. For 20 kHz, the correlation between the ice echo and the inverted echo from the air-filled pan was 0.82 at $f = g = 0$, and peaked at 0.98 at $f = 0.6$ and $g = 11$. The correlation values for all frequencies are shown in Figure 40;

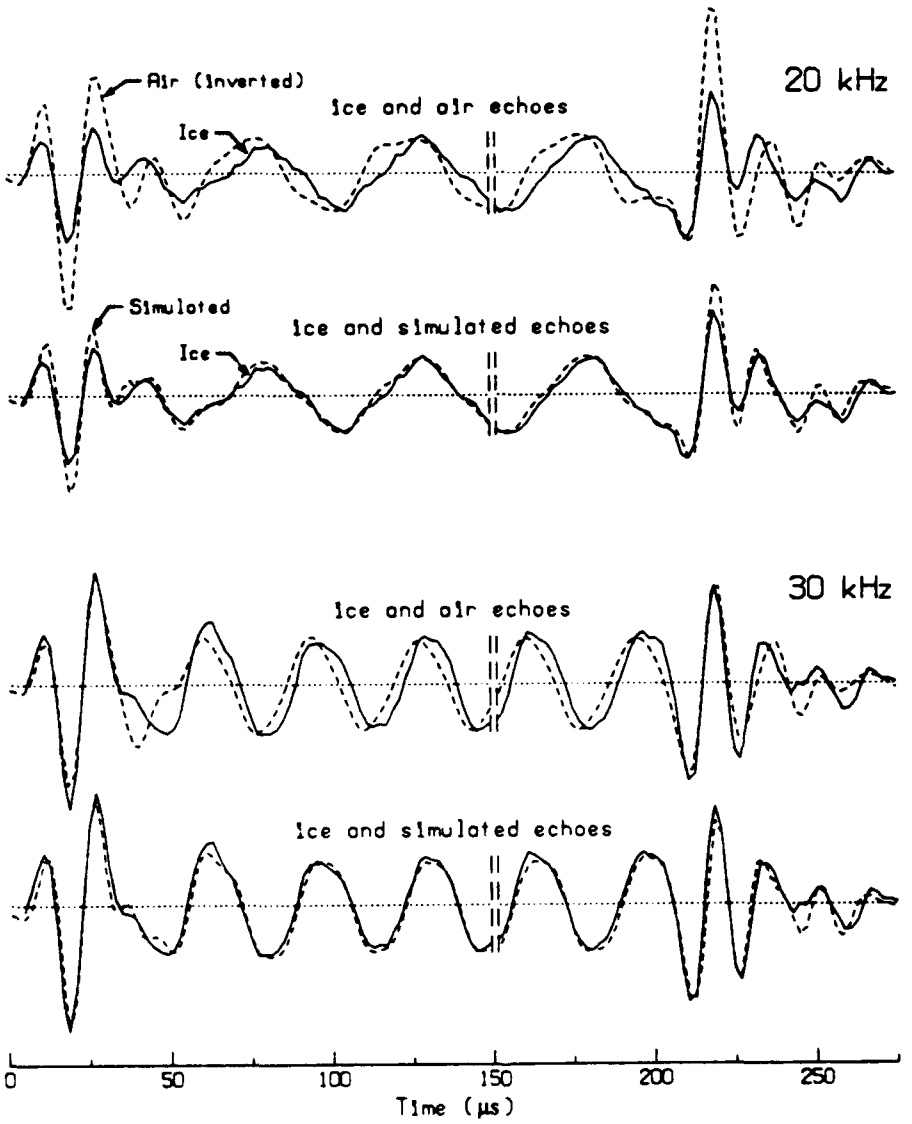

Figure 39. Improvement in correlation between echoes from 58-cm ice block and inverted return from an air-filled pan when adding a delayed air echo.

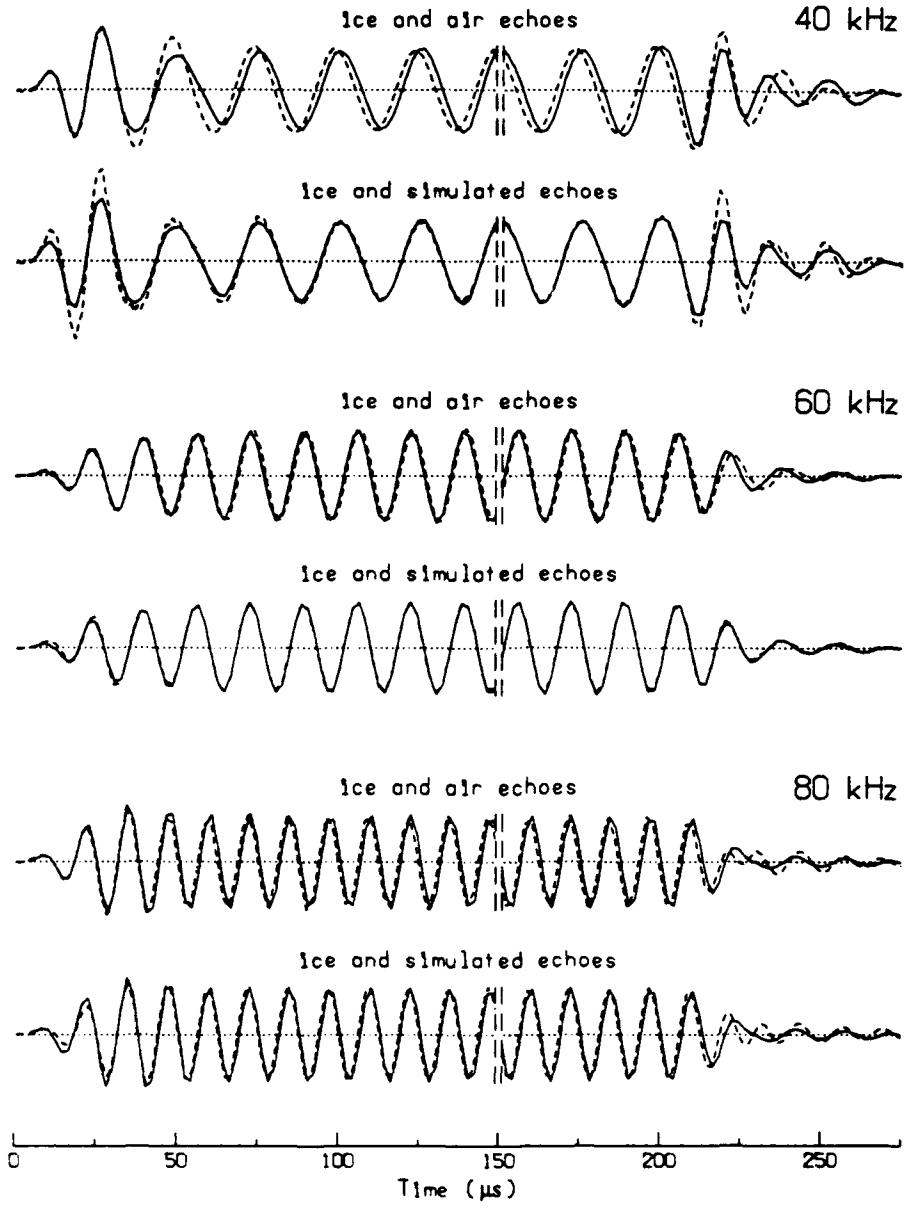

Figure 39, cont.

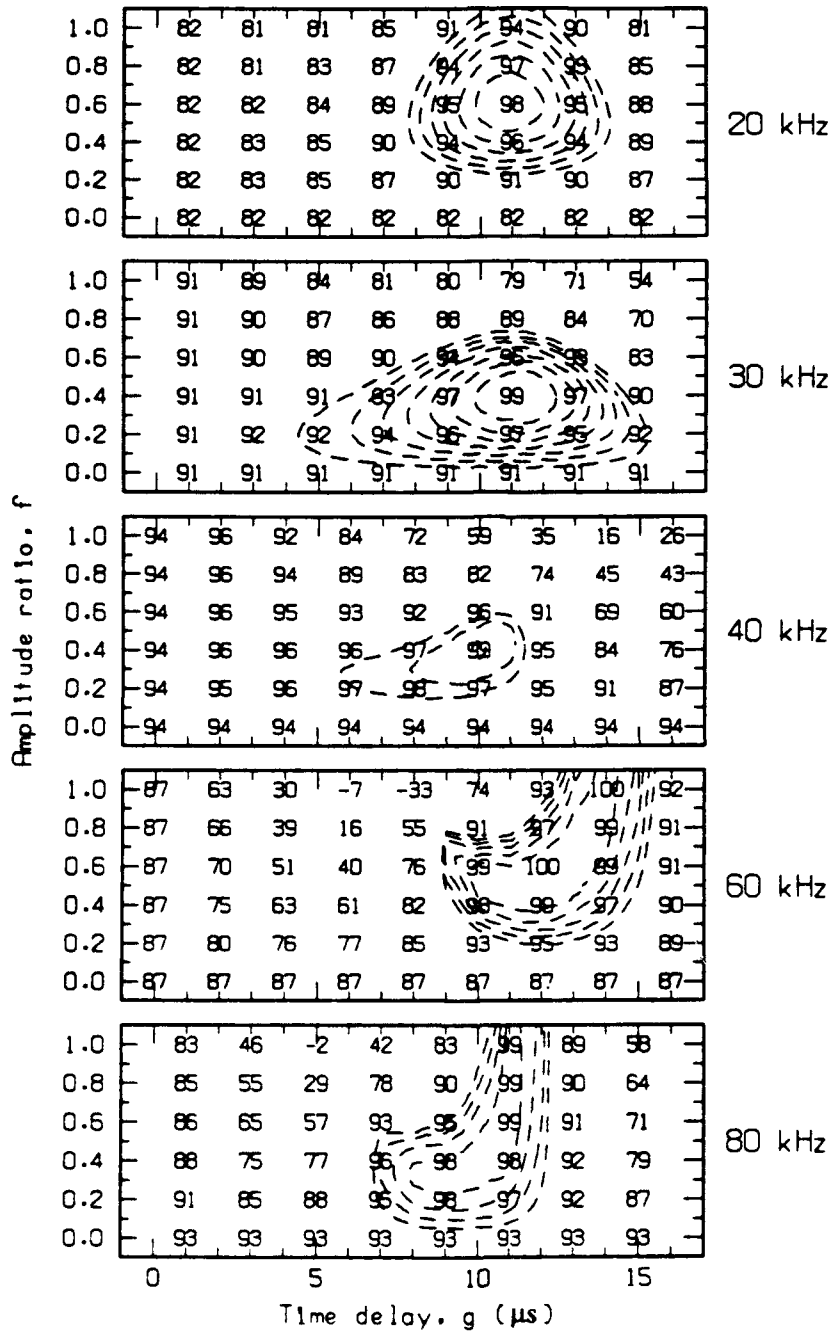

Figure 40. Variation of cross correlation coefficient (shown as percent) between the ice echo and a simulated echo consisting of the inverted echo from the air-filled pan with an added replica, as a function of the amplitude and delay of the added echo.

contour lines have been drawn for correlation coefficient values near maximum and at a few successively lower values to show the sensitivity of the determinations to f and g.

The correlations between the ice echoes and the air echoes without the added replica, the values of f and g that gave the highest correlation between the ice echoes and the simulated echoes with the added replica, and the values of the highest correlation are shown in Table 24 for all frequencies. The values are very consistent, with an average of $f = 0.5$ and $g = 11$.

Table 24. Summary of the amplitude ratios and delays at each frequency that gave a peak in the correlation between ice echoes and a simulation based on air echoes.

Frequency (kHz)	Correlation Ice–Air	f	g (μs)	Correlation Ice–Simulation
20	0.818	0.6	11	0.977
30	0.906	0.4	11	0.988
40	0.946	0.4	10	0.995
60	0.870	0.5	12	0.999
80	0.936	0.7	11	0.992
	Average	0.5	11	

A delay of $g = 11$ μs corresponds to a distance of 1.4 cm into the ice if we assume a sound speed of 2600 m/s (as estimated from examination of Figure 10 and Figures 41 and 42 in Section VI.C). This may be the depth into the ice at which the pores close and the growing platelets merge into a solid structure, i.e., the extent of the region called the "skeletal transition layer."

A delay of 11 μs corresponds to a phase shift of 0.22 cycle at 20 kHz and 0.44 cycle at 40 kHz. Thus if the two-reflection model is correct, we should see a transition from somewhat constructive interference at 20 kHz (amplitude ratio of 1.20) to destructive interference at 40 kHz (amplitude ratio of 0.54), or a difference of 7 dB. The target

strength of the 58-cm block measured during the ice-block experiment (Figure 26) was about 5 dB lower (referenced to theory) at 40 kHz than at 20 kHz, indicating that the decrease with frequency was due to a combination of two reflections.

For another approach, consider that the ice reflections involve three media: the ice, the skeletal layer, and the water. The densities and sound speeds of the ice and the water are known, and the density of the skeletal layer must lie between that of the ice and the water. Let us calculate the sound speed in the skeletal layer that would give the ratio of 0.5 obtained by the simulation method for reflections from the upper and lower surfaces. The sound speed in the ice (shown in Figure 43a in Section VI.C) is about 3610 m/s. The density near the lower surface of the ice, say at −2°C and a salinity of 5 ppt, is given by Cox and Weeks[9] as 0.93. The density of the skeletal layer is assumed to be about mid-way between that of ice and water, or 0.98.

Medium	Sound Speed, c (m/s)	Density, ρ (g/cm^3)	Acoustic Impedance, ρc
Ice	3610	0.93	3357
Skeletal layer	Unknown	0.98	Unknown
Water	1440	1.02	1469

The one-way absorption in the skeletal layer is 1–2 dB (see summary in Section VII.C). If we assume the smallest value, 1 dB each way, we obtain a total of 2 dB.

For each interface, with ρc ratio N, the amplitude reflection coefficient at normal incidence is

$$R = \frac{N-1}{N+1} . \tag{15}$$

For an incident sound wave normal to the lower surface, the ratio of the return from the upper interface to the return from the lower can be shown to be

$$\text{ratio} = mR_b \frac{1-R_a^2}{R_a} , \tag{16}$$

where R_a and R_b are the reflection coefficients for the lower and upper interfaces, respectively, and m represents the skeletal layer absorption (equal to 0.79 for the assumed absorption of 2 dB). Trial and error shows that a skeletal-layer sound speed of 2462 m/s gives a ratio of 0.5, the value given by the simulation method. This sound speed is in fair agreement with the measurements shown in Figure 10 and Figure 43a in Section VI.C, demonstrating a consistency in the various measurements.

VI. VERTICAL TRANSMISSIONS THROUGH THE ICE

This experiment was conceptually quite simple: position a source in the water, put a receiver in a shallow hole in the ice directly above the source, and measure the sound transmitted through the ice at several frequencies; then deepen the hole and repeat the process, taking a final reading with the receiver in the water below the completed hole. From the arrival time and the measured distance between the source and the receiver, the sound speed profile can be estimated. From the change in sound level with depth, absorption can be calculated.

A. Experimental Arrangement

The three-point tethering system (Figure 1) was used to suspend a sound source 29 m under the ice. Since the source was free to move, it could be positioned directly below a receiver at several different locations. Two transducers were used as the sound source on separate occasions: an ITC 1042 with an omnidirectional beam pattern and a small 22 × 22-element array with a narrow beam. (See descriptions in Section IV.B.)

A second ITC 1042 transducer was used as the receiver. It was mounted inside a 5.1-cm-diameter aluminum pipe with its tip flush with the end of the pipe. A tape measure was affixed to the pipe for reading the depth of the transducer relative to a fixed reference. The fixed reference was a swinging arm attached to a vertical pipe previously frozen into the ice. The arm was an L-shaped piece of aluminum supported by a piano hinge along the vertical side. The horizontal part was 60 cm long and could be swung in and out of place during hole-augering operations without changing its vertical position. This vertical rigidity was necessary to obtain accurate depth readings for the sound-speed measurements.

B. Experimental Procedure

For each location chosen for the receiver, a pipe was frozen vertically in the ice about 40 cm away, and the swinging arm attached. The next task was to locate the source directly beneath the receiving hydrophone. To accomplish this, the hydrophone was lowered into the water through a hole offset 1 m away from the desired location. The source was then activated and moved around, by moving the surface ring of the three-point tether, until the arrival time of the received pulse reached a minimum, indicating the source was directly beneath the receiver. The source was then moved 1 m in the direction required to correct for the offset and bring it directly beneath the location chosen for the receiver. After the snow was removed from the surface at that location, the pipe holding the receiver pipe was positioned vertically with the hydrophone end resting on the ice. The arm was swung against the pipe, and a reference "zero-depth" was read on the tape measure affixed to the pipe. The pipe was then removed, and the arm swung out of the way. A shallow 10-cm-diameter hole was augered manually at the chosen location, warmed seawater was poured in to improve the acoustic coupling between the transducer and the ice, and the pipe then set in the hole. A new depth reading was taken, and a series of pulses was transmitted through the ice and recorded. Considerable slush was generated both by the augering and by subsequent freezing, and this slush was difficult to remove. Ice chips were usually found trapped within the cavity between the receiving hydrophone and the surrounding pipe, and may have affected the signal received.

The procedure was repeated at hole-depth intervals of 10–20 cm. The intention was to take finer steps near the bottom in order to profile the skeletal-layer transition zone in greater detail. However, because of the weaker ice in this layer and poor control with the manually operated auger, the auger usually broke unexpectedly through the last 10–20 cm and into the water below. A set of measurements with the receiver in the water was taken for reference.

At each depth, several cw pulses at different frequencies were transmitted upward through the ice and received by the hydrophone. The monitored transmit pulse (at 1/100 of the actual output level) and the received waveform were recorded on the Nicolet oscilloscope disks along with relevant information such as frequency, gain, depth, etc. Table 25 lists the runs made.

The measurements made on 27 March contain data from two holes on opposite sides of the pipe supporting the swinging arm. For these measurements the source transducer was kept stationary at a horizontal position midway between the holes, and the receiver was moved alternately from one hole to the other.

C. Sound Speed Profiles from One-Way Transmissions

The stored data were recalled onto the digital oscilloscope and examined. Pulses at the various frequencies appeared to arrive at the same time, but the waveform of the highest frequency was used for timing because it provided the best detection of the leading edge of the pulse. At each depth, the pulse's arrival time was resolved to an accuracy equivalent to the sampling rate (see Table 25) used on the Nicolet oscilloscope. The sampling interval of 0.5 μs used for hole 1 is equivalent to a distance of about 0.19 cm in the ice. This is twice as large as the uncertainty in the depth readings (0.1 cm) and

Table 25. Measurements of vertical transmissions through the ice. Receiving transducer was an ITC 1042 for all measurements.

Date	Hole No.	Data Disk	Transmitting Transducer	Pulse Length (ms)	Digitizing Interval on Scope (μs)	Frequency (kHz)
26 March 88	1	ABS 15,16	22×22	0.2	0.5	30,40,60,80,100, 120,160,200
27 March 88	2,3	Block 3,4	ITC 1042	0.2	1.0	20,30,40,60,80
16 April 88	4	ABS 19-21	ITC 1042	0.2	2.0	20,30,40,60,80

results in an error, depending on the depth interval, of up to 4% in the sound speed. For the other holes, the error is 2–4 times as large as for hole 1.

The sound speed was computed by simply dividing the depth interval between measurements by the difference in the travel times for the two measurements defining the interval. The quotient obtained for each depth interval is considered the average speed at the mid-point of that interval. In addition, a value for the top layer (between the top of the ice and the first measurement) and one for the bottom layer (between the last measurement and the bottom of the ice) can also be obtained from the data. The sound speed in the top layer is obtained by merely taking the depth of the first measurement point and dividing by one-half the difference between the travel times of the direct pulse and the pulse reflected from the top of the ice; in this case, these pulses overlapped, but could be resolved using a digital inverse filtering technique.[10] The sound speed in the bottom layer was computed from the measurement in the water and the lowest measurement in the ice as outlined in Figure 41. The sound speed profiles obtained are shown in Figure 42.

A large scatter is observed in all four profiles. The exceptionally large scatter in the data from hole 4 is hard to explain. The timing resolution was about 2 μs, too small to cause the variations observed in the measured sound speeds. If only one depth reading had been wrong, there should have been a high value adjacent to each low value. Instead, the data show two consecutive high values over 5000 m/s. This would require that two successive readings (either time or depth) be in error.

The results for holes 2 and 3, which were measured alternately, are repeated in Figure 43a with the less accurate value for the top layer of the ice omitted. They are in fair agreement, with both indicating a lower sound speed in the bottom of the ice. Profiles derived from the measured values of temperature, salinity, and density for two ice cores taken from the same experimental site[11] are shown in Figure 43b for comparison. Here too, the sound speed decreases in the skeletal-layer transition zone at the bottom of the ice.

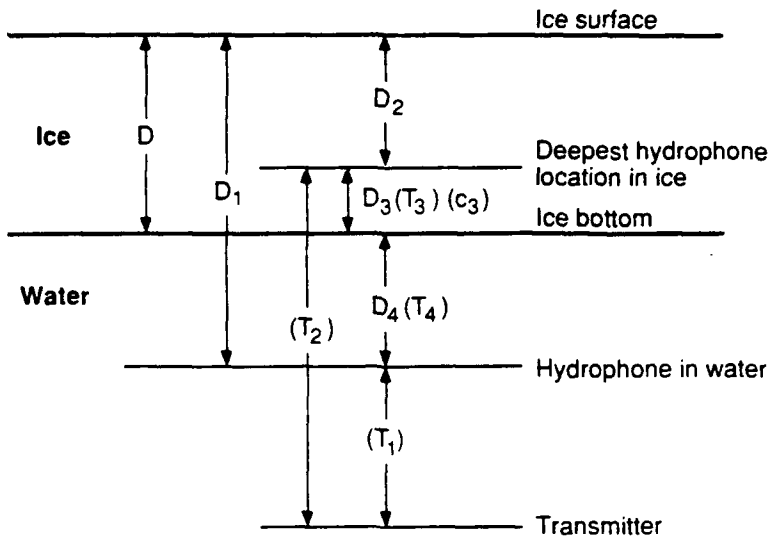

Measurements

D = ice thickness

D_1, D_2 = depth readings on pipe scale, referenced to the surface reading

T_1, T_2 = measured one-way travel times

c_w = sound speed in the water

Calculations

Travel times

$T_4 = D_4 / c_w$

$T_3 = T_2 - T_1 - T_4$

$= T_2 - T_1 - D_4 / c_w$

$= T_2 - T_1 - (D_1 - D) / c_w$

Sound speed in skeletal-layer transition zone

$c_3 = D_3 / T_3 = (D - D_2) / T_3$

Figure 41. Relationships used in computing the sound speed in the skeletal-layer transition zone.

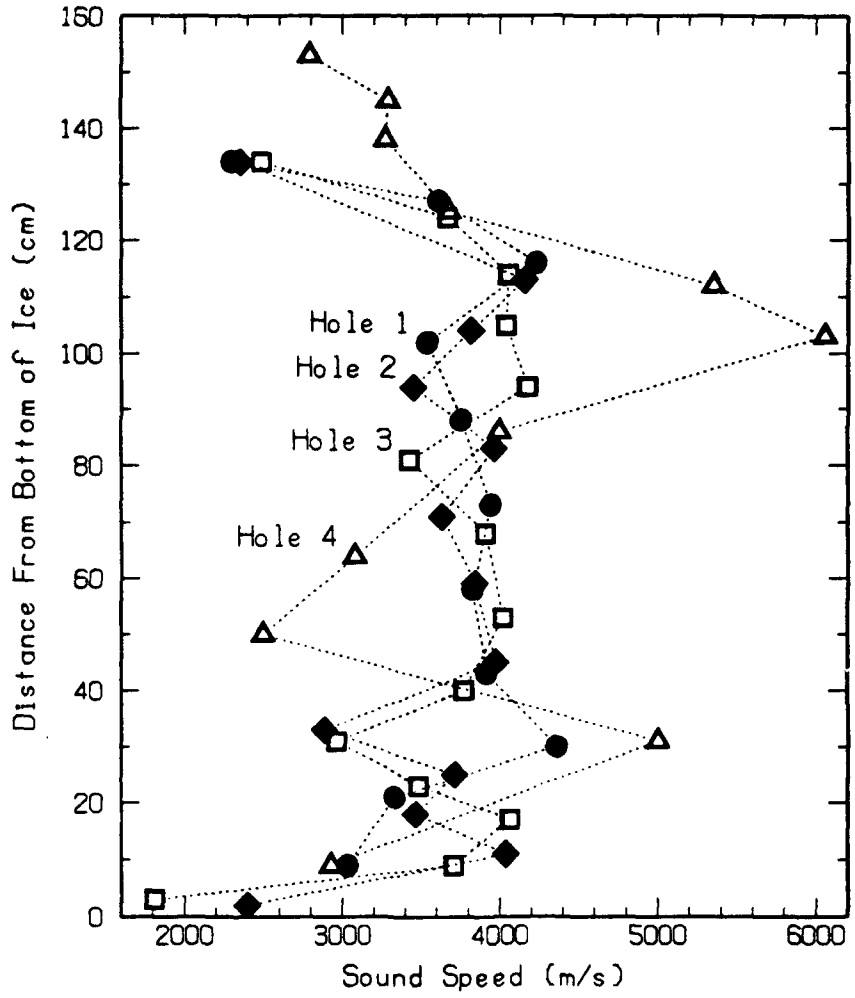

Figure 42. Measured sound speed profiles in the ice, computed from one-way transmissions at 80 kHz on 27 March 1988.

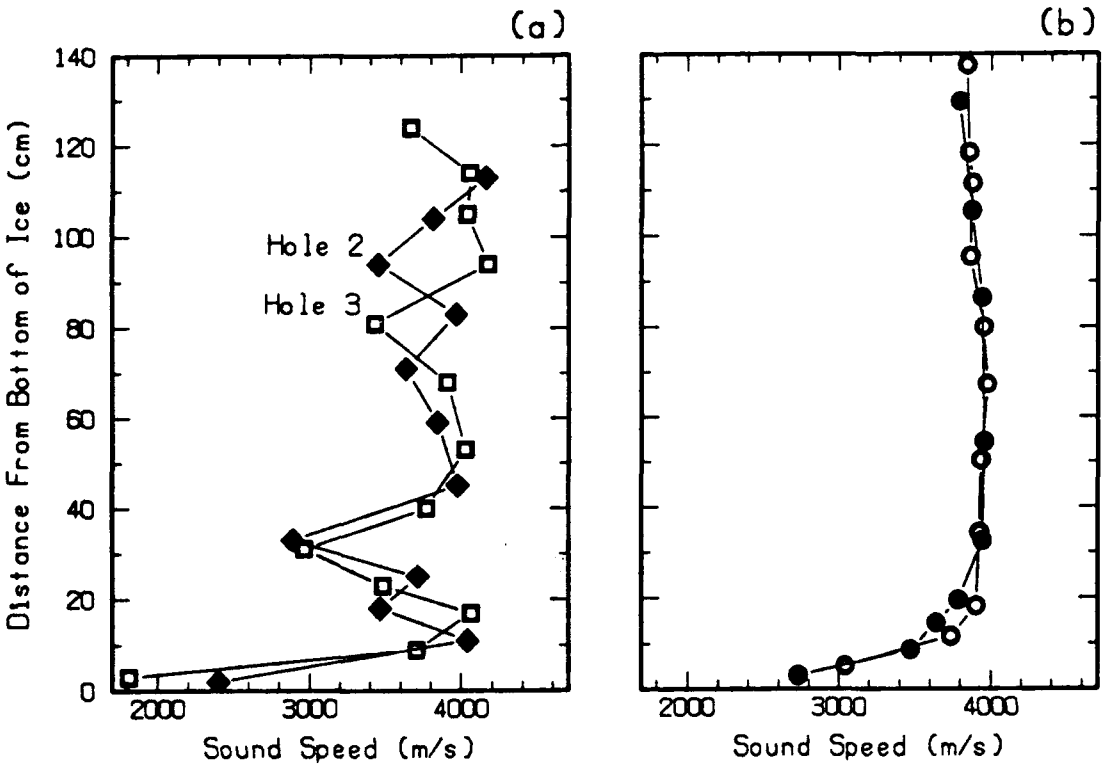

Figure 43. (a) A replot of two directly measured sound speed profiles made as the transducer was moved alternately from one hole to the other on 27 March 1988. (b) Profiles derived from the measured temperature, salinity, and density of sawed off pieces of two ice cores taken nearby on 25 March and 3 April 1988.

The unweighted average sound speed in the ice column computed for each of the four holes is 3623, 3517, 3587, and 3814 m/s, respectively, for an average of 3635 m/s. The last value, for hole 4, is highly questionable, since the profile varies so widely. However, it agrees well with the averages of the profiles derived from the temperature, salinity, and density measurements, whereas for the first three holes these averages are about 200 m/s lower.

D. Absorption Calculated from One-Way Transmissions

The stored data recorded during the one-way transmission measurements were recalled from the Nicolet disks, and the peak values of the transmit voltage and received waveform were read and recorded for each pulse. Some waveforms were not flat topped, and eyeball averaging was performed. Figure 44 shows the waveforms obtained for six of the frequencies (30, 40, 60, 80, 100, and 120 kHz) recorded at hole 1. The readings at 160 and 200 kHz have been omitted because the waveforms generally had very low amplitudes owing to the poor response of the ITC 1042 at these frequencies. To compare the levels at different depths in a hole, we computed the received signal levels relative to 1 V transmitted as follows:

$$L = 20\log(V_r R'/100V_x) - \text{gain}\,, \tag{17}$$

where V_r is the received voltage, V_x is the recorded transmit voltage, and R' is the range adjusted to correct for the additional spreading in the ice. The logarithm is to base 10.

The measured sound levels are listed in Table 26. Figures 45a and 45b are vertical profiles of the sound levels received at each hole. The received level has been corrected for spreading loss, both in the water and in the ice, by $R' = R + xc_i/c_w$, where R is the range from the transmitter to the under-ice surface, x is the distance into the ice, and c_i and c_w are the sound speed in the ice and the water, respectively (see Appendix B). Despite some large scatter, the slope of the profile appears to increase with frequency.

According to the absorption model of McCammon and McDaniel[1] discussed in Section III.H, the absorption should be higher at the bottom of the ice, where the temperature is higher, than at the top of the ice. Their model includes a factor 0.06 which we labeled k. To test the temperature and frequency dependence of the model, we calculated a value of k for each frequency and each hole and examined the constancy of the calculated k's.

Equation (6) in Section III.H gives the absorption in ice of thickness t with a constant temperature gradient. For a transmission distance d into the ice from below, the loss can be expressed

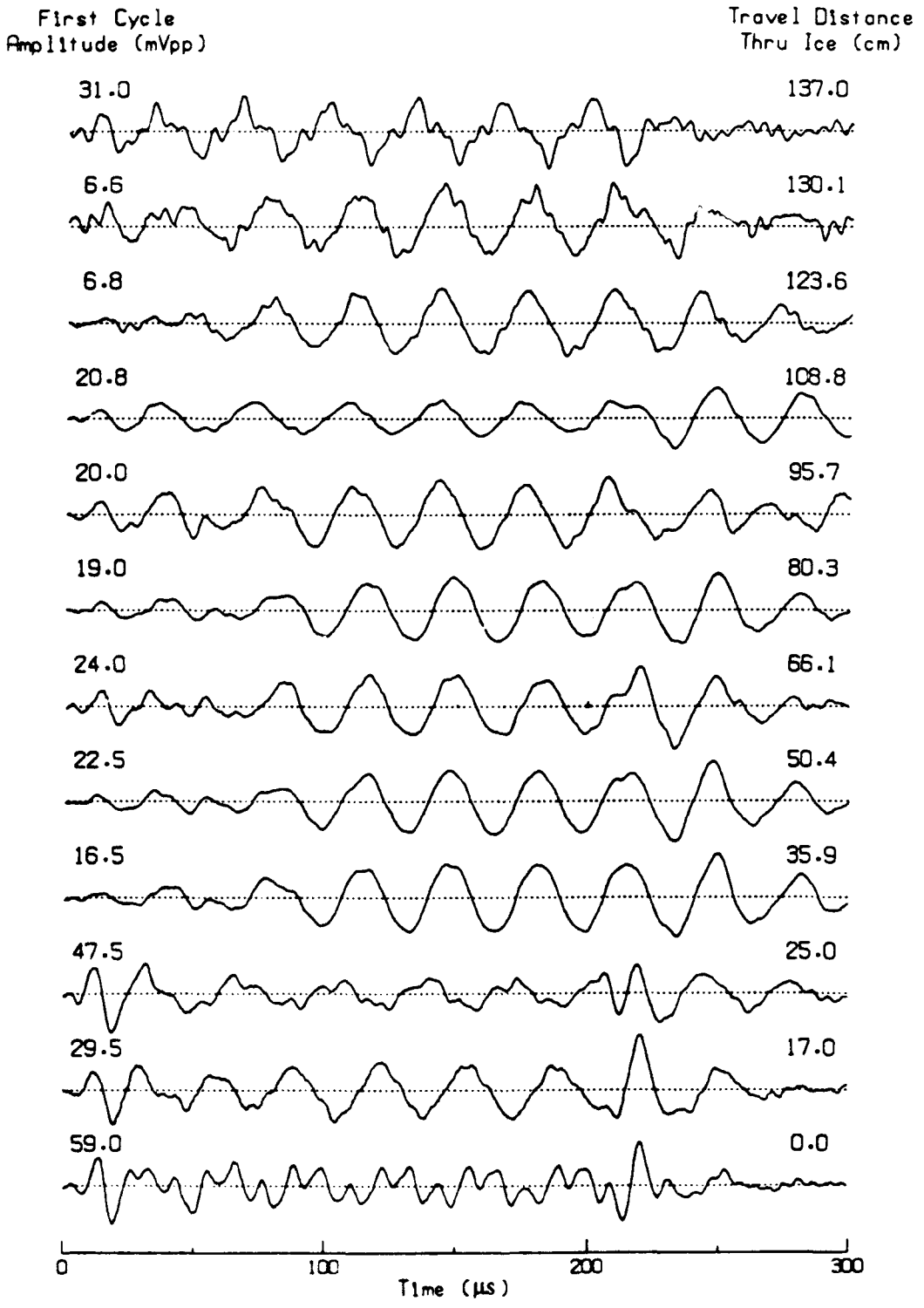

Figure 44a. Pulses received at several depths in the ice from a transducer placed below hole 1; frequency, 30 kHz.

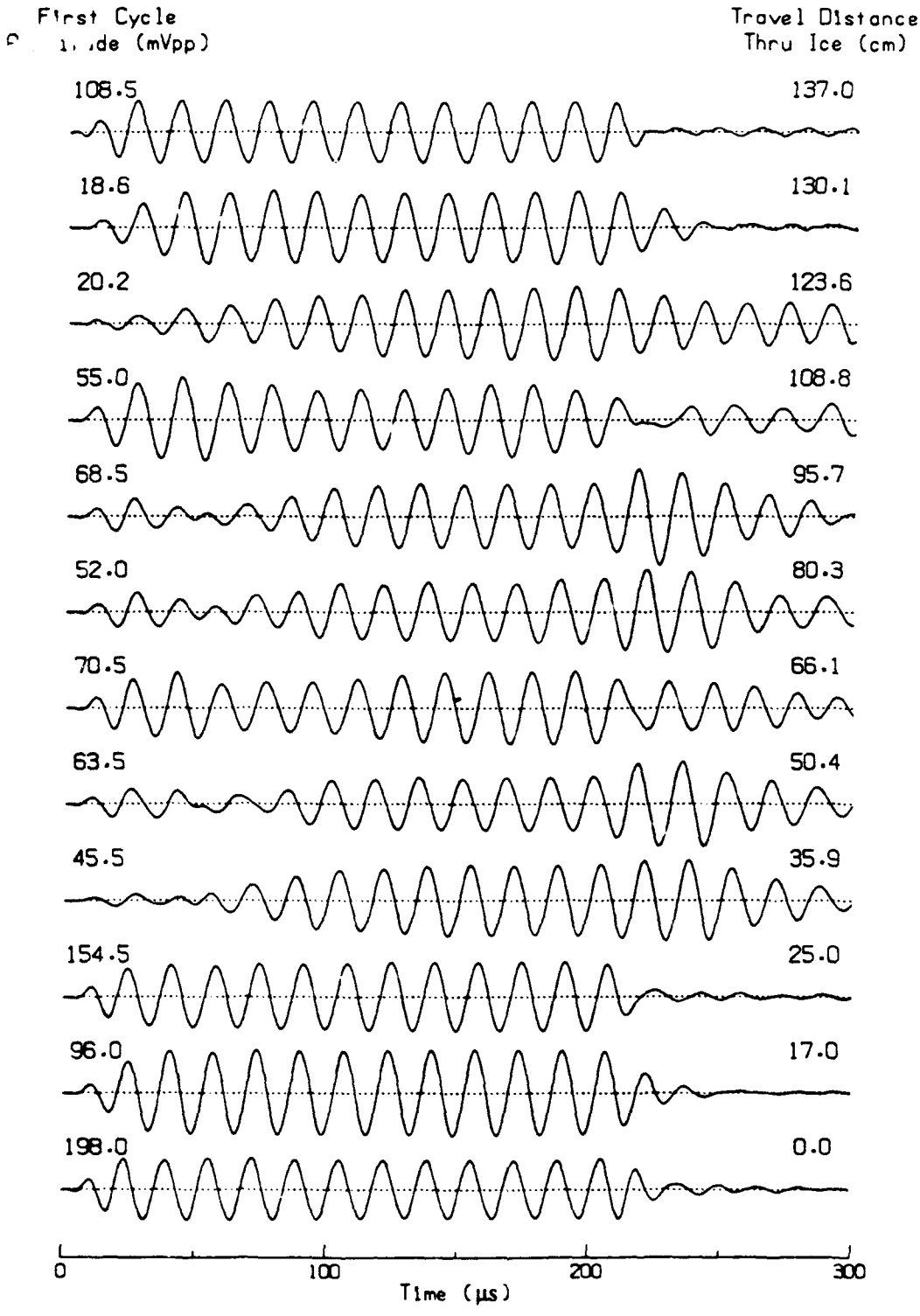

Figure 44b. Pulses received at several depths in the ice from a transducer placed below hole 1; frequency, 40 kHz.

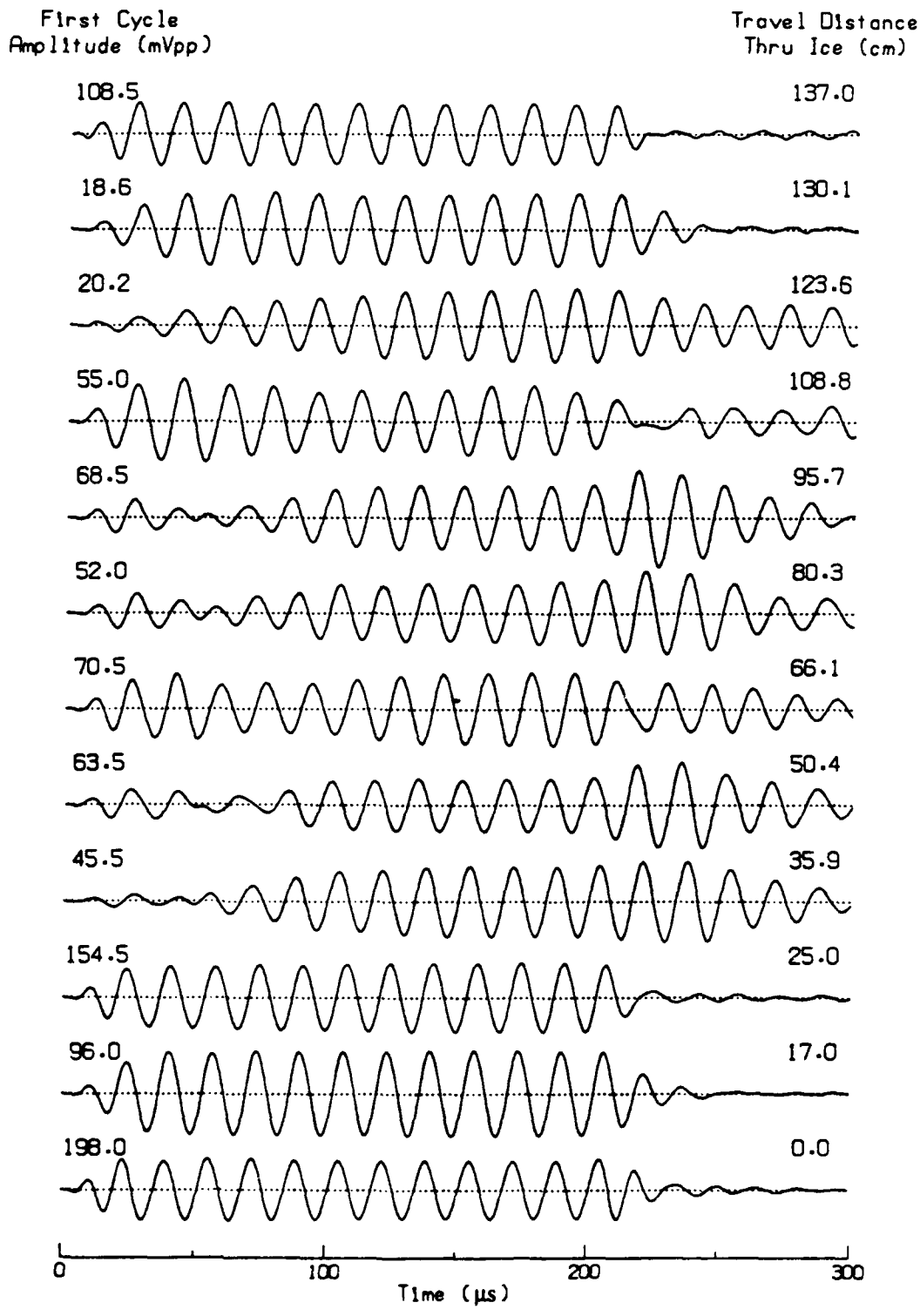

Figure 44c. Pulses received at several depths in the ice from a transducer placed below hole 1; frequency, 60 kHz.

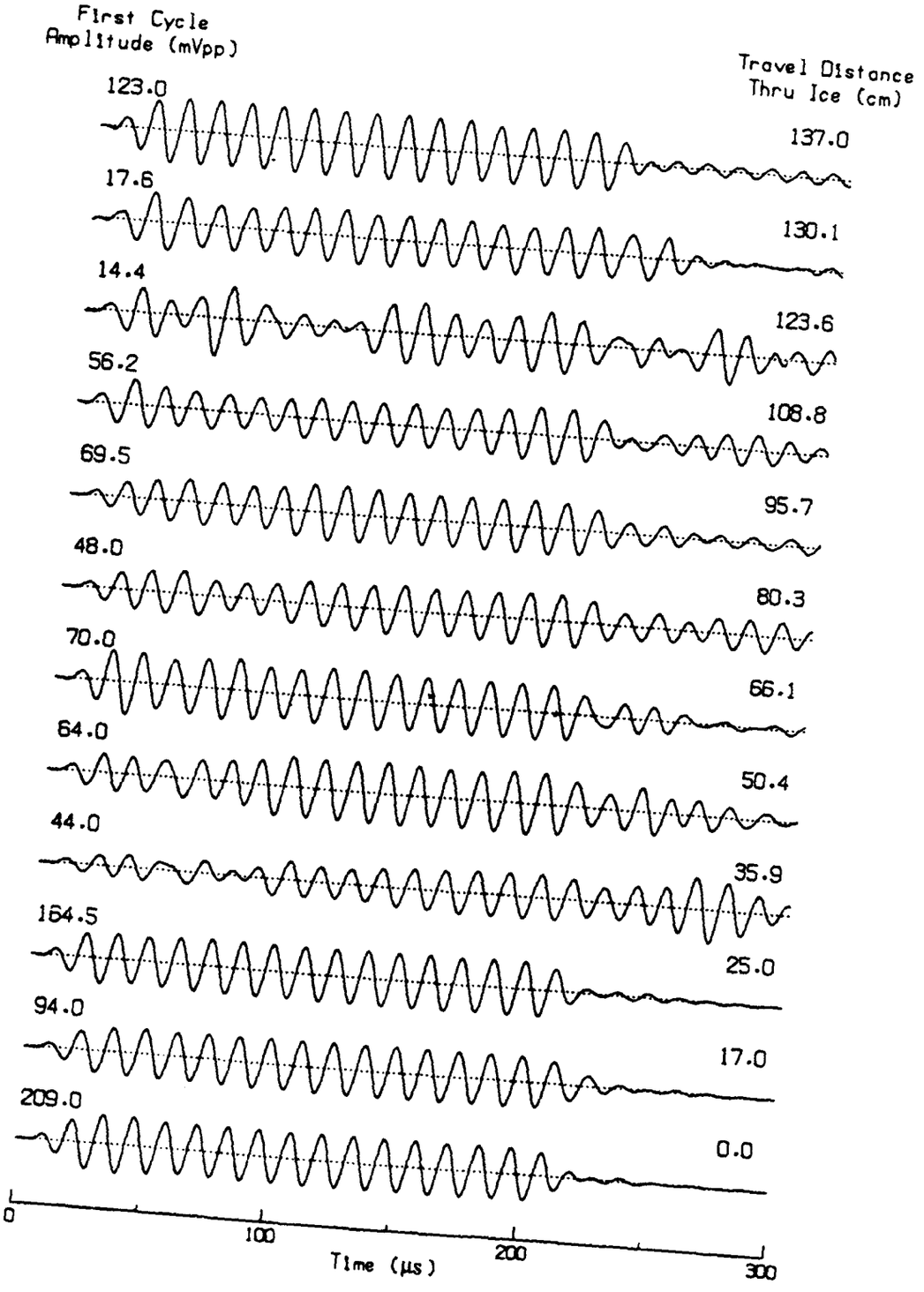

Figure 44d. Pulses received at several depths in the ice from a transducer placed below hole 1; frequency, 80 kHz.

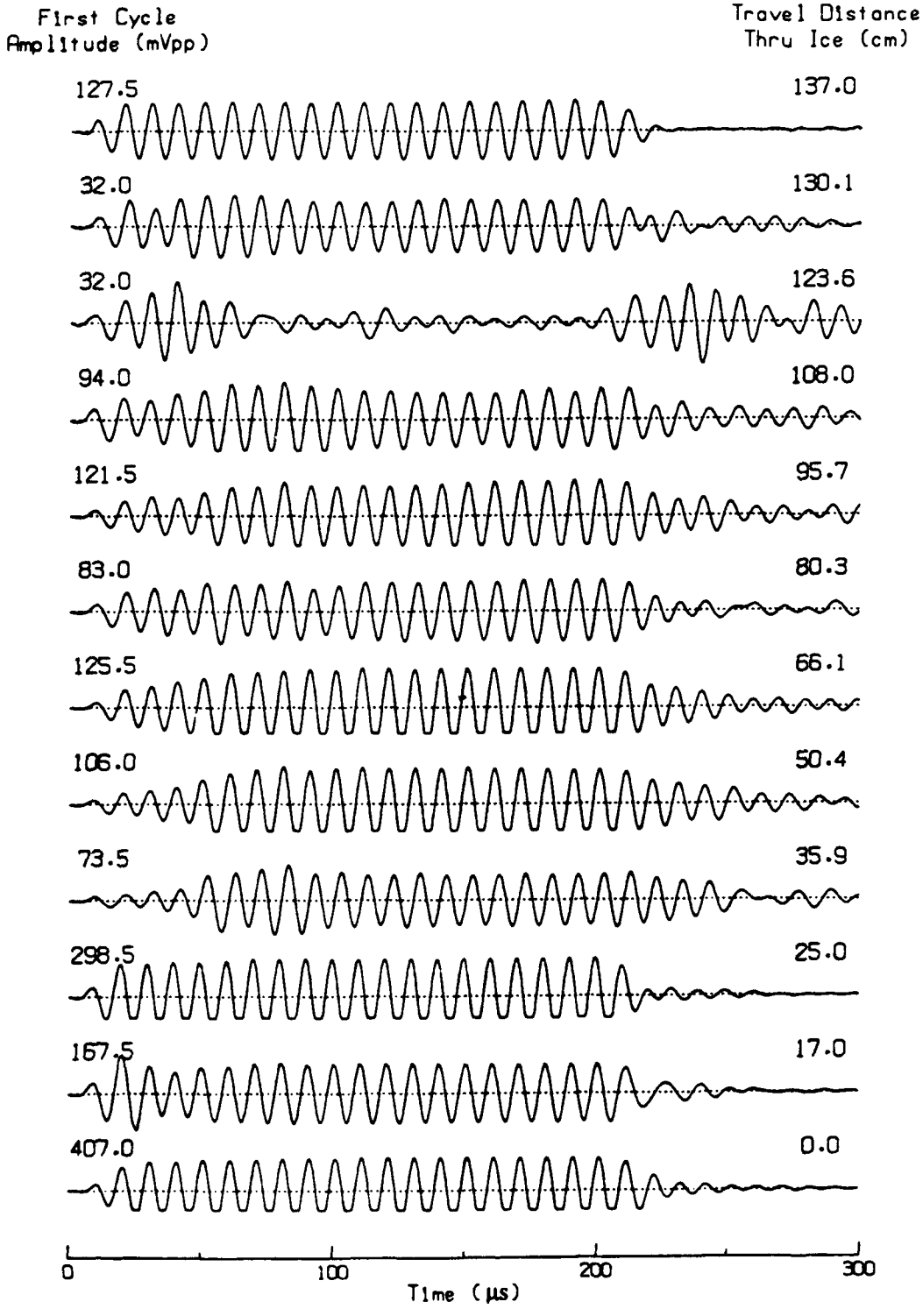

Figure 44e. Pulses received at several depths in the ice from a transducer placed below hole 1; frequency, 100 kHz.

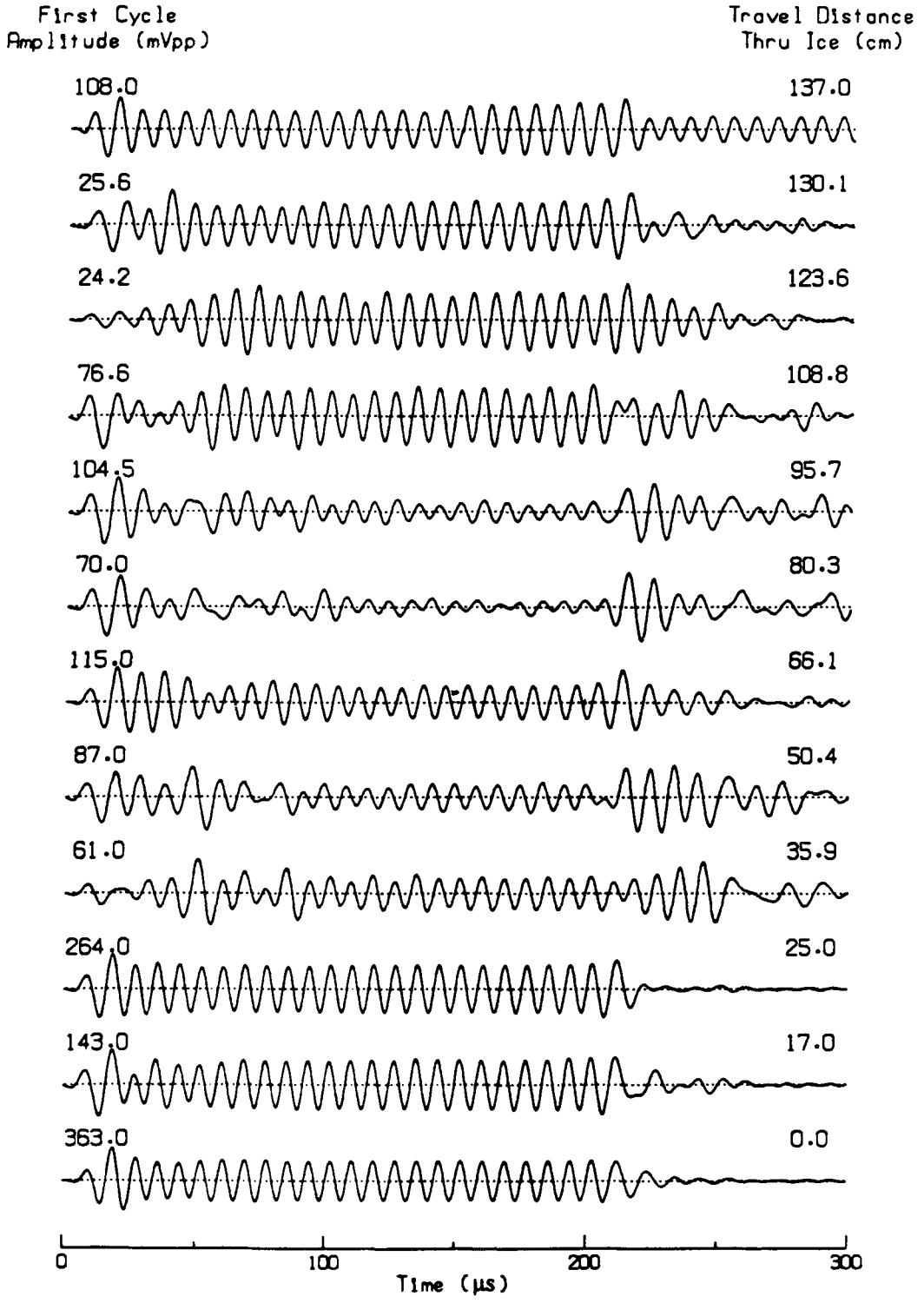

Figure 44f. Pulses received at several depths in the ice from a transducer placed below hole 1; frequency, 120 kHz.

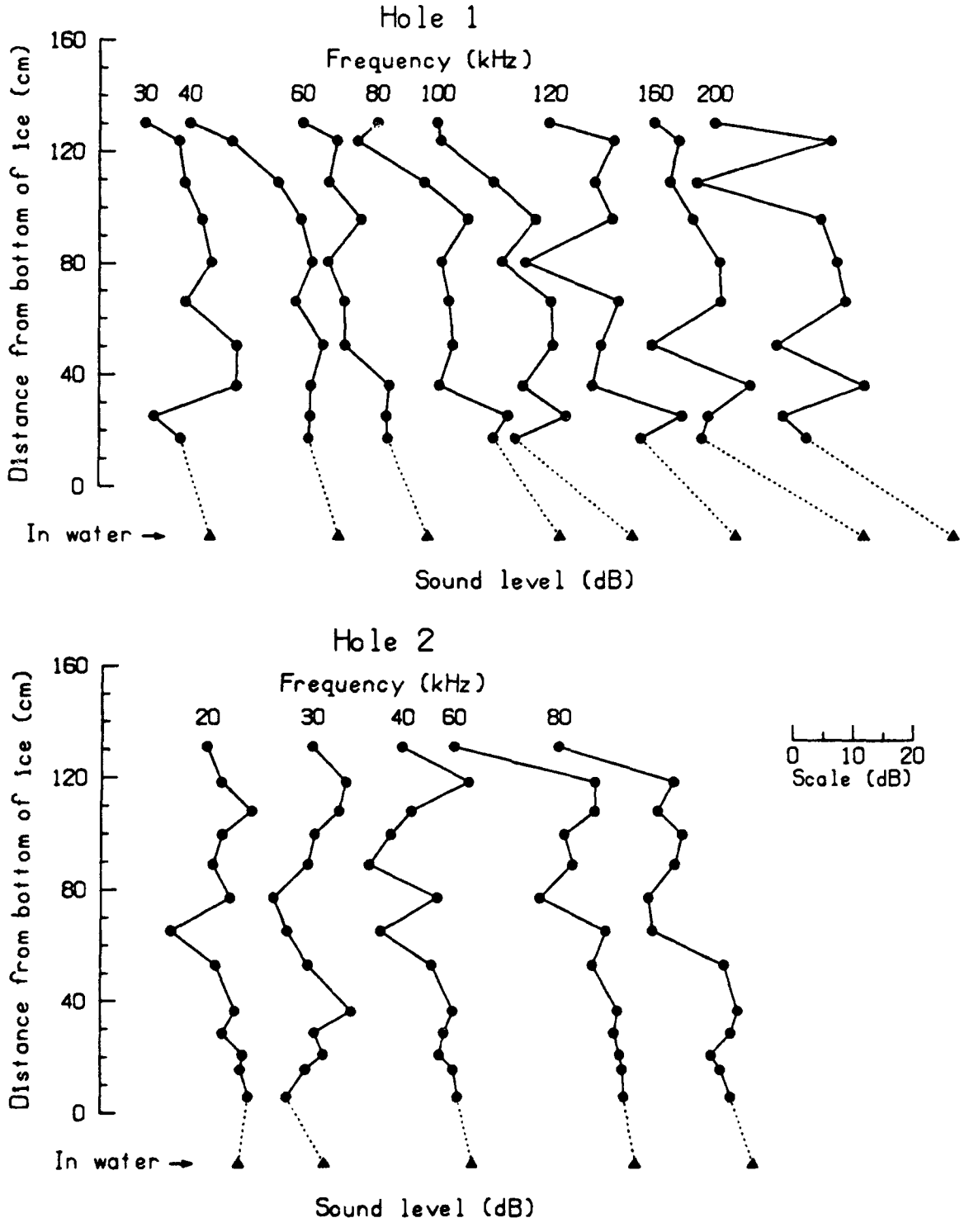

Figure 45a. Measured sound levels at holes 1 and 2 for all frequencies.

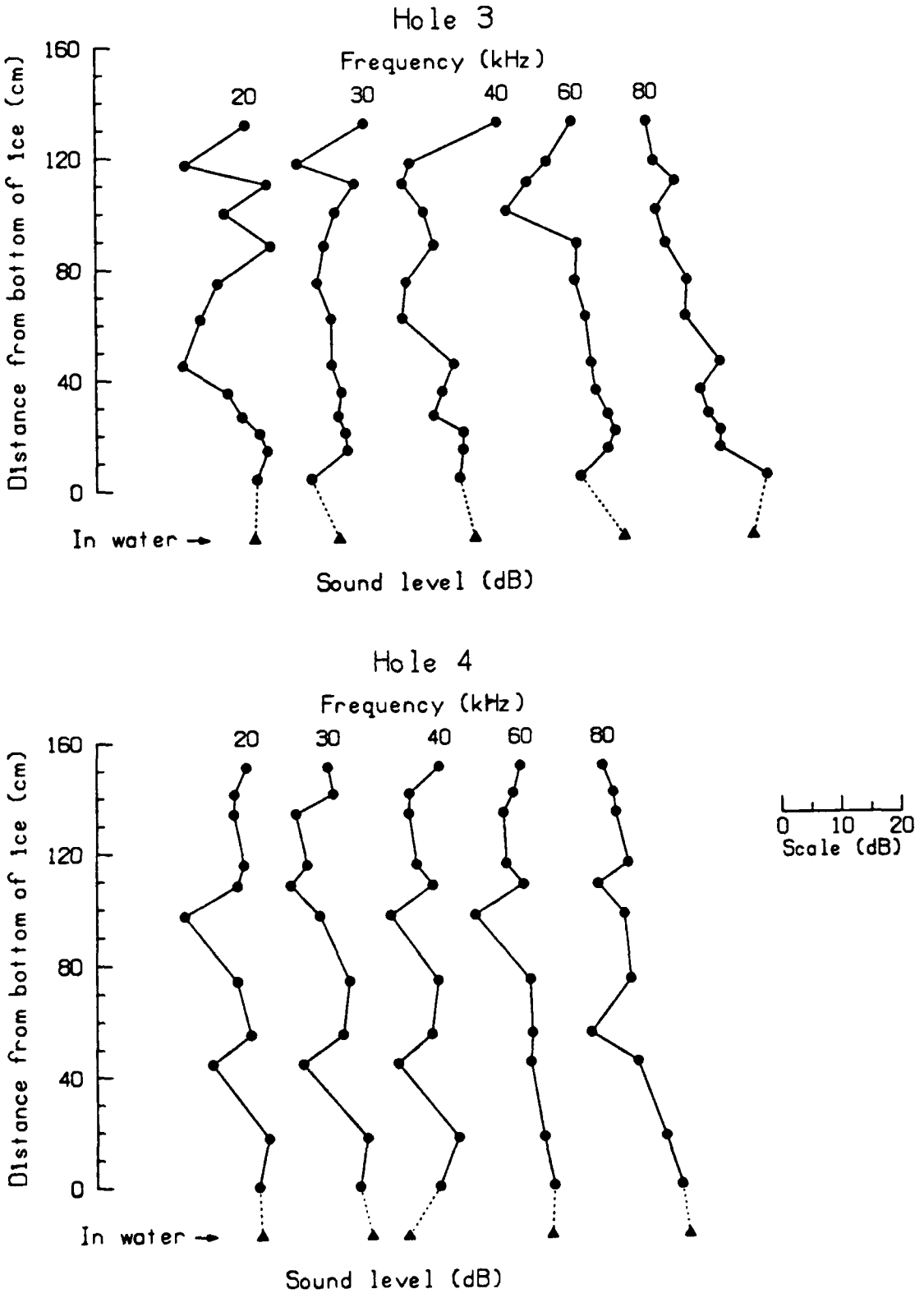

Figure 45b. Measured sound levels at holes 3 and 4 for all frequencies.

Table 26. Measured steady-state sound levels (in decibels) after travel through ice of various thicknesses at four locations. All levels are corrected for spreading loss in the water and in the ice. The 22×22 transducer was used as the transmitter for hole 1 and the ITC 1042 for the other holes.

Hole 1

Ice Thickness (cm)	Frequency (kHz) 30	40	60	80	100	120	160	200
130.1	-53.4	-58.0	-42.2	-43.3	-38.8	-43.4	-53.5	-73.9
123.6	-47.7	-51.0	-36.4	-46.6	-38.1	-32.6	-49.4	-54.4
108.8	-46.7	-43.3	-37.7	-35.4	-29.3	-35.7	-50.8	-76.8
95.7	-43.8	-39.4	-32.3	-28.0	-22.2	-32.8	-47.0	-56.0
80.3	-42.3	-37.6	-37.9	-32.5	-27.9	-47.3	-42.6	-53.4
66.1	-46.5	-40.3	-35.1	-31.2	-19.6	-31.7	-42.3	-51.9
50.4	-38.0	-35.7	-35.0	-30.5	-19.3	-34.6	-53.7	-63.3
35.9	-38.1	-37.8	-27.6	-32.8	-24.3	-36.1	-37.4	-48.8
25.0	-51.8	-37.9	-28.1	-21.3	-17.1	-21.2	-44.4	-62.3
17.0	-47.4	-38.2	-27.9	-23.8	-25.6	-28.0	-45.5	-58.4
-18.2[a]	-42.3	-33.0	-21.0	-12.5	-5.9	-12.1	-18.3	-33.7

Hole 2

Ice Thickness (cm)	Frequency (kHz) 20	30	40	60	80
131.0	-20.3	-15.7	-16.1	-23.8	-23.9
118.5	-17.9	-10.1	-4.9	-0.3	-4.8
108.1	-12.8	-11.1	-14.4	-0.2	-7.3
99.7	-17.7	-15.2	-17.9	-5.3	-3.3
89.0	-19.2	-16.3	-21.5	-3.9	-4.5
77.1	-16.4	-22.1	-10.1	-9.4	-8.9
65.1	-26.2	-19.8	-19.6	1.6	-8.2
52.8	-18.7	-16.3	-11.0	-0.6	3.7
36.5	-15.5	-9.0	-7.4	3.6	6.0
28.7	-17.6	-15.2	-8.9	3.0	4.8
20.9	-14.2	-13.6	-9.6	4.0	1.6
15.7	-14.6	-16.6	-7.3	4.4	3.1
6.0	-13.3	-19.8	-6.6	4.7	4.8
-55.2[a]	-14.7	-13.3	-3.9	6.8	8.8

Hole 3

Ice Thickness (cm)	Frequency (kHz) 20	30	40	60	80
131.4	-18.4	-10.4	0.4	-0.3	-8.8
117.1	-28.4	-21.7	-14.4	-4.5	-7.6
109.8	-14.8	-12.0	-15.6	-7.8	-4.0
99.7	-21.9	-15.3	-12.1	-11.3	-7.2
87.8	-14.2	-17.2	-10.4	0.5	-5.6
74.6	-23.0	-18.3	-15.0	0.2	-2.0
61.7	-25.9	-16.0	-15.7	1.9	-2.3
45.0	-28.9	-16.0	-7.1	2.8	3.4
35.0	-21.4	-14.3	-9.0	3.6	0.2
26.4	-19.1	-14.9	-10.5	5.6	1.5
20.3	-16.2	-13.7	-5.5	6.8	3.5
14.0	-14.9	-13.4	-5.6	5.6	3.4
3.8	-16.6	-19.4	-6.1	1.1	11.3
-55.6[a]	-17.1	-14.8	-3.6	8.3	8.9

Hole 4

Ice Thickness (cm)	Frequency (kHz) 20	30	40	60	80
150.9	-26.3	-27.9	-15.3	-10.2	-15.5
141.2	-28.3	-27.0	-20.3	-11.4	-13.7
134.0	-28.4	-33.3	-20.4	-13.1	-13.3
115.6	-26.7	-31.4	-19.1	-12.6	-11.2
108.1	-27.8	-34.2	-16.4	-9.7	-16.3
97.2	-36.6	-29.3	-23.5	-17.9	-11.9
74.0	-27.8	-24.3	-15.5	-8.6	-10.8
54.9	-25.6	-25.4	-16.6	-8.3	-17.5
44.4	-31.9	-32.1	-22.2	-8.5	-9.6
17.4	-22.6	-21.3	-12.1	-6.3	-4.9
0.0	-24.2	-22.5	-15.2	-4.6	-2.2
-11.0[a]	-23.8	-20.5	-20.5	-5.0	-1.0

[a]Receiving transducer in the water below the ice.

$$\text{loss} = (d)(k)[3f6^{(2/3)}]\,\frac{(-T_1)^{1/3}-(-T_0)^{1/3}}{T_0-T_1}\quad \text{dB}\,, \tag{18}$$

where

k = coefficient in absorption model

T_0 = water temperature below the ice (°C)

T_1 = ice temperature at receiver depth (°C)

f = frequency (kHz).

For ice of thickness t with temperature T_2 at the top surface, and assuming a constant temperature gradient, the temperature at the receiver a distance d above the bottom is

$$T_1 = T_0 + (T_2-T_0)\frac{d}{t}\,. \tag{19}$$

For a sound level L_0 in the ice at the bottom, and letting

$$q = 3f6^{2/3}\,\frac{(-T_1)^{1/3}-(-T_0)^{1/3}}{T_0-T_1}\,, \tag{20}$$

the sound level at distance d into the ice can be expressed

$$L = L_0 - kqd\,, \tag{21}$$

where q is a function of T_1 and thus a function of d.

For each set of measured sound levels at several depths in the four tests at five frequencies, we plotted L versus qd and applied a first-order least-squares regression to the set of data for each frequency and each hole to obtain values for L_0 and k. The data points obtained in the water were not included in the least-squares fit because of the additional loss at the water–ice interface. Table 27 gives the k's calculated for each frequency and each hole. As mentioned before, the effect due to spreading was included as a correction to the measured sound level L.

Table 27. Values computed for absorption constant k *in Eq. (21) for measurements at the four holes.*

Frequency (kHz)	Hole 1[a]	Hole 2[b]	Hole 3[b]	Hole 4[c]
20	--	0.18	0.14	0.14
30	0.21	–0.05	–0.02	0.23
40	0.46	0.22	0.09	0.04
60	0.26	0.30	0.20	0.10
80	0.31	0.27	0.20	0.12
100	0.23	--	--	--
120	0.15	--	--	--
160	0.12	--	--	--
200	0.10	--	--	--

[a]Data set ABS-15
[b]Data set BLOCK-3
[c]Data set ABS-19

The k's exhibit a large scatter. The average is 0.17 with a standard deviation of 0.11. The negative values of k obtained at 30 kHz for holes 2 and 3 indicate an increase in the sound level with range instead of a decrease, mainly because of the lower sound levels measured near the bottom of the ice. The higher-frequency data (160 and 200 kHz) for hole 1 are also disturbing, because the drop in k indicates that the absorption coefficient is not proportional to frequency, as modeled.

The average k, 0.17, is about three times the value of 0.06 used in the McCammon-McDaniel model. Their model was based on horizontal transmissions whereas ours were in the vertical direction. Intuitively, we would have expected the vertically oriented brine channels to cause more absorption for horizontal transmissions.

E. Alternate Absorption Analysis

An expanded view of the reflected waveform shows that the first cycle is apparently a transient near the resonant frequency of the transmitting transducer. This is followed by a gradual transition to the driving frequency, which dominates after about two cycles of that frequency. As the receiver was lowered in the successively deepened hole in the ice, these first cycles appear to have less variation than the steady-state cycles that follow. The steady-state return apparently includes some deflected or reflected paths that combine and interfere with the direct pulse. To avoid this interference, we recalculated the absorption based on the first cycle only, thereby limiting our investigation of frequency dependence to the variation in frequency of the first cycle.

In Figure 44 we note that the first cycle has a frequency near the resonant frequency of the transducer regardless of the driving frequency. During the next few cycles, the frequency changes gradually to the driving frequency. The numbers at the left in Figure 44 give the peak-to-peak voltage of the first cycle, and those at the right give the distance the sound traveled through the ice. Using Eq. (17), we computed a signal level L, normalized for differences in transmit voltage, receiver gain, and refraction, and plotted L versus qd to determine the slope of the line given by Eq. (21). When computing q, we used a temperature of −25°C for the top of the ice for all holes even though the air temperature at the time of the measurements at hole 4 had warmed to −10°C. We assumed that the ice, with some snow cover, probably did not change temperature appreciably in the 2 days between the measurements at hole 1 and hole 4. Figure 46 shows plots of the return amplitude of the first cycle at successive distances through the ice for holes 1–4. The labeled frequencies are the driving frequencies, which differ from the first-cycle frequencies. After replotting signal level against qd (not shown), we computed a least-squares line; the slope of this line gives a value for k in the absorption equation, (4).

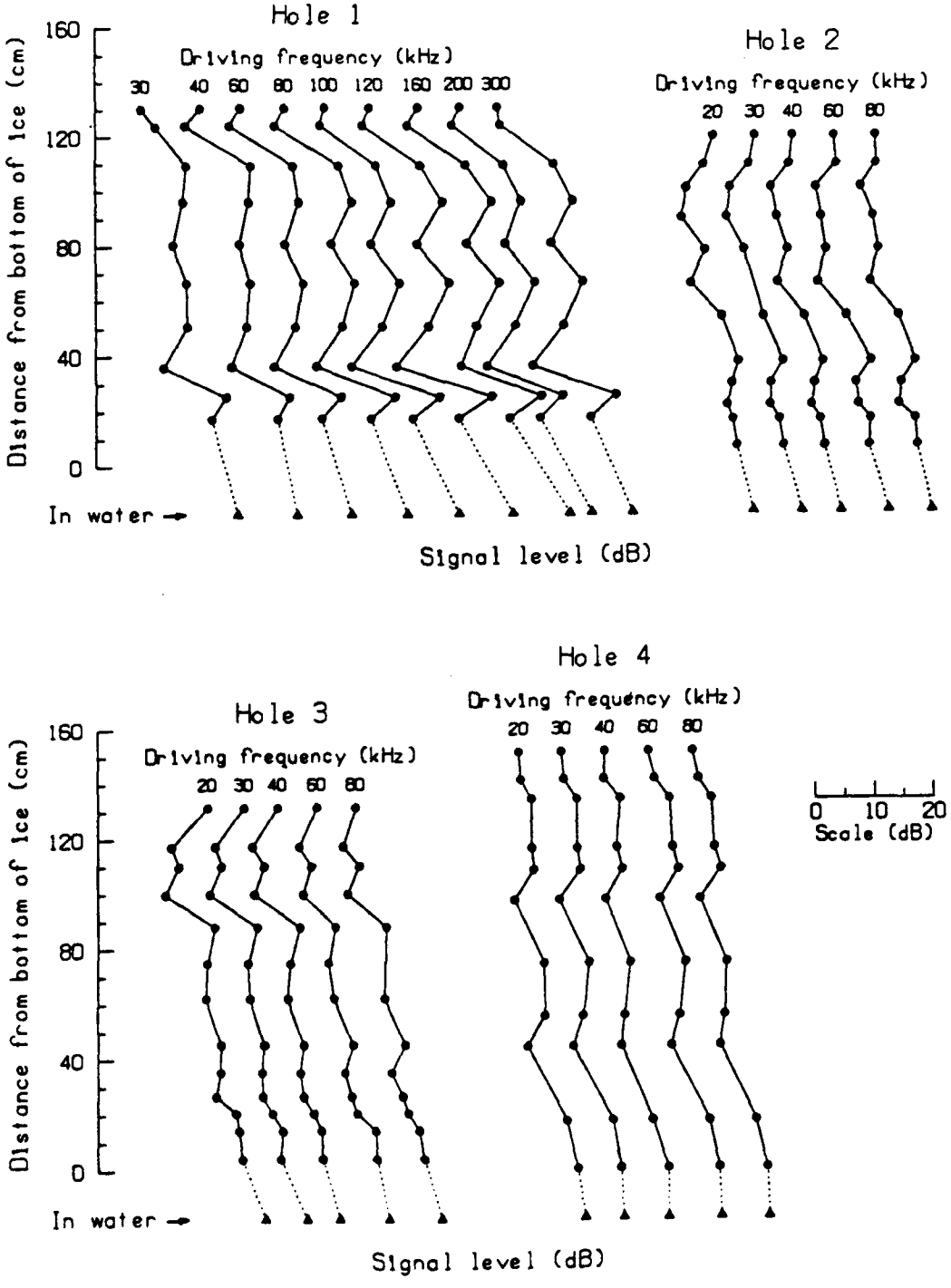

Figure 46. Signal level of first cycle versus thickness of ice for holes 1–4. When replotted against qd, as shown in Eq. (21), the slope is the constant k. The frequency of the first cycle varied only from 60–94 kHz as the driving frequency increased.

Note the high correlation among the five pings for the data taken at each depth. This indicates that the variation in signal level was the same at all frequencies, and thus the first few cycles did not involve any type of interference. The variations may have been caused by inadequate coupling between the receiving transducer and the ice, even though water was placed in the bottom of the hole to enhance the coupling.

Table 28 and Figure 47 show the k's calculated for holes 1–4 for the different first-cycle frequencies. For hole 1, we used the 22×22 transducer for transmitting; for the other holes, we used the ITC 1042. Since hole 1 had a different transducer and a different range of frequencies, it was treated separately, resulting in an average k of 0.21. The results for the other three holes were averaged together, giving a k of 0.17. The agreement between holes is fair. The overall average for k is 0.19 ± 0.02, three times that given by the McCammon-McDaniel model for horizontal transmission. The value of k is about the same as that obtained in the previous section (VI.D), but the accuracy of the result is five times better.

These measurements indicate that the absorption coefficient for vertical transmission is given by

$$\alpha = 0.19f\left[\frac{-6}{T}\right]^{2/3} \text{ dB/m}. \tag{22}$$

For 20 kHz, this gives an absorption coefficient of 7.9 dB/m at −2°C and 1.5 dB/m at −25°C.

Why was the amplitude of the first cycle so uniform with depth in the ice and the amplitude of the later cycles so erratic? This may be caused by later arrivals, either from surfaces above the hydrophone or from rays deflected at the interface. The signal usually reached steady state in 0.1 ms. Reflections from the surface of the water placed in the hole to improve coupling would arrive within this time if the surface was less than 7 cm above the transducer. Except for the first measurement, holes 1–3 had much more water than that. A deflected ray that intercepted the ice 65 cm off to one side would arrive at the receiver near the top of the ice 100 μs later if it had been deflected 25° as it entered the ice—a path that might be possible.

Table 28. Summary of absorption constants k determined from transmissions through several thicknesses of ice at four holes.

Location	Transmitted Frequency (kHz)	First Cycle Frequency (kHz)	k	Correlation Coefficient	Average k
Hole 1	30	60	0.21	0.73	
	40	66	0.24	0.76	
	60	72	0.24	0.74	
	80	83	0.22	0.71	
	100	93	0.19	0.71	
	120	96	0.19	0.69	
	160	91	0.23	0.75	
	200	83	0.20	0.71	
	300	94	0.19	0.71	Hole 1 = 0.21 ± 0.01
Hole 2	20	57	0.174	0.78	
	30	58	0.174	0.82	
	40	61	0.167	0.85	
	60	66	0.169	0.84	
	80	73	0.166	0.91	
Hole 3	20	57	0.212	0.83	
	30	58	0.205	0.86	
	40	61	0.202	0.88	
	60	66	0.215	0.94	
	80	73	0.205	0.94	
Hole 4	20	57	0.143	0.87	
	30	58	0.141	0.87	
	40	61	0.144	0.91	
	60	66	0.139	0.90	
	80	73	0.138	0.93	Holes 2–4 = 0.17 ± 0.01
					Overall = 0.19 ± 0.02

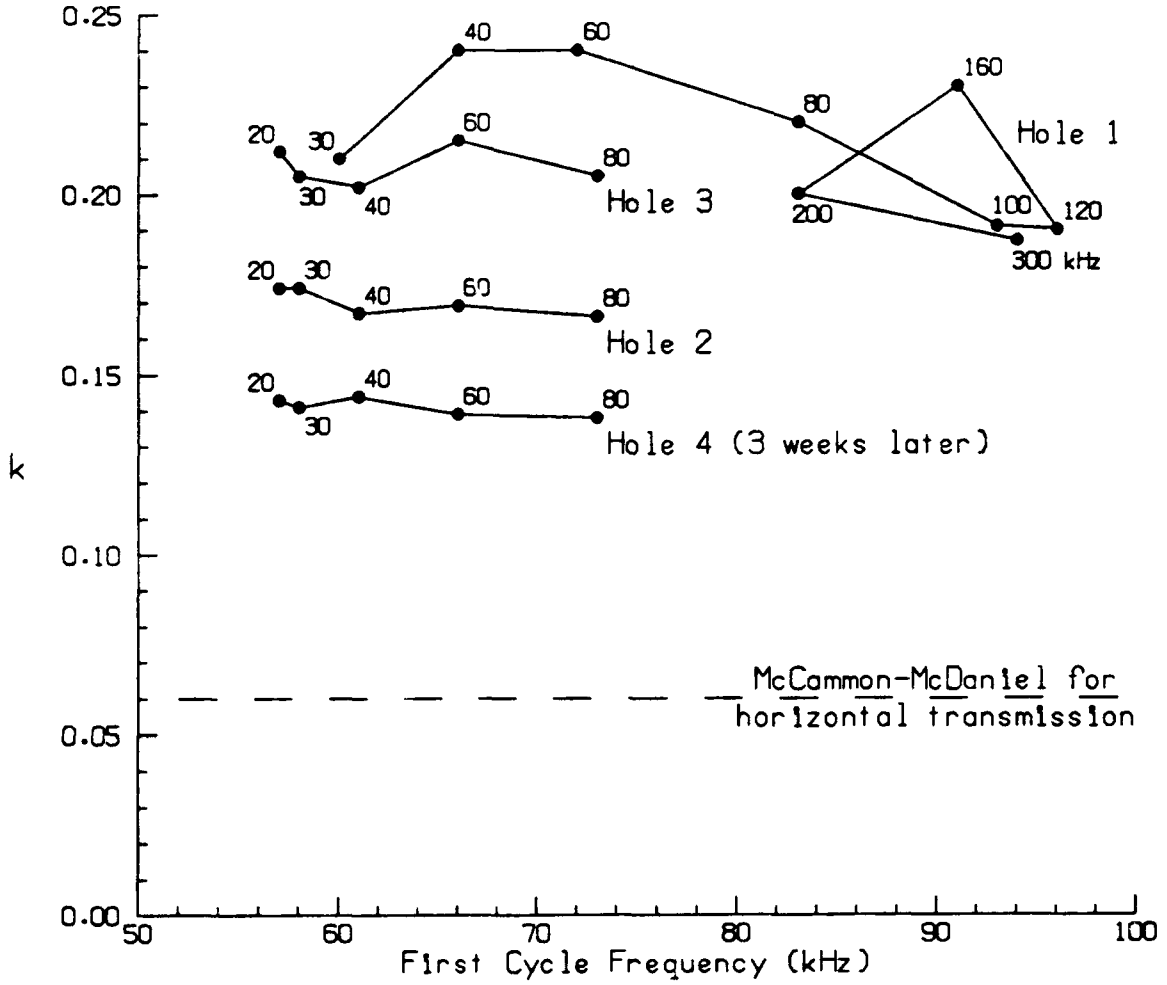

Figure 47. The coefficient k in the absorption model, $\alpha = kf\left[\frac{-6}{T}\right]^{2/3}$, as determined by one-way transmissions at four locations (holes 1–4).

Is there a higher absorption in the skeletal layer than in the ice above? This was determined by comparing the signal level just inside the ice with the level in the water below the ice. The signal level in the ice was obtained from the zero axis intercepts in Figure 46. The signal levels in the water were measured after each set of in-ice measurements. The difference between the in-ice and in-water sound levels is due to the change in amplitude at the interface plus the extra loss in the skeletal layer. For the change in amplitude at the interface, we referred to Figure 23, which shows the amplitude reflection coefficients, R_a. The amplitude of the sound entering the ice should have been $1 + R_a$ times the incident amplitude. We compared this gain, $20\log(1+R_a)$, with the total loss to determine the loss due to absorption in the skeletal layer. This difference is shown for all holes and all frequencies in Tables 29 and 30. Because the spread in first-cycle

Table 29. Measured total loss in signal level at the interface and calculated absorption loss in the skeletal layer for hole 1, using the 22×22 transducer as the transmitter.

Transmitted Frequency (kHz)	First Cycle Frequency (kHz)	L_0 from[a] Best-Fit Line (dB)	Received Amplitude (V_{pp})	L at Receiver[b] Below the Ice (dB)	Total Loss (dB)
30	60	−31.6	109	−30.3	1.3
40	66	−26.2	154	−27.3	−1.1
60	72	−16.2	532	−16.5	−0.3
80	83	−15.4	636	−15.0	0.4
100	93	−11.1	1272	−8.9	2.2
120	96	−13.0	1096	−10.2	2.8
160	91	−17.8	624	−15.1	2.7
200	83	−23.6	342	−20.4	3.2
300	94	−27.5	170	−26.4	1.1
				Average Loss	1.4 ±0.5 dB
				Gain at interface with R_a = 0.09	0.7 dB
				Sum is skeletal layer absorption loss	2.1 dB

[a] For simplicity, we used a transmitter voltage V_x of 1.0 V, peak to peak, even though there were small variations.

[b] For the signal level below the ice, Eq. (17) inputs are R = 28 m, G = 0, V_x = 0.5 V, peak to peak.

frequency was small, we treated all the data together. The results are shown at the bottoms of the tables. For hole 1, we calculate an absorption of 2.1 dB for the skeletal layer. For holes 2, 3, and 4, the results are quite consistent, giving an average of 2.2 dB.

Table 30. Measured total loss in signal level at the interface and calculated absorption loss in the skeletal layer for holes 2–4, using the ITC 1042 transducer as the transmitter.

Transmitted Frequency (kHz)	First Cycle Frequency (kHz)	L_0 from Best-Fit Line			L at Receiver Below the Ice			Total Loss (dB)
		Hole 2 (dB)	Hole 3 (dB)	Average (dB)	Hole 2 (dB)	Hole 3 (dB)	Average (dB)	
20	52	−17.5	−16.4	−16.9	−16.5	−14.1	−15.3	1.6
30	53	−13.2	−12.6	−12.9	−11.8	−10.1	−11.0	1.9
40	57	−11.6	−10.4	−11.0	−10.4	−9.3	−9.8	1.2
60	60	−6.0	−4.4	−5.2	−4.6	−3.8	−4.2	1.0
80	62	−1.3	−0.2	−0.8	−1.1	+0.6	−0.2	0.6
		Hole 4			1st	2nd		
20	52	−18.4			−16.9	−16.1	−16.5	1.9
30	53	−14.7			−13.3	−14.1	−13.7	1.0
40	57	−12.4			−11.5	−11.5	−11.5	0.9
60	60	−10.3			−9.5	−10.0	−9.7	0.6
80	62	−8.9			−7.9	−8.6	−8.3	0.6

Average loss (equal weight per hole) 1.2 ± 0.1 dB

Gain at interface, with $R_a = 0.12$ 1.0 dB

Sum is skeletal layer absorption loss 2.2 dB

VII. SUMMARY OF ACOUSTIC PROPERTIES OF THE ICE

A. Sound Speed

1. Average Speed

The average vertical sound speeds in the ice calculated from the acoustic measurements of arctic ice made by APL in 1988 are summarized below:

Calculated from front- and back-surface reflections

Submerged cylindrical blocks (140-cm-thick-ice) ..... 3480 m/s
Growing ice in hole (50-cm-thick ice) ..... 3360 m/s
Ice cover (140-cm-thick ice) ..... 3642 m/s
Ice adjacent to first growing ice hole (139-cm-thick ice) ..... 3757 m/s
Ice adjacent to second growing ice hole (142-cm-thick ice) ..... 3640 m/s

Calculated from one-way transmissions

Ice cover (140-cm-thick ice) ..... 3635 m/s

In calculating an average value for the ice cover in Spring 1988, we have omitted the growing-ice result because the skeletal layer has a lower sound speed, and thus thinner ice may have a lower average. The average and the standard deviation from the average for the latter four measurements, all in the natural 139–140-cm-thick ice cover, are

$$\text{Average sound speed} = 3669 \pm 29 \text{ m/s} . \qquad (23)$$

Equations relating elastic strength properties to the physical properties (temperature, salinity, and density) give a result about 100 m/s higher, possibly because the skeletal layer is not included. The equations do not apply to the skeletal layer because the ice is not homogeneous.

2. *Sound Speed Profile*

A sound speed profile calculated from measurements of the temperature, salinity, and density in ice core sections taken in 1988 showed a constant value in the solid ice but a pronounced decrease in sound speed in the section at the bottom containing the skeletal-layer transition zone. Measurements of acoustic reflection from growing ice (Section III) and acoustic transmission through the ice (Section VI) showed a similar dropoff in sound speed near the bottom of the ice cover. The average sound speed for the lower 2–3 cm appears to be about 2000 m/s. It is quite possible that there may be a gradual transition of the sound speed in the skeletal layer to the water sound speed of 1440 m/s.

B. Amplitude Reflection Coefficient

The measured amplitude reflection coefficients are shown in Figure 48 along with the results from the ice-block experiments[2,5] and with measurements of thin ice by Stanton et al.[12] We offer two explanations for the decrease in R_a with frequency and another for some of the irregularities.

1. *Decrease Due to Surface Variations*

A surface variation, or roughness, with a scale near 1/4 wavelength (1.8 and 0.4 cm for 20 and 100 kHz) will cause differences of 180° in the phase of the reflections and therefore destructive interference. The large decrease in R_a seen in Figure 48 between 20 and 100 kHz could be caused by a surface variation somewhere between 1.8 and 0.4 cm. The lower surface of an 84-cm-diameter, cylindrical block of ice taken from the field used for the acoustic measurements was measured with a probe and found to have a peak-to-peak deviation of 0.85 ± 0.3 cm from a plane. Thus surface variation alone may provide sufficient phase cancellation to lower the reflections.

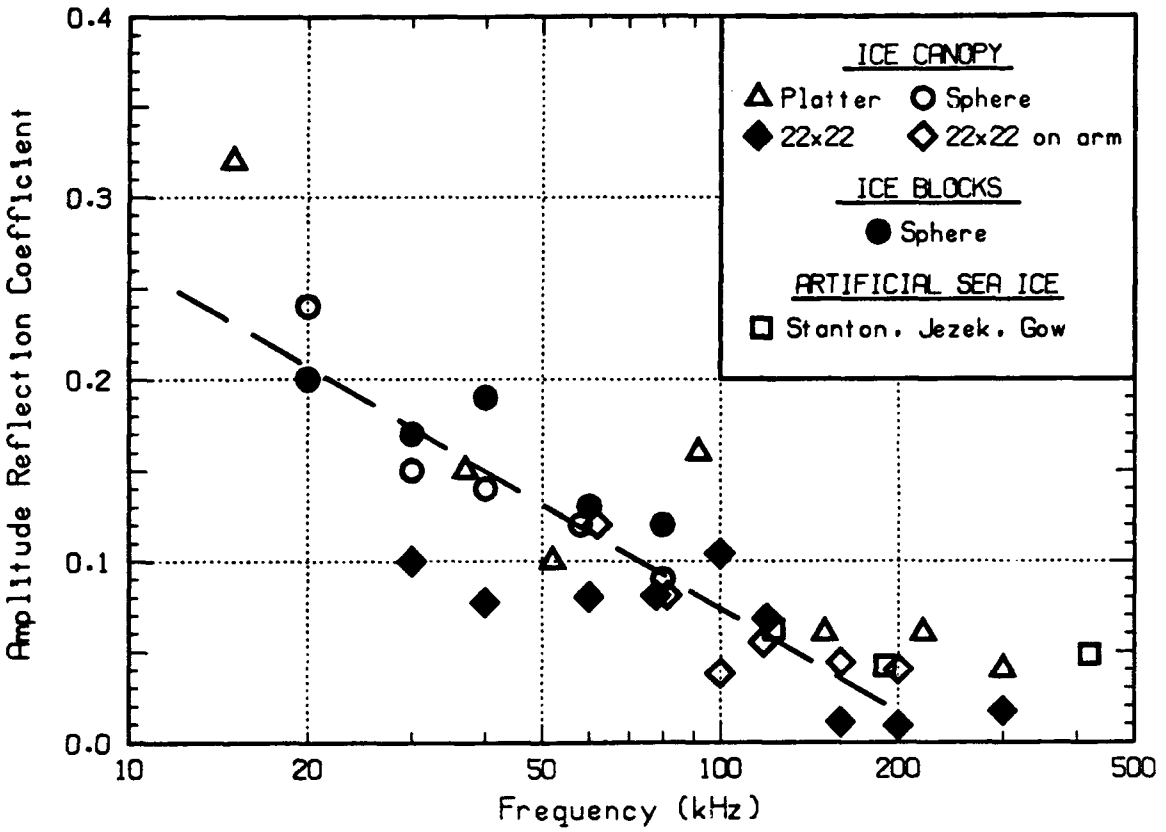

Figure 48. Reflection coefficients for the underside of the ice. Data from the ice-block experiment and from Stanton et al.[12] are included for comparison. The line $R_a = 0.454 - 19\log f$ is the best fit of a line to the APL data for frequencies below 200 Hz.

2. *Decrease Due to Variations in Sound Speed Profile*

Calculations of the sound speed profile in the ice show a gradual decrease near the bottom in the skeletal-layer transition zone. With such a profile, the amplitude reflection coefficient can no longer be expected to be the value calculated for the acoustic impedance change from water to average ice. A model of a fluid medium in which the sound speed varies arbitrarily with depth was generalized by Winebrenner[13] and used to

predict that the sound speed profile shown in Figure 49b will produce the amplitude reflection coefficient curve plotted in Figure 49a, which is a good fit to the measured results.

At lower frequencies, we consider that, for acoustic purposes, the ice is represented by its bulk properties of sound speed and density. The transition from ice to water involves an impedance change that corresponds to R_a = 0.41. The curve should be asymptotic to this value at low frequencies, as it appears to be in Figure 49a.

The modeled profile shown in Figure 49b drops off more sharply than the measured profile in Figure 43. However, measurements in the dropoff region are very difficult to make and thus may be in error. We feel that the agreement is good enough that the model deserves further study and testing.

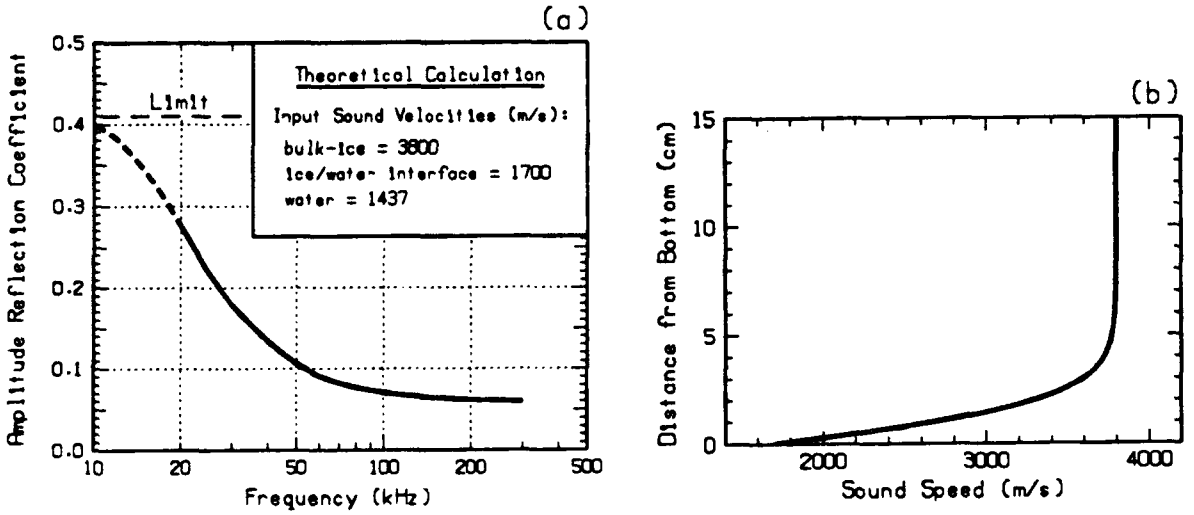

Figure 49. Frequency-dependent reflection coefficient (a) calculated for the hypothetical sound speed profile (b) that was selected to take into account the two general regions of the ice, i.e., the skeletal-layer transition zone and the columnar zone. Below 20 kHz, calculations show that the reflection coefficient tends toward the low-frequency limit as computed from bulk properties.

3. *Irregularities Due to Interference*

Another possibility is that the skeletal layer provides two abrupt impedance changes, one at the bottom and one at the top. Deviations from a smooth frequency dependence may occur because the two resulting closely spaced reflections would exhibit interference effects. Some echoes measured from the bottom of a 58-cm-diameter ice block were examined in detail and shown to be the sum of two reflections—one from the bottom and another, at half the amplitude, from the top of the skeletal layer—spaced 11 μs apart. The interference between two such reflections would reduce the amplitude by one-half at 45 kHz and increase the amplitude by 1.5 at 91 kHz. Some evidence of this effect can be seen in Figure 48, in which high values are seen at 90–100 kHz for the platter and the 22×22 transducers. No data were taken at 45 kHz, so it is impossible to tell whether there is a corresponding dip at that frequency.

C. Sound Absorption

Two methods were used to measure sound absorption in the ice. In the first, the absorption was measured directly from one-way transmissions through the ice. One possible source of error with this method is that a different ping was used for each thickness of ice, and the transmitted signal may have varied. To avoid the effect of reflections or interfering paths, we computed the absorption coefficient using only the first cycle of the transmissions. The measurements give a value of 0.19 ± 0.02 for the absorption coefficient k used in the McCammon-McDaniel model, $\alpha = kf(-6/T)^{2/3}$; McCammon and McDaniel used $k = 0.06$ to match the horizontal measurements made by Langleben[14] at −6°C. Some measurements of the sound level in the water just below the ice indicate a loss of 2.3 dB in the skeletal layer.

In the second method, the absorption was determined from reflections from the lower and upper surfaces of the ice. This method assumes that we can estimate the reflectivity of the upper face and that all sound not specularly reflected from the lower surface enters the ice. All returns from the 140-cm-thick ice indicate a loss of about 1 dB

each way in the skeletal layer, followed by an absorption in the ice that is again about three times that of the McCammon-McDaniel model.

In contrast, the absorption calculated for the returns from growing ice in the 2×2-m hole was quite erratic and high, 10 times the McCammon-McDaniel value. A possible explanation for these high values is that there was more supercooled water in the protected hole and that the crystals grew without disturbance from the current, forming a very irregular surface which caused considerable scattering. This caused a reduction in R_a, which, as seen in Figure 5, reached a value much lower than expected after 100 hours of freezing and remained low for the duration of the experiment. On passing downward through the lower surface, the return was also reduced by scattering. In our calculations, scattering losses are ignored. The reduction in the return from the upper surface due to scattering results in an apparently high absorption.

In summary, the absorption calculated directly from the first cycle of vertical transmissions through the ice, thus avoiding extraneous paths and reflections, is considered quite accurate. The absorption obtained by comparing reflections from the lower and upper surfaces of the ice is less accurate but in good agreement. Although we do not claim to have substantiated the temperature and frequency dependence of the McCammon-McDaniel model, which was for horizontal transmissions, we find that these dependencies are good for our vertical measurements at 15–100 kHz in ice with a linear temperature profile from −2 to −25°C; however, we calculate a constant of 0.19 rather than their 0.06. Our recommended model for absorption of sound transmitted vertically in the ice at these frequencies and under these conditions is

$$\alpha = 0.19f(-6/T)^{2/3} \quad \text{dB/m}, \tag{24}$$

where f is the frequency in kilohertz and T is the temperature in degrees Celsius. The skeletal layer and transition zone appear to have an extra absorption of 2 dB.

For the uniform temperature profile often observed in the ice, the average absorption is

$$\bar{\alpha} = (0.19)(3) f 6^{2/3} \frac{(-T_2)^{1/3} - (-T_1)^{1/3}}{T_1 - T_2} \tag{25}$$

$$= 1.9 f \frac{(-T_2)^{1/3} - (-T_1)^{1/3}}{T_1 - T_2} \text{ dB/m},$$

where T_1 and T_2 are the temperature at the top and bottom of the ice, respectively.

It should be noted, however, that our measurements were in first-year ice. Multiyear ice has a lower salinity, having gone through one or more melt seasons. The Pounder and Langleben[15] measurements, the major source for the McCammon-McDaniel model, were made in sea ice that had a salinity of 1 ppt in the 1967 measurements and 4 ppt in the 1969 measurements. The salinity of the ice in our measurements was higher, varying from 4–9 ppt. The absorption loss, and also the sound speed, in sea ice is expected to be a function of brine porosity and air porosity, plus the temperature effect on the (pure) ice as a matrix material. Further work, perhaps under laboratory controlled conditions, is required to establish the combined effects of salinity and temperature on the acoustic absorption of sea ice. Until such refinements are made, we believe that Eq. (24) provides the best estimate to use in analyzing the performance of sonar systems.

D. Use of Reflections to Measure Ice Thickness

Much interest has been expressed in measuring ice thickness acoustically from below. Such measurements would be particularly helpful for sea-ice penetration studies, where the greatest interest is in first-year ice, which ranges in thickness from a few centimeters to 2 m. Multiyear ice is thicker and, in general, much stronger because of desalinization over the previous melt season(s). The accuracy of thickness estimates becomes more important as the thickness increases because of the square-law relationship of penetrating force to ice thickness. The following factors need to be considered in designing equipment for measuring ice thickness:

(1) The amplitude reflection coefficient R_a decreases with frequency.

(2) Absorption loss in the ice increases with frequency.

(3) For best measurement of the difference between the arrivals times of reflections from the front and back faces of first-year ice, the amplitude of the two returns should be roughly equal so that the rise times of the pulses can be estimated with similar error.

(4) In general, the higher the frequency, the better the time resolution.

(5) Highly directive vertical beams are required for measurement accuracy, and such beams require a primary transmission of high frequency.

For general surveys of ice with a thickness of several meters, a parametric sonar may provide a low-frequency system that will satisfy some requirements. The above considerations also apply to the choice of the difference frequency and to ice thickness/accuracy tradeoffs.

The opposing effects of a decrease in reflectivity with frequency and an increase in absorption with frequency must be compared to determine at what frequency the reflection from the back face will have an amplitude near that of the reflection from the front face.

To do this, we use Eq. (3) to calculate the ratio of the back-face amplitude to the front-face amplitude from the total two-way absorption loss, $2L$;

$$\frac{V_2}{V_1} = 10^{-2L/20} \frac{(1-R_a^2)(R_b)}{R_a(1+tN/R)} . \tag{26}$$

For R_a we use the value $R_a = 0.454 - 0.19f$ from Figure 48. For L we use the line in Figure 24, which has the relation

$$L = 0.8 + 0.22qt \quad \text{(dB)} . \tag{27}$$

For typical arctic conditions, this can be written

$$L = 0.8 + 0.144ft \quad \text{(dB)} \tag{28}$$

using Eq. (8), i.e., $q = 0.655f$. To get the total absorption loss $2L$, we multiply this by 2. A plot of V_2/V_1 as a function of ice thickness and frequency, as given by Eq. (26) with $R_b = -1$ and for no refraction correction, is shown in Figure 50. The curve for $V_2 = V_1$ indicates the best frequency to use for thickness of ice t. For example, if the thickness is expected to be about 1 m, use 60 kHz; for a thickness of 2 m, use 20 kHz. For a system with a single frequency, a compromise frequency could be selected for the thicknesses considered most important.

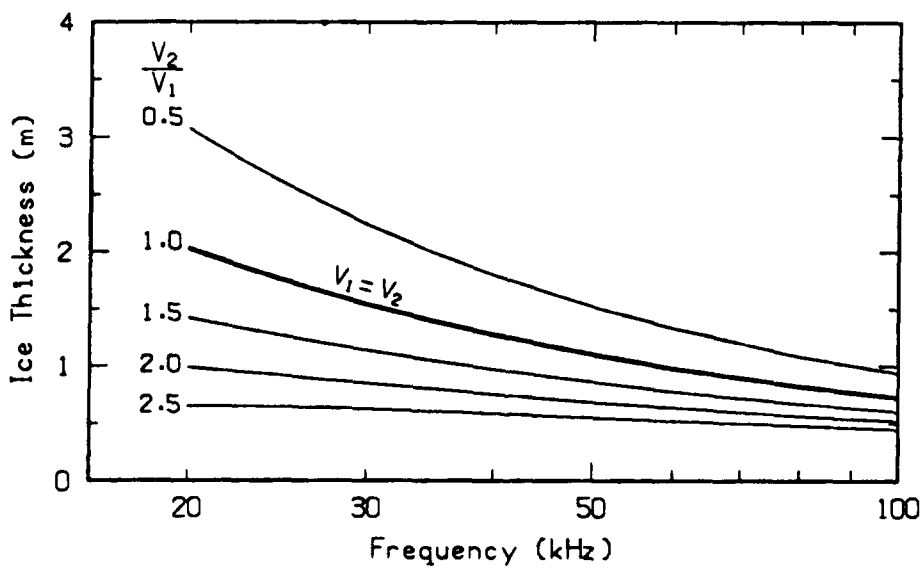

Figure 50. Amplitude ratio of upper surface reflection to lower surface reflection as a function of frequency.

VIII. REFERENCES

1. D.F. McCammon and S.T. McDaniel, The influence of the physical properties of ice on reflectivity, *J. Acoust. Soc. Am., 77:*499–507 (1985).

2. G.R. Garrison, R.E. Francois, T. Wen, and W.J. Felton, Acoustic Reflections from Cylindrical Blocks of Arctic Ice, 1988, APL-UW TR 8815, Applied Physics Laboratory, University of Washington, Seattle, January 1990.

3. R.E. Francois and J.G. Harrison, A thermal drill for making large holes in sea ice, *OCEANS'75,* 303–310, 1975.

4. D.L. Anderson, Growth rate of sea ice, *J. Glaciol. 3:*1170–1172 (1961).

5. G.R. Garrison, R.E. Francois, T. Wen, and R.P. Stein, Acoustic Reflections from Cylindrical Blocks of Arctic Ice, 1986, APL-UW 8707, Applied Physics Laboratory, University of Washington, Seattle, August 1988.

6. B.M. Marks and E.E. Mikeska, Reflections from focused liquid-filled spherical reflectors, *J. Acoust. Soc. Am., 59:*813–817 (1976).

7. R.J. Urick, *Principles of Underwater Sound* (McGraw-Hill, New York, 1975).

8. R.E. Francois, K.L. Williams, G.R. Garrison, P.D. Mourad, and T. Wen, ICE KEELS I: Intrinsic physical/acoustic properties of sea ice and scattering from ice surfaces (U), *U.S. Navy Journal of Underwater Acoustics, 39:* 1203–1228 (1989). [unclassified portion of secret document]

9. G.F.N. Cox and W F. Weeks, Equations for determining the gas and brine volumes in sea-ice samples, *J. Glaciol., 29:*306–316 (1983).

10. S. Senmoto and D.G. Childers, Signal resolution via digital inverse filtering, *IEEE Trans. Aerospace Electr. Sys., AES-8:* 633–640 (1972).

11. T. Wen, W.J. Felton, J.C. Luby, W.L.J. Fox, and K.L. Kientz, Environmental Measurements in the Beaufort Sea, Spring 1988, APL-UW TR 8822, Applied Physics Laboratory, University of Washington, Seattle, March 1989.

12. T. K. Stanton, K. C Jezek, and A. J. Gow, Acoustical reflection and scattering from the underside of laboratory grown sea ice: Measurements and predictions, *J. Acoust. Soc. Am., 80:* 1486–1494 (1986).

13. D. Winebrenner, Acoustic backscattering from sea ice at 10–100 kHz, unpublished report, Applied Physics Laboratory, University of Washington, Seattle, January 1991.

14. M. P. Langleben, Attenuation of sound in sea ice, 10–500 kHz, *J. Glaciol., 8:* 399–406 (1969).

15. E. R. Pounder and M. P. Langleben, Acoustic attenuation in sea ice, in *International Association of Scientific Hydrology, 77* (Ice Research Project, McGill University, Montreal, Canada, 1968) pp. 161–169.

APPENDIX A

Tables of Under-Ice Acoustic-Reflection Measurements

The echoes that were recorded on diskette in the field with the Nicolet oscilloscope were examined, and the average voltages of various echoes were read manually. The following three tables give the resulting data for the three transducers used in the measurements.

Table A1. Measurements of reflection from the upper and lower surfaces of the ice canopy with the ITC 1042 transducer.

Track No.	Freq. (kHz)	T_x (V_p)	Received Sphere (mV_p)	Received V_1 (mV_p)	Received V_2 (mV_p)	Gain (dB)	CAL (dB)	Sphere[a] TS (dB)	Reflection[b] Gain (dB)	Amplitude[c] Reflection Coef., R_a
				Location N2, E23						
1	20	189	108	764	1167	72	−75	−6.6	−9.7	0.33
2	30	220	181	698	1164	72	−70	−8.2	−16.5	0.15
3	40	182	210	650	1168	72	−65	−10.1	−20.3	0.10
4	60	156	1396	2430	2256	72	−50	−7.0	−22.4	0.08
5	80	145	718	1344	944	72	−50	−12.0	−26.5	0.05
				Location N18, E23						
6	20	189	134	470	690	72	−75	−4.7	−13.9	0.20
7	30	214	206	538	908	72	−70	−6.8	−18.5	0.12
8	40	187	420	998	600	72	−65	−4.3	−17.1	0.14
9	60	156	1298	3492	2408	72	−50	−7.7	−19.2	0.11
10	80	145	940	2456	1552	72	−50	−9.6	−21.9	0.08
				Location N40, E16						
11	20	189	92	468	436	72	−75	−8.0	−14.0	0.20
12	30	212	190	540	776	72	−70	−7.5	−18.5	0.12
13	40	182	302	1068	742	72	−65	−6.9	−15.9	0.16
14	60	164	920	4816	1494	72	−50	−11.1	−17.1	0.14
15	80	141	880	2656	848	72	−50	−10.0	−20.0	0.10
				Location N24, E16						
16	20	199	92	412	596	72	−75	−8.4	−16.5	0.15
17	30	213	227	492	588	72	−70	−5.9	−19.2	0.11
18	40	185	378	856	644	72	−65	−5.1	−18.5	0.12
19	60	157	1406	3490	810	72	−50	−7.0	−19.2	0.11
20	80	142	1222	2752	848	72	−50	−7.2	−20.0	0.10
				Location N24, E40						
1	20	194	66	391	492	66	−75	−11.1	−9.7	0.33
2	30	212	100	360	752	66	−70	−13.0	−13.9	0.20
3	40	185	208	552	864	66	−65	−10.3	−14.9	0.18
4	60	159	695	2136	1188	66	−50	−13.3	−17.7	0.13
5	80	140	592	1665	1049	66	−50	−13.4	−18.5	0.12
				Location N40, E40						
6	20	192	30	299	371	66	−75	−17.8	−12.0	0.25
7	30	217	73	348	404	66	−70	−16.0	−15.4	0.17
8	40	186	169	591	568	66	−65	−12.1	−15.4	0.17
9	60	155	505	2725	1314	66	−50	−15.9	−15.4	0.17
10	80	140	379	1384	686	66	−50	−17.3	−19.2	0.11

[a]Sphere TS = $20\log(V/T_X)$ − CAL − Gain + $40\log R + 2\alpha R$. For a return time of 33.0 ms, R = 23.8 m and $2\alpha R$ was 0.2, 0.4, 0.6, 0.8, and 1.0, respectively, for the five frequencies.

[b]Reflection gain = $20\log(V_1/T_X)$ − CAL − Gain + $20\log 2R + 2\alpha R$. For a return time of 39.4 ms, R = 28.2 m.

[c]Define R_a by Reflection Gain = $20\log R_a$.

Table A2. Measurements of reflections from both ice surfaces with the platter transducer.

Track No.	Freq. (kHz)	Pulse Length (ms)	Time (ms)	Transmit T_x (V_{pp})	Received V_1 (V_{pp})	Received V_2 (V_{pp})	Cal (dB)	Reflection Gain[a] (dB)	Amplitude Reflection Coef.,[b] R_a
				Location 1a					
1	15	0.35	13.8	47.2	1.07	1.69	−36.4	−10.5	0.30
2	37	0.35	13.7	165.6	2.86	1.94	−31.6	−17.6	0.13
3	52	0.35	13.7	47.8	3.50	0.98	−14.6	−22.0	0.08
4	92	0.20	13.7	249.6	3.46	0.83	−30.2	−20.7	0.09
5	150	0.20	13.7	304.8	2.50	0.95	−28.0	−27.3	0.04
6	220	0.03	13.7	198.4	1.34	0.56	−21.9	−34.8	0.02
7	300	0.05	13.7	186.4	1.84	0.54	−21.0	−31.9	0.03
				Location 1b					
8	15	0.35	12.0	49.6	1.31	–	−36.4	−10.4	0.30
9	37	0.35	12.0	164.0	3.82	2.62	−31.6	−16.2	0.16
10	52	0.35	12.0	23.0	2.96	1.52	−14.6	−18.3	0.12
11	92	0.20	12.0	122.4	4.34	0.97	−30.2	−13.7	0.21
12	150	0.20	12.0	157.6	2.08	0.85	−28.0	−24.4	0.06
13	220	0.03	12.0	189.0	6.95	0.87	−21.9	−21.3	0.09
14	300	0.05	12.0	186.0	5.30	1.12	−21.0	−24.0	0.06
				Location 2a					
1	15	0.35	11.5	48.0	–	–	-36.4	–	–
2	37	0.35	11.5	164.8	3.54	2.38	−31.6	−17.2	0.14
3	52	0.35	11.5	23.8	1.99	0.94	−14.6	−22.3	0.08
4	92	0.20	11.5	122.0	2.82	0.59	−30.2	−17.8	0.13
5	150	0.20	11.5	157.6	1.71	0.62	−28.0	−26.4	0.05
6	220	0.03	11.5	172.8	2.78	0.62	−21.9	−28.9	0.04
7	300	0.05	11.5	192.8	2.93	0.97	−21.0	−29.9	0.03
				Location 2b					
2	15	0.35	11.2	46.8	1.50	1.78	−36.4	−9.3	0.34
3	37	0.35	11.1	81.4	1.98	2.61	−31.6	−16.5	0.15
4	52	0.35	11.1	23.6	2.75	1.34	−14.6	−19.8	0.10
5	92	0.20	11.1	121.6	4.72	0.74	−30.2	−13.7	0.21
6	150	0.20	11.1	159.2	1.84	0.77	−28.0	−26.2	0.05
7	220	0.03	11.1	197.6	6.91	0.85	−21.9	−22.5	0.08
8	300	0.05	11.1	227.2	4.21	1.22	−21.0	−28.6	0.04
				Location 3a					
1	15	0.35	11.0	46.2	1.44	2.10	−36.4	−9.7	0.33
2	37	0.35	10.8	164.0	4.24	3.25	−31.6	−16.2	0.16
3	52	0.35	10.8	22.9	2.72	1.68	−14.6	−19.9	0.10
4	92	0.20	10.8	124.0	4.36	1.08	−30.2	−14.7	0.18
5	150	0.20	10.8	158.4	3.10	1.09	−28.0	−21.9	0.08
6	220	0.03	10.8	194.4	7.43	1.10	−21.9	−21.9	0.08
7	300	0.05	10.8	186.4	5.72	1.81	−21.0	−24.4	0.06

[a] Range = 7.8 to 10.0 m, Spreading loss = $20 \log 2R$ = 23.9 to 26.0 dB, Absorption loss = $2\alpha R$ = 0.1 to 1.3 dB, Receiver Gain = 40 dB

[b] Define R_a by Reflection Gain = $20 \log R_a$

Table A3. Measurements of reflections from both ice surfaces with the 22×22 transducer.

Track No	Freq (kHz)	Pulse Length (ms)	Time (ms)	Transmit T_x (V_{pp})	Received V_1 (V_{pp})	Received V_2 (V_{pp})	Cal (dB)	Reflection Gain[a] (dB)	Amplitude Reflection Coef.,[b] R_a
				Location N13, E32					
10	30	0.50	39.3	183.0	131	91	−67.8	−19.7	0.10
11	40	0.50	39.3	182.0	120	93	−64.4	−23.6	0.07
12	60	0.50	39.3	149.0	242	87	−57.7	−22.2	0.08
13	80	0.50	39.3	90.4	300	–	−51.1	−22.4	0.08
14	100	0.50	39.3	52.0	500	–	−45.0	−19.2	0.11
15	120	0.50	39.3	33.0	360	–	−39.0	−23.9	0.06
16	160	0.50	39.3	29.2	158	–	−28.0	−40.6	0.009
17	200	0.50	39.3	28.2	490	–	−20.3	−37.7	0.013
18	300	0.20	39.3	54.0	300	–	−30.5	−35.9	0.016
				Location N22, E30					
1	30	0.50	38.9	191.9	123	166	−67.8	−20.7	0.09
2	40	0.50	39.6	187.2	129	132	−64.4	−23.2	0.07
3	60	0.50	39.6	155.2	203	52	−57.7	−24.0	0.06
4	80	0.50	39.6	91.6	350	64	−51.1	−21.1	0.09
5	100	0.50	39.6	51.6	355	–	−45.0	−22.0	0.08
6	120	0.50	39.6	32.4	320	–	−39.0	−24.7	0.06
7	160	0.50	39.6	28.4	84	–	−28.0	−45.7	0.005
8	200	0.50	39.6	29.5	432	–	−20.3	−39.1	0.011
9	300	0.20	39.6	56.0	348	–	−30.5	−34.8	0.018
				Location N12, E22					
10	30	0.50	39.3	187.0	140	167	−67.8	−19.3	0.11
11	40	0.50	39.3	187.0	144	233	−64.4	−22.3	0.08
12	60	0.50	39.3	158.0	215	106	−57.7	−23.8	0.06
13	80	0.50	39.3	104.0	385	102	−51.1	−21.5	0.08
14	100	0.50	39.3	58.4	396	–	−45.0	−22.2	0.08
15	120	0.50	39.3	37.6	326	–	−39.0	−25.9	0.05
16	160	0.50	39.3	31.2	210	–	−28.0	−38.7	0.012
17	200	0.50	39.3	28.8	244	–	−20.3	−43.9	0.006
18	300	0.20	39.3	59.6	262	–	−30.5	−37.9	0.013
				Location N13, E14					
1	30	0.50	39.2	187.0	114	175	−67.8	−21.1	0.09
2	40	0.50	39.2	190.0	143	143	−64.4	−22.5	0.08
3	60	0.50	39.2	163.0	231	102	−57.7	−23.4	0.07
4	80	0.50	39.2	107.0	428	94	−51.1	−20.8	0.09
5	100	0.50	39.2	58.4	638	–	−45.0	−18.1	0.12
6	120	0.50	39.2	37.9	360	–	−39.0	−25.1	0.06
7	160	0.50	39.2	31.0	160	125	−28.0	−41.0	0.009
8	200	0.50	39.2	30.7	266	–	−20.3	−43.8	0.006
9	300	0.20	39.2	57.0	263	–	−30.5	−37.5	0.013
				Location N28, E16					
10	30	0.50	38.5	185.6	118	203	−67.8	−20.9	0.09
11	40	0.50	38.5	188.8	125	173	−64.4	−23.8	0.06
12	60	0.50	38.5	168.0	292	216	−57.7	−21.8	0.08
13	80	0.50	38.5	100.0	322	–	−51.1	−22.9	0.07
14	100	0.50	38.5	60.0	470	–	−45.0	−21.1	0.09
15	120	0.50	38.5	37.6	387	–	−39.0	−24.6	0.06
16	160	0.50	38.5	31.6	238	–	−28.0	−37.9	0.013
17	200	0.50	38.5	30.0	252	–	−20.3	−44.2	0.006
18	300	0.20	38.5	60.0	368	–	−30.5	−35.3	0.017

[a] Range = 26.9 to 28.5 m, Spreading loss = $20 \log 2R$ = 34.6 to 35.1 dB, Absorption loss = $2\alpha R$ = 0.4 to 3.7 dB, Receiver Gain = 60 dB

[b] Define R_a by Reflection Gain = $20 \log R_a$

Table A3. Measurements of reflections from both ice surfaces with the 22×22 transducer, cont.

Track No	Freq (kHz)	Pulse Length (ms)	Time (ms)	Transmit T_x (V_{pp})	Received V_1 (V_{pp})	Received V_2 (V_{pp})	Cal (dB)	Reflection Gain[a] (dB)	Amplitude Reflection Coef.,[b] R_a
				Location N40, E16					
1	30	0.50	37.5	189.0	152	175	-67.8	-19.1	0.11
3	40	0.50	37.5	187.0	162	173	-64.4	-21.7	0.08
4	60	0.50	37.5	170.0	340	128	-57.7	-20.9	0.09
5	80	0.50	37.5	105.0	260	89	-51.1	-25.4	0.05
6	100	0.50	37.5	59.6	537	–	-45.0	-20.2	0.10
7	120	0.50	37.5	38.4	436	–	-39.0	-24.0	0.06
8	160	0.50	37.5	32.4	212	–	-28.0	-39.4	0.011
9	200	0.50	37.5	28.8	314	–	-20.3	-42.2	0.008
10	300	0.20	37.5	56.6	424	–	-30.5	-33.9	0.020
				Location N28, E28					
11	30	0.50	38.6	189.0	118	173	-67.8	-21.0	0.09
12	40	0.50	38.6	190.0	151	180	-64.4	-22.2	0.08
13	60	0.50	38.6	164.0	260	127	-57.7	-22.6	0.07
14	80	0.50	38.6	104.0	342	–	-51.1	-22.7	0.07
15	100	0.50	38.6	61.0	513	–	-45.0	-20.5	0.09
16	120	0.50	38.6	38.0	390	–	-39.0	-24.6	0.06
17	160	0.50	38.6	32.0	156	–	-28.0	-41.7	0.008
18	200	0.50	38.6	31.3	522	–	-20.3	-38.2	0.012
19	300	0.20	38.6	60.0	390	–	-30.5	-34.7	0.018
				Location N40, E28					
1	30	0.50	37.6	189.0	144	163	-67.8	-19.5	0.11
2	40	0.50	37.6	189.0	144	150	-64.4	-22.8	0.07
3	60	0.50	37.6	165.0	275	125	-57.7	-22.4	0.08
4	80	0.50	37.6	106.0	541	59	-51.1	-19.1	0.11
5	100	0.50	37.6	59.2	602	–	-45.0	-19.1	0.11
6	120	0.50	37.6	37.0	376	–	-39.0	-24.9	0.06
7	160	0.50	37.6	31.8	218	–	-28.0	-39.0	0.011
8	200	0.50	37.6	30.0	214	–	-20.3	-45.9	0.005
9	300	0.20	37.6	57.0	344	–	-30.5	-35.7	0.016
				Location N40, E40					
10	30	0.50	37.5	186.0	138	184	-67.8	-19.8	0.10
11	40	0.50	37.5	184.0	180	208	-64.4	-20.6	0.09
12	60	0.50	37.5	163.0	346	170	-57.7	-20.3	0.10
13	80	0.50	37.5	105.0	438	86	-51.1	-20.9	0.09
14	100	0.50	37.5	60.0	710	–	-45.0	-17.8	0.13
15	120	0.50	37.5	37.4	743	–	-39.0	-19.1	0.11
16	160	0.50	37.5	31.2	250	–	-28.0	-37.7	0.013
17	200	0.50	37.5	29.4	366	–	-20.3	-41.1	0.009
18	300	0.20	37.5	58.6	380	–	-30.5	-35.1	0.018
				Location N28, E40					
1	30	0.50	38.5	189.0	141	225	-67.8	-19.5	0.11
2	40	0.50	38.5	190.0	186	231	-64.4	-20.4	0.10
3	60	0.50	38.5	163.0	393	146	-57.7	-19.0	0.11
4	80	0.50	38.5	104.0	341	–	-51.1	-22.7	0.07
5	100	0.50	38.5	60.0	688	–	-45.0	-17.8	0.13
6	120	0.50	38.5	37.4	702	–	-39.0	-19.4	0.11
7	160	0.50	38.5	31.2	358	–	-28.0	-34.3	0.019
8	200	0.50	38.5	29.7	516	–	-20.3	-37.9	0.013
9	300	0.20	38.5	59.8	318	–	-30.5	-36.5	0.015

APPENDIX B

Refraction Correction for Back-Face Reflection

Transmitted sound enters the ice from below as shown in Figure B1. From Snell's Law

$$\frac{\sin\theta_1}{c_1} = \frac{\sin\theta_2}{c_2}\,, \tag{B1}$$

and thus

$$\frac{\sin\theta_2}{\sin\theta_1} = \frac{c_2}{c_1} = N\,. \tag{B2}$$

Figure B1 shows the geometrical relationships

$$b = 2t\tan\theta_2 \tag{B3}$$

$$a = R\tan\theta_1\,, \tag{B4}$$

and, from the larger triangle,

$$a + b = r_2\tan\theta_1\,. \tag{B5}$$

Combining Eqs. (B3), (B4), and (B5), we obtain

$$r_2\tan\theta_1 = R\tan\theta_1 + 2t\tan\theta_2\,, \tag{B6}$$

$$(r_2 - R)\tan\theta_1 = 2t\tan\theta_2 \tag{B7}$$

$$\frac{r_2 - R}{2t} = \frac{\tan\theta_2}{\tan\theta_1}\,. \tag{B8}$$

For small angles, the sine and tangent are nearly equal, and the above ratio is approximately equal to N. Solving for r_2, we obtain

$$r_2 = 2tN + R\,. \tag{B9}$$

The spreading loss for the upper-surface return is over a distance $2(R + r_2)$ compared with $2R$ for the lower-surface return. This causes a reduction in amplitude by $1/F$, where

$$F = \frac{R + r_2}{2R}\,. \tag{B10}$$

Substituting r_2 from above, we obtain

$$F = \frac{2R + 2tN}{2R} = 1 + tN/R\,. \tag{B11}$$

To compensate for the additional spreading loss of the back-face reflection caused by passage through the ice, the amplitude of the back-face return must be multiplied by F to normalize results.

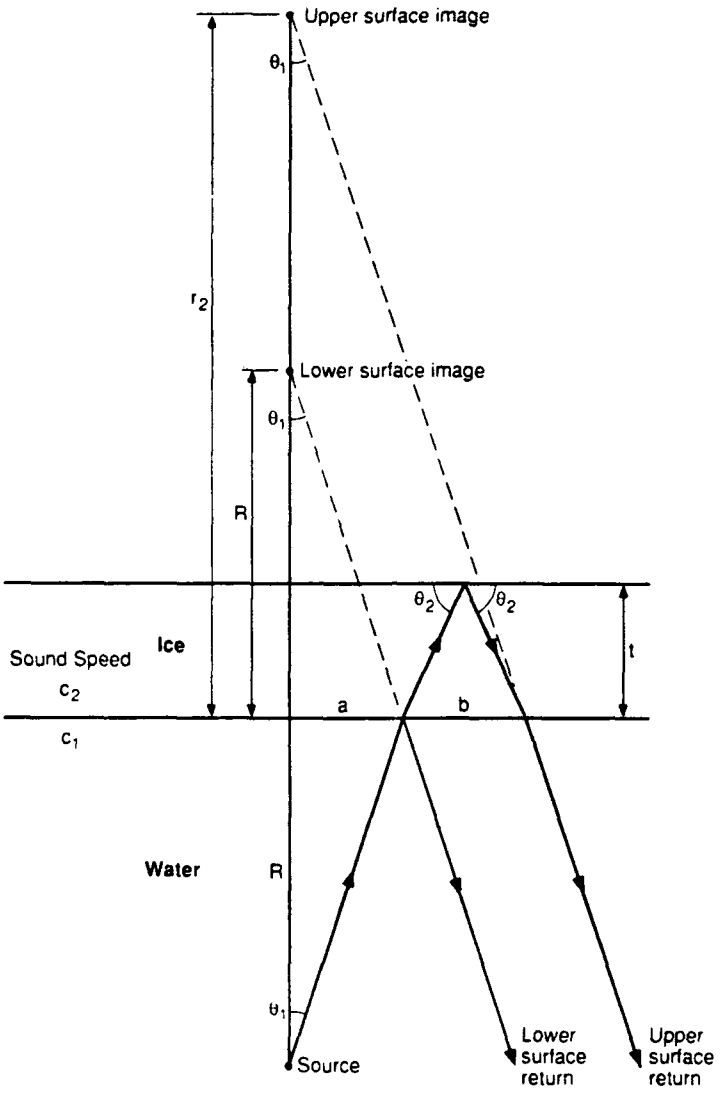

Figure B1. Refraction effects when sound enters the ice and then, after reflection off the upper surface, passes from the ice into the water.

REPORT DOCUMENTATION PAGE

Form Approved OMB No. 0704-0188

1a REPORT SECURITY CLASSIFICATION: Unclassified	1b RESTRICTIVE MARKINGS
2a SECURITY CLASSIFICATION AUTHORITY	3 DISTRIBUTION / AVAILABILITY OF REPORT: Approved for public release; distribution is unlimited
2b DECLASSIFICATION / DOWNGRADING SCHEDULE	
4 PERFORMING ORGANIZATION REPORT NUMBER(S): APL-UW TR 9005	5 MONITORING ORGANIZATION REPORT NUMBER(S): N/A
6a NAME OF PERFORMING ORGANIZATION: Applied Physics Laboratory University of Washington; 6b OFFICE SYMBOL (If applicable)	7a NAME OF MONITORING ORGANIZATION: N/A
6c ADDRESS (City, State, and ZIP Code): 1013 N.E. 40th Street Seattle, WA 98105	7b ADDRESS (City, State, and ZIP Code): N/A
8a NAME OF FUNDING / SPONSORING ORGANIZATION: NOARL; 8b OFFICE SYMBOL (If applicable): Code 242	9 PROCUREMENT INSTRUMENT IDENTIFICATION NUMBER: N00039-91-C-0072
8c ADDRESS (City, State, and ZIP Code): Stennis Space Center, MS 39529-5004	10 SOURCE OF FUNDING NUMBERS: PROGRAM ELEMENT NO: 62435N; PROJECT NO; TASK NO; WORK UNIT ACCESSION NO

11 TITLE (Include Security Classification)

Sound Speed, Reflectivity, and Absorption Measurements in Arctic Ice in 1988

12 PERSONAL AUTHOR(S)

T. Wen, G.R. Garrison, R.E. Francois, R.P. Stein, W.J. Felton

13a TYPE OF REPORT	13b TIME COVERED	14 DATE OF REPORT (Year, Month, Day)	15 PAGE COUNT
Technical	FROM _____ TO _____	March 1991	140

16 SUPPLEMENTARY NOTATION

17 COSATI CODES			18 SUBJECT TERMS (Continue on reverse if necessary and identify by block number)
FIELD	GROUP	SUB-GROUP	Sound speed; Arctic acoustics; Absorption; Skeletal layer of pack ice; Reflectivity; 20-300 kHz
08	03		
17	07		

19 ABSTRACT (Continue on reverse if necessary and identify by block number)

Acoustic measurements at 20–300 kHz were made in the Arctic in Spring 1988 to study sound speed and absorption within the ice canopy and the reflectivity of the water-ice interface. An average sound speed of 3669 ±29 m/s was found for first-year ice, with evidence that the speed varied from 3800 m/s in solid ice to 2000 m/s in the so-called skeletal layer at the lower boundary. The absorption, α, for vertical transmissions was found to be three times as high as that given in the literature for horizontal transmissions; the recommended frequency and temperature dependence is $\alpha = 0.19f(-6/T)^{2/3}$ for temperatures between $T = -2$ and $T = -20$°C. The reflectivity of the lower surface of the ice decreased from 0.2 at 20 kHz to 0.04 at 200 kHz for sound impinging at normal incidence. A simple model that treats the echoes as the sum of reflections from two surfaces, one at the interface between the water and the skeletal layer and one at the transition from the porous skeletal layer to solid ice, matches the experimental results with reasonable accuracy.

20 DISTRIBUTION / AVAILABILITY OF ABSTRACT	21 ABSTRACT SECURITY CLASSIFICATION
☐ UNCLASSIFIED/UNLIMITED ☒ SAME AS RPT ☐ DTIC USERS	Unclassified
22a NAME OF RESPONSIBLE INDIVIDUAL: Robert A. Fisher	22b TELEPHONE (Include Area Code): (601) 688-5520; 22c OFFICE SYMBOL: 242

Initial Distribution List for APL-UW TR 9005

Assistant Secretary of the Navy
(Research, Engineering and Systems)
Department of the Navy
Washington, DC 20350 [2 cp]

Chief of Naval Operations
Department of the Navy
Washington, DC 20350-2000

OP 02
OP 22
OP 223
OP 225
OP 07
OP 071
OP 095
OP 96T
OP 0962E
OP 0962X
OP 098

Director of Defense Research
Office of Assistant Director (Ocean Control)
The Pentagon
Washington, DC 20301-5000

Defense Technical Information Center
Cameron Building #5
Alexandria, VA 22304-6145

Office Chief of Naval Research
Department of the Navy
800 N. Quincy Street
Arlington, VA 22217-5000

OCNR 00
OCNR 000A
OCNR 112
OCNR 1125
OCNR 1125AR
OCNR 1125OA
OCNR 1222T
OCNR 124
OCNR 125 [2 cp]
OCNR 1223

Office of Naval Research
R. Silverman, Resident Representative
315 University District Bldg., JD-16
1107 N.E. 45th Street
Seattle, WA 98195
(Cover Letter & Distribution List Only)

Office of Naval Technology
Department of the Navy
Ballston Center Tower #1
800 N. Quincy Street
Arlington, VA 22217-5000

Code 22
Code 23
Code 23D
Code 231
Code 233
Code 232
Code 234

Director
Defense Advanced Research Project Agency
1400 Wilson Boulevard
Arlington, VA 22209

Commanding Officer
Naval Intelligence Support Center
4301 Suitland Road
Washington, DC 20390

Commanding Officer
Naval Polar Oceanographic Center
4301 Suitland Road
Washington, DC 20390-5140

Library

Center for Naval Analyses
4401 Ford Avenue
P.O. Box 16268
Alexandria, VA 22302-0268

Attn: Technical Information Center

Commander
Space and Naval Warfare Systems Command (NC1)
(SPAWAR)
Department of the Navy
Washington, DC 20363-5100

SPAWAR 03
PMW-180
PMW-181
PMW-182
PMW-182-2

Commander
Naval Sea Systems Command
Department of the Navy
Washington, DC 20362

NSEA 05R
NSEA 06
NSEA 06U2
NSEA 06U3B
NSEA 06UR
NSEA 06UR-45
NSEA 06URB
NSEA 922
Code PM0-402
Code PM0-406
Code PM0-407

Commanding Officer
Naval Underwater Systems Center
Newport, RI 02840

Library [2 cp]
Code 00
Code 22201
Code 382
Code 3824
Code 801
Code 81
Code 8211 [2 cp]
Code 8212
Code 8231
Code 82391 [2 cp]

Officer-in-Charge
New London Laboratory
Naval Underwater Systems Center
New London, CT 06320

Library
Code 01Y [2 cp]
Code 341
Code 2111
Code 2113
Code 3423

Commander
Naval Air Systems Command Hq.
Department of the Navy
Washington, DC 20361

AIR 340L

Commander
Naval Weapons Center
China Lake, CA 93555

Library

Commander
Naval Surface Warfare Center
White Oak
Silver Spring, MD 20903-5000

Library [2 cp]
Code R-01
Code R-43 [2 cp]
Code U-04
Code U-06
Code U-42 [2 cp]

Commander
Naval Ocean Systems Center
San Diego, CA 92152-5000

Library
Code 00
Code 19 [3 cp]
Code 541
Code 844 [3 cp]

Commanding Officer
Naval Civil Engineering Laboratory
Port Hueneme, CA 93043-5003

Library
Code L1B
Code L14
Code L43 [2 cp]

Director
Naval Research Laboratory
Washington, DC 20375

Library
Code 5100
Code 5550
Code 5123
Code 6090

Commanding Officer
Naval Coastal Systems Center
Panama City, FL 32407

Library
Code 2120

Commanding Officer
Naval Oceanographic and Atmospheric
Research Laboratory
Stennis Space Center, MS 39529-5004

Library [2 cp]
Code 113
Code 200
Code 240
Code 242 [3 cp]
Code 252

Commanding Officer
Naval Oceanographic Office
Stennis Space Center, MS 39522-5001

Code OA
Code OAR
Code OARU

Commander
Naval Air Development Center
Warminster, PA 18974

Library
Code 3031 (A. Horbach)

Commander
David Taylor Research Center
Bethesda, MD 20084

Library
Code 1720
Code 1908

Commanding Officer
Naval Submarine School
Box 70
Naval Submarine Base -- New London
Groton, CT 06340

Superintendent
Naval Postgraduate School
Monterey, CA 93943-5100

Library [2 cp]
Code 68

Commander, SECOND Fleet
Fleet Post Office
New York, NY 09501

Commander, THIRD Fleet
Fleet Post Office
San Francisco, CA 96601

Commander Submarine Force
U.S. Atlantic Fleet
Norfolk, VA 23511

Code 00
Code 019
Code 22
Code N311

Commander Submarine Force
U.S. Pacific Fleet
Pearl Harbor, HI 96860

Code 00
Code N2
Code N21

Commander
Submarine Squadron THREE
Fleet Station Post Office
San Diego, CA 92132

Commander
Submarine Group FIVE
Fleet Station Post Office
San Diego, CA 92132

Commander
Submarine Development Squadron TWELVE
Box 70
Naval Submarine Base - New London
Groton, CT 06340

Code N20

Dr. Knut Aagaard
Pacific Marine Environmental Laboratory
NOAA
7600 Sand Point Way NE, Building 3
Bin C15700
Seattle, WA 98115-0070

Director
Applied Research Laboratories
The University of Texas at Austin
P.O. Box 8029
Austin, TX 78713-8029

Library
Dr. J. Huckaby

Director
Applied Research Laboratory
The Pennsylvania State University
State College, PA 16801

C. Ackerman
R. Ingram [2 cp]
E. Liszka
S. McDaniel
F. Symons, Jr.
J. Kisenwether

University of Washington
Oceanography Dept. [2 cp]